ATRX Protects Cells Against Replication-Induced Genomic Instability

Danton Ivanochko

M.Sc. Thesis

This thesis is submitted to
the Faculty of Graduate and Postdoctoral Studies
in partial fulfillment of the requirements for the degree of

Master of Science
in Biochemistry
with a specialization in Human and Molecular Genetics

Department of Biochemistry, Microbiology, and Immunology
Faculty of Medicine University of Ottawa,
Ontario, Ontario, Canada

Dedicated to my parents.

Abstract

Expansive proliferation of neural progenitor cells (NPCs) is a prerequisite to the temporal waves of neuronal differentiation that generate the six-layered cerebral cortex. NPC expansion places a heavy burden on proteins that regulate chromatin packaging and genome integrity, which is further reflected by the growing number of developmental disorders caused by mutations in chromatin regulators. Accordingly, mutations in ATRX, a chromatin remodelling protein required for heterochromatin maintenance at telomeres and simple repeats, cause the ATR-X syndrome. Here, we demonstrate that proliferating ATRX-null cells accumulate DNA damage, while also exhibiting sensitivity to hydroxyurea-induced replication fork stalling. Specifically, PARP1 hyperactivation and replication-dependent double strand DNA breakage indicated replication fork protection defects, while DNA fiber assays confirmed that ATRX was required to protect replication forks from degradation. Interestingly, inhibition of the exonuclease MRE11 by the small molecule mirin could prevent degradation. Thus, ATRX is required to limit replication stress during NPC expansion.

Acknowledgements

First and foremost, I would like to thank my supervisor, Dr. David Picketts, for his guidance and support during my undergraduate and graduate studies.

Thanks to the members of my thesis advisory committee, Dr. Jean-François Couture and Dr. Michael McBurney, for their insight during the orchestration of this research.

Thanks to all the Picketts' lab members, especially Dr. Michael Huh, Dr. Matthew Todd, and Dr. Matias Alvarez-Saavedra, for their mentorship and training. Special thanks to Keqin Yan, whose technical support was an invaluable aspect to all our research in the lab.

Thanks to Victoria J. Looking forward to our next chapter!

Finally, I would like to thank my parents, as none of this would have been possible without their love and support.

Table of Contents

List of Abbreviations

1^o, 2^o etc	Primary, secondary etc…
ALT	Alternative Lengthening of Telomeres
ART	ADP-ribosyl transferase
ATP	Adenosine triphosphate
BrdU	5-bromo-2'-deoxyuridine
CcnA	Cyclin A
Da	Dalton (equevelent to g/mol)
Da	Daltons
DDR	DNA damage response
DMEM	Dulbecco's Modified Eagle Medium
DMR	Differentially methylated regions
dNTP	Deoxyribose nucleoside triphosphates
DSB	dsDNA break
DSBR	dsDNA break repair
dsDNA	doube strand DNA
DT	Dorsal telencephalon
E_	Embryonic day _
EdU	5-ethynyl-2'-deoxyuridine
ERV	Endogenous retroviral element
EtBr	Ethidium bromide
EZH2	Enhancer of zeste homolog 2
FACT	Facilitates chromatin transcription
FBS	Fetal bovine serum
FDR	False discovery rate
gDNA	genomic DNA
H3K9me3	Tri-methylation of lysine 9 on histone 3
HP1	Heterochromatin Protein 1
HR	homologous recombination
HRP	Horse-radish peroxidise
HU	Hydroxyurea
KI	Knockin
KO	Knock out
MMEJ	Microhomology mediated end-joining
MPC	Myogenic precursor cells
MRN	MRE11-RAD50-NSB1
MZ	Marginal zone
ncRNA	non-coding RNA
NGS	Next-generation sequencing
NHEJ	nonhomologous end-joining
NMR	nuclear magnetic resonance
NPC	Neuronal progenitor cell

OMIM	Online Mendelian Inheritance in Man
PAR	poly (ADP-ribose)
PARP	poly (ADP-ribose) polymerase
PARPi	PARP inhibition
pATM	phosphorylation of the ATM kinase on Serine 1981
PBS	Phosphate buffered saline
PCR	polymerase chain reaction
PFA	paraformaldehyde
RFLP	Restriction fragment length polymorphism
RNAi	RNA interference
shRNA	short hairpin RNA
siRNA	small interfering RNA
SP	Subplate
SSDB	ssDNA break
ssDNA	single strand DNA
SVZ	Subventricular zone
TUNEL	Terminal deoxynucleotidyl transferase dUTP nick end labeling
UV	Ultraviolet
VZ	Ventricular zone
WT	Wild-type
XIST	X-inactive specific transcript
γH2A.X	phosphorylation of the histone H2A variant H2A.X on serine 139

List of Figures and Illustrations

List of Tables

1. Introduction

1.1.1 Characterization of a novel disease

In 1980, a direct method for genetic testing entered the fray of molecular diagnostics when the analysis of restriction fragment length polymorphisms (RFLPs) was first demonstrated using human genomic samples [1]. In a short time, RFLP analysis was being used to assess a field of idiopathic conditions, including one set of 3 unrelated patients presenting with milder forms of α-thalassemia, usually caused by loss of α-globin expression, as well as varying degrees of mental retardation [2]. It raised the question – was this a genetic coincidence or a new syndrome? Additional patients soon followed, which indicated that deleterious mutations mapping to the α-globin locus on the p13.3 arm of chromosome 16 (denoted as 16p13.3) could only account for the symptoms in a proportion of afflicted patients [3]. Dysregulation of a trans-acting factor pertinent for 16p13.3 expression was proposed to explain these remaining cases, which also exhibited an X chromosome-linked inheritance pattern [4] [3] [5] [6]. Linkage analysis of multiple afflicted families helped narrow the focus within the Xq13.1-q21.1 region, where the causative gene was later discovered [7] [8] [9].

1.1.2 Discovery of ATR-X syndrome: α-thalassemia, mental retardation, X-Linked

In 1995, mutations in the X-linked gene, *XH2* (later renamed *ATRX*), were identified as being causative for the ATR-X syndrome [10]. Now, with a distinct genetic identifier by which to group patients, it became clear that ATR-X syndrome comprised a clinically heterogeneous set of features that often ranged in their severity between patients. As an X-linked disease, pathogenic variants are either inherited from carrier females (**Figure 1A**), or

arise as *de novo* mutations. ATR-X syndrome is a developmental disorder, associated with postnatal growth deficiency and symptoms that can be characterized as either neurological or non-neurological. Non-neurological symptoms can include genital and skeletal abnormalities, a distinctive facial dysmorphia, and α-thalassaemia, while the neuronal symptoms can present as mental retardation, microcephaly, cerebellar atrophy, hypomyelination, and epilepsy (**Figure 1A**) [11] [12] [13].

1.1.3 Clinical mutational analysis

As of 2006, 168 cases of ATR-X syndrome had been reported, indicating the general rarity of this orphan disease [14]. Causative mutations include missense, nonsense, altered splicing, small insertions or deletions (indels) and gross rearrangements, although they are largely missense mutations. However, when the protein expression levels have been examined in detail, some residual expression of ATRX has been detected in patients' cells regardless of their mutation [15] [16]. This appears to hold true, even in the cases of upstream nonsense mutations, which seems to indicate that ATR-X null mutations are non-viable and that all other mutations possess a hypomorphic quality [17] [15]. Furthermore, these mutations are disproportionately biased towards loci encoding the two conserved functional domains of the ATRX protein [18] [19]. When we mapped 109 unique ATR-X causing mutations that had been reported to the date of this thesis (June 20th, 2016), we were able to confirm this location bias (**Figure 1B**). Specifically, the N-terminal ADD domain accounted for ~34% of unique mutations, while the C-terminal ATPase/Helicase domain accounted for ~41% of unique mutations. If the unique ATR-X causing mutations were evenly distributed across the protein, then we would expect the proportional unique mutation densities to be ~8% and ~28%, respectively. Interestingly, another mutational analysis also included the frequency of identical causal mutations and found the ADD and

ATPase/Helicase domains accounted for ~49% and ~30% of all causal mutations, respectively [15].

There have been several attempts to define a phenotype-genotype correlation between the range and severity of symptoms in patients afflicted with ATR-X syndrome relative to the location and manner of their mutations. One study of 22 patients had suggested that while all observed patients displayed some level of mental retardation, those with mutations in the ADD domain correlated with more severe psychomotor and physical anomalies relative to those with mutations located within the ATPase/Helicase domain of the protein [18]. Interestingly, a mild form of ATR-X syndrome has been associated with a nonsense mutation in exon 2 (c.109C>T, p.R37X), which leads to an N-terminally truncated protein product due to the production of an alternatively spliced transcript [20] [21]. These patients are fortunate to possess protein product containing both the ADD and ATPase/Helicase domains, although the protein is expressed at a slightly lower level [20]. This evidence indicates that the disease severity is also dose dependent.

At the molecular level, biochemical analysis has indicated that particular mutations influence protein expression levels, perhaps by their contribution to the overall stability of the molecule. Structural determination of the ADD domain has indicated that mutations to the highly conserved cysteine residues required for zinc binding lead to lower protein expression levels compared to mutations of the hydrophilic surface residues [19]. Additionally, homology modeling of the ATPase/Helicase domain, using the zebrafish Snf2-family member Rad54, indicated that hydrophobic to hydrophilic mutations also destabilizes the protein molecule [22]. Interestingly, modern molecular genetics has elucidated one phenotype-genotype correlation, albeit in an indirect manner. ATRX functions in part through targeted genomic localization and the polymorphic nature of ATRX's genomic

targets has been correlated with the severity of specific symptoms. This has been exemplified by the variable levels of α-thalassemia observed in ATR-X patients, resulting from downregulated α-globin gene expression causing HbH inclusions [23]. Specifically, the downregulation of α-globin gene expression strongly correlated with the size of the polymorphic ψζ VNTR tandem repetitive sequence proximal to the α-globin loci, which ATRX is known to bind [24] [25]. Therefore, while ATR-X function and expression may influence the severity of ATR-X symptoms, so too does the nature of its genomic targets.

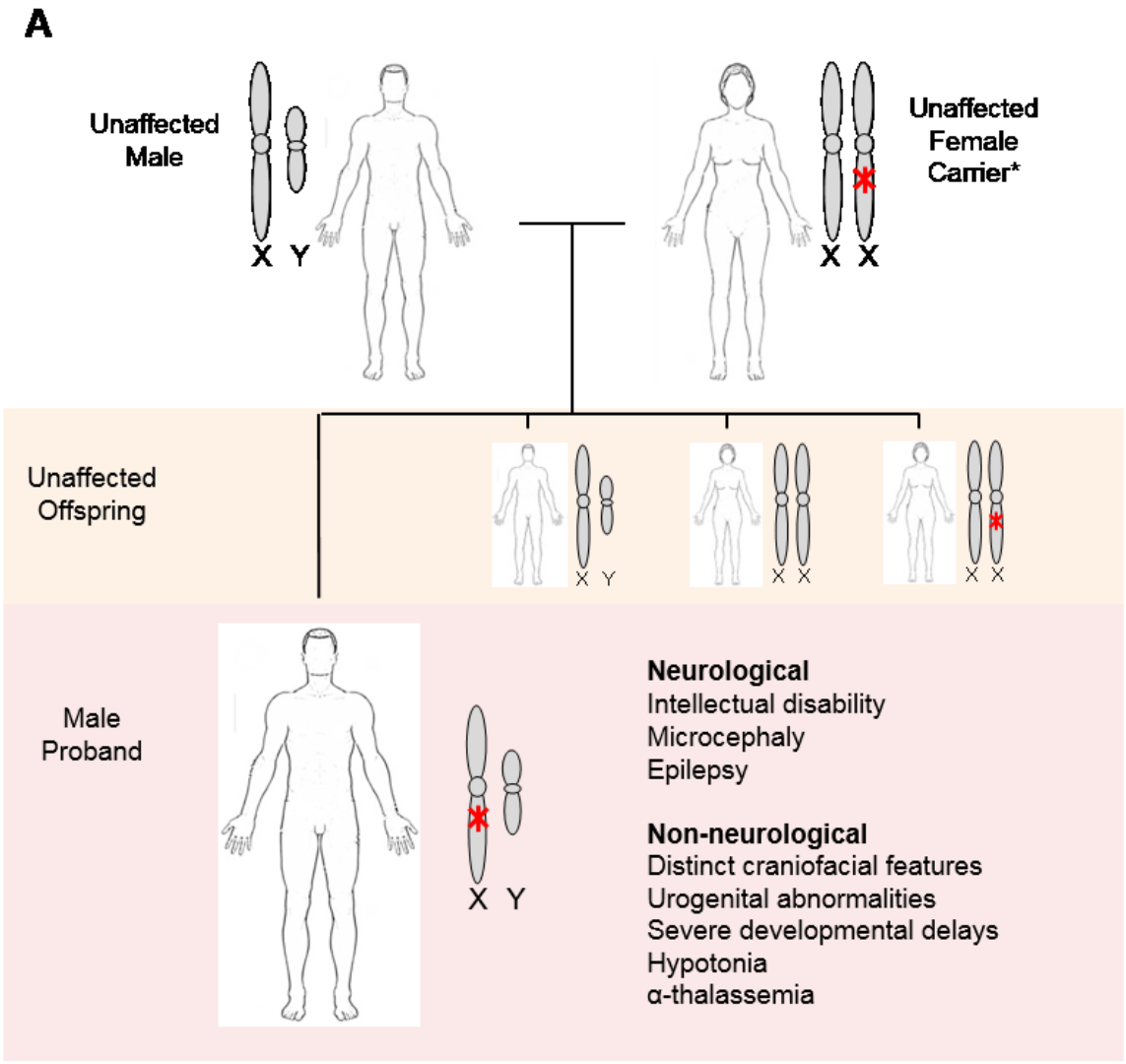
A
Unaffected Male
X Y
Unaffected Female Carrier*
X X
Unaffected Offspring
X Y
X X
X X
Male Proband
X Y
Neurological
Intellectual disability
Microcephaly
Epilepsy
Non-neurological
Distinct craniofacial features
Urogenital abnormalities
Severe developmental delays
Hypotonia
α-thalassemia

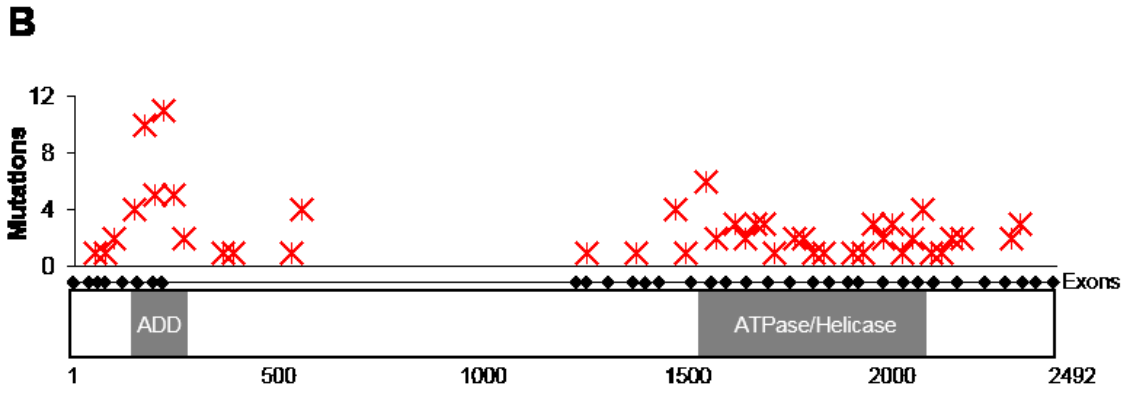
B
Mutations
12
8
4
0
Exons
ADD
ATPase/Helicase
1
500
1000
1500
2000
2492

Figure 1. ATR-X syndrome: α-Thalassemia, mental retardation, X-Linked
(**A**) ATR-X syndrome is an example of an X-linked disease. Causal mutation can arise in an unaffected maternal carrier or de novo in a male proband who presents with an assortment of neuronal and non-neurological symptoms.
(**B**) A map of 109 unique ATR-X causing mutations that had been reported to the date (June 20th, 2016) were aligned to the full length ATRX amino acid sequence. Mutations were binned into 50 amino acid increments and the number of mutations per bin was quantified on the y-axis. The ADD and ATPase/Helicase domains have been labeled for reference.
Panel B references: [10] [26] [27] [28] [23] [29] [30] [31] [32] [33] [34] [35] [36] [37] [38] [39] [40] [41] [42] [43] [44] [45] [46] [47] [48] [15] [49] [50] [51] [52] [22] [53] [54] [13] [55] [56] [21] [57] [58] [59]

1.2.1 The ATRX protein.

The *ATRX* gene encodes an atypical chromatin associated enzyme that still requires a comprehensive biochemical characterization. *ATRX* is transcribed into its mRNA message, which is in turn alternatively spliced to yield 2 main isoforms. The full length, 283 kDa ATRX protein is identified by its N-terminal ADD domain and its C-terminal ATPase/helicase domain, while an ~200kDa C-terminally truncated minor isoform called ATRX-t, possesses only the N-terminal ADD domain (**Figure 2A**) [60]. Early work characterizing the ATRX protein sequence determined that it belonged to the SNF2-family of chromatin remodelers as inferred by the conserved ATPase/Helicase domain (**Figure 2B**) [27] [61]. Additionally, the ADD domain, aptly named for is conservation between ATRX and the DNA methyltransferases, DNMT3 and DNMT3L, is comprised of a GATA-type zinc finger linked to a PHD-type zinc finger and a C-terminal α helix (**Figure 2B**). To date, the ATRX ADD domain remains the only ATRX structural domain that has been directly solved by either x-ray crystallography or nuclear magnetic resonance (NMR) spectroscopy [19] [16] [62] [63].

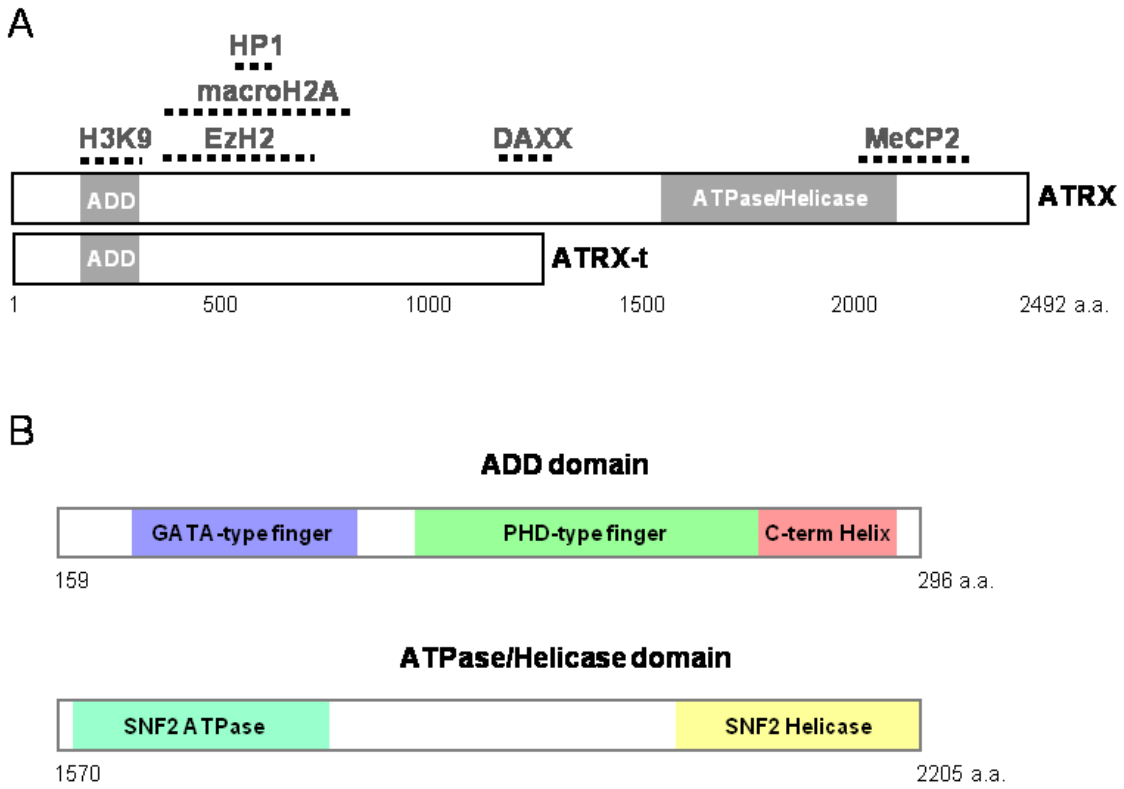

Figure 2. A map of ATRX's primary amino acid sequence, with mapped protein-interaction domains.

(**A**) The full length ATRX protein is 283 kDa and contains an N-terminal ADD domain and a C-terminal ATPase/helicase domain, while an ~200kDa C-terminally truncated minor isoform (ATRX-t), possesses only the N-terminal ADD domain. ATRX's ADD domain recognizes the tri-methylated covalent modification of histone 3 lysine 9. Additionally, both ATRX and ATRX-t, can interact with HP1, macroH2A and the PRC2 complex member EzH2. Potentially, only full length ATRX can interact with the DAXX protein to form a histone H3.3 chaperone complex, while only full length ATRX can interact with MeCP2.
(**B**) The ADD (ATRX-DNMT3-DNMT3L) domain is composed of a GATA-type zinc finger followed by a PHD-type zinc finger and a C-terminal α-helix. The ATPase/Helicase domain belongs to the SNF2 family of ATPase/Helicases and is homologous to the RAD54 helicase protein.

To illustrate ATRX in the context of its chromatin environment, we used the RaptorX protein modeling software to develop an anatomical representation of the full length protein and placed this predicted structure next to a dinucleosome array (**Table 1, Figure 3**) [64] [65]. RaptorX aligned the ATRX sequence to three previously solved structures from the RCSB Protein Data Bank. As expected the previously solved ADD domain structure was selected for amino acids 151-301 and the homologous RAD54 structured derived from zebrafish was used to predict the SNF2 ATPase/Helicase domain, while a portion of the remaining C-terminus was matched to the BRO1/V domain of the human anti-apoptotic protein known as ALIX (**Table 1**). When the predicted structural domains were aligned to the ATRX primary sequence, we observed that a large portion of the junction between the ADD domain and SNF2 domain, as well as short sections of the N- and C- terminus, lacked any defined structural predictions (**Figure 3A**). Interestingly, these regions are largely barren from any mutations that are associated with ATR-X syndrome, suggesting a limited functional consequence to the amino acid sequences beyond a domain-linking feature (**Figure 1B**). The predicted ATRX structure was juxtaposed with the solved structure of a nucleosome placed in tandem array (**Figure 3B**) [66]. Consequently, this theoretical model indicates the scale of the ATRX protein in regards to its native chromatin environment.

Table 1. Predicted structural model of the full length ATRX protein. RaptorX software was used to model the full length ATRX protein using previously solved, closely identical structures as templates. The colour corresponds to the modeled domain in **Figure 3**, and the indicated amino acids were modeled with the indicated template, identified by the specifc Protein Data Bank (PDB) code. The p-value indicates the likelihood of a predicted model being worse than the best of a set of randomly-generated models for the indicated domain. Of the full length protein, 1025 (41%) residues were modeled and 1467 (59%) positions were predicted as disordered.

Colour	Amino Acids	Template (organism)	PBD code	p-value
Red	151-301	ATRX's ADD domain (Human)	2JM1	2.01×10^{-10}
Magenta	1544-2248	RAD54's SWI2/SNF2 domain (Zebrafish)	1Z3I	1.63×10^{-16}
Cyan	2249-2417	ALIX's BRO1/V domain (Human)	2OEV	1.17×10^{-02}

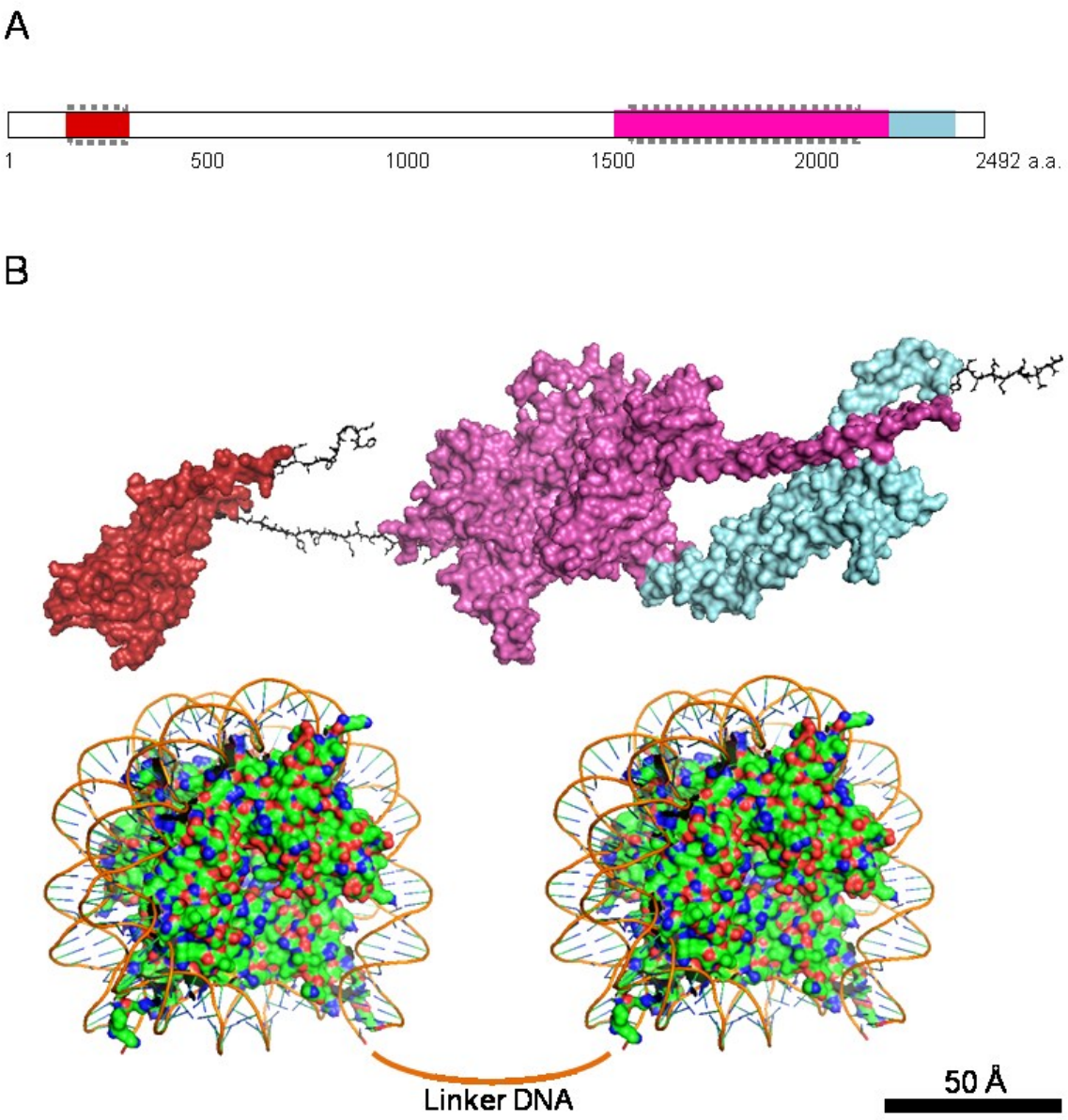

Figure 3. The predicted ATRX secondary structure modeled with chromatin.
(**A**) The primary, full length ATRX sequence map with coloured indicators of the predicted structural domains in panel (**B**) and **Table 1**. The N-terminal ADD domain and the C-terminal ATPase/Helicase domain are designated with the dotted lines.
(**B**) The predicted structure of the full length ATRX protein was placed next to a dinucleosome array composed of two identical human nucleosome core particles (PDB: 5AV6). Structures were manipulated with PyMOL (v1.7.4) software. Scale bar is relative to both ATRX and the nucleosomes.

1.2.2 The ATRX interactome

The ATRX protein has several characterized interactions associated with its nuclear functions including heterochromatin maintenance and response to DNA damage (**Table 2**). With regards to heterochromatin maintenance, ATRX's ADD domain recognizes a specific epigenetic chromatin profile including the post-translational modifications of the histone H3 tail with unmodified lysine 4 and tri-methylated lysine 9, while also being tolerant of serine 10 phosphorylation status (H3K9me3±S10ph) (**Figure 2A**) [67] [16] [63]. Downstream of the ADD domain, ATRX interacts with several heterochromatin-associated proteins including Heterochromatin protein 1 (HP1, the HP1α paralog has been specifically demonstrated) via a degenerate PxVxL motif and with the histone H2A variant, macroH2A, via an unspecified interaction motif (**Figure 2A**) [68] [69] [70]. At a region of ATRX's C-terminal end, which partially overlaps the SNF2 Helicase domain, ATRX interacts with the transcriptional repressor known as Methyl CpG binding protein 2 (MeCP2) (**Figure 2A**) [71]. Additional heterochromatin interactions that are less well documented include HP1β, as well as SMC1A and SMC3 of the Cohesin complex (**Table 2**) [72] [73].

With regards to ATRX chromatin remodeling function, the SNF2 domain has been demonstrated to possess an ATPase activity that can be stimulated by either DNA or mononucleosomes [74]. Upstream of this ATPase domain lies ATRX's DAXX-interaction domain (**Figure 2**) [75]. ATRX and DAXX form an ATP-dependent chromatin-remodeling complex that functions to deposit H3.3-H4 dimers into heterochromatin associated with repetitive DNA regions [76] [77] [78] [79]. Furthermore, ATRX-dependent H3.3 deposition has been directly associated with the maintenance of the H3K9me3 modification by histone methyltransferases, SUV39H1 and SETDB1 (also known as ESET) [80] [81] [82] [83]. One high-throughput screen identified the Facilitates chromatin transcription (FACT) complex

members, SUPT16H and SSRP1, as potential interacting partners with ATRX, perhaps relevant for nucleosome assembly, although there has not been any follow-up published to date [84]. In addition to binding with DAXX for the purpose of chromatin remodeling, an ATRX region downstream of the ADD domain is thought to bind to the histone methyltransferase subunit of Polycomb repressive complex 2 (PRC2), known as Enhancer of zeste homolog 2 (EZH2), which is required to write the H3K27me3 heterochromatin mark [85] [86]. However, recent evidence suggests that the EZH2 interaction may actually be an artifact of a shared RNA-interaction [87].

So far, the only published example of ATRX's specific interaction with an RNA molecule comes from a 2014 paper which carefully suggested that ATRX remodels the 2^{o} structure of the X-inactive specific transcript (XIST) noncoding RNA (ncRNA) [87]. Here the authors found that ATRX specifically binds the Repeating Adenine (RepA) motif of XIST and stimulates XIST binding to PRC2. Additionally, they indicated that ATRX, PRC2, and the RepA-sequence of XIST could form a 4^{o} structural complex that was dependent on the ATPase activity of ATRX. In contrast to RNA, ATRX interactions with DNA have been more thoroughly characterized. Chromatin immunoprecipitation assays have demonstrated that ATRX localizes to repetitive and guanine (G)-rich DNA loci *in vivo*, particularly at telomeres, retrotransposons and simple repeats, while also specifically binding to G-quadruplex (G4) structured DNA *in vitro* [24] [63] [80] [88] [89].

A growing body of evidence has amassed to suggest that ATRX interacts with several DDR proteins (**Table 2**). The best characterized of this group is ATRX's interaction with the MRN dsDNA break repair (DSBR) complex, which is composed of MRE11, RAD50 and NBS1 [84] [90]. The MRN complex facilitates the homologous recombination (HR) DSBR pathway, while a second and less well characterized interaction of ATRX, which is known as the

DNAPK complex (composed of DNAPKcs, Ku70 and Ku80), is recognized to facilitate the nonhomologous end-joining (NHEJ) DSBR pathway [91] [84]. Several additional, lower confidence interactions include the ssDNA binding protein, RPA1, the DNA damage response (DDR) and cell cycle progression master-regulator, p53, and two members of the 9-1-1 cell-cycle checkpoint complex, known as RAD1 and RAD9A [84].

Table 2. The published ATRX protein interactome.
ATRX protein-protein interactions are indicated by the gene and protein interactor, with notes on the functional significance of the interaction, as well as the method of interaction determination and the referenced article where the interaction was first reported.

ATRX interactor		Function	Detection method		
Gene	**Protein**		**High-throughput**	**Low-throughput**	**Refs**
DAXX	DAXX	H3.3 chaperone	IP-MS	IP-W	[74] [84]
CBX5	HP1α	Heterochromatin, H3K9me3		IP-W	[68]
CBX1	HP1ß	Heterochromatin, H3K9me4	IP-MS		[72]
PML	PML	PML-nuclear bodies		IP-W	[92]
EZH2	EZH2	PRC2 complex, H3K27me3		2-H, IP-W	[85] [87]
MRE11A	MRE11	DSBR, HR, MRN, exonuclease	IP-MS	IP-W	[84] [90]
RAD50	RAD50	DSBR, HR, MRN, DNA binding	IP-MS	IP-W	[84] [90]
NBN	NBS1	DSBR, HR, MRN complex	IP-MS	IP-W	[84] [90]
MECP2	MECP2	Binds both 5-methylcytosine (5mC)		2-H, IP-W	[71] [73]
XRCC6	KU70	Helicase, DSBR, NHEJ, DNAPK	IP-MS		[84]
XRCC5	KU80	Helicase, DSBR, NHEJ, DNAPK	IP-MS		[84]
PRKDC	DNAPKcs	DSBR, NHEJ, DDR kinase	IP-MS		[84]
H2AFY	macroH2A.1	Transcriptional repression	IP-MS	IP-W	[69] [87]
epigenetic*	H3K9me3	Heterochromatin		ITC, Crystal	[16]
epigenetic*	H3K9me3S10ph	Mitotic pericentromeres		IP-W, Crystal	[63]
SUPT16H	SUPT16H	FACT complex	IP-MS		[84]
SSRP1	SSRP1	FACT complex	IP-MS		[84]
RPA70	RPA1	RPA, ssDNA, HR, BER, NER	IP-MS		[84]
TP53	p53	Cell growth arrest, apoptosis	IP-MS		[84]
RAD9A	RAD9A	9-1-1 cell-cycle checkpoint	IP-MS		[84]
RAD1	RAD1	9-1-1 cell-cycle checkpoint	IP-MS		[84]

Table 2. The published ATRX protein interactome (continued).

ATRX interactor		Function	Detection method		Refs
Gene	Protein		High-throughput	Low-throughput	
NEK1	NEK1	DDR kinase		2-H	[93]
HIST1H1C	Histone H1.2	Binds to linker DNA	IP-MS		[84]
many**	Histone H2A	Core nucleosome component	IP-MS		[84]
many**	Histone H2B	Core nucleosome component	IP-MS		[84]
many**	Histone H3	Core nucleosome component	IP-MS	Crystal	[84] [62]
many**	Histone H4	Core nucleosome component	IP-MS		[84]
SMC1A	SMC1A	Cohesin complex, HR		IP-W	[73]
SMC3	SMC3	Cohesin complex, HR		IP-W	[73]
ZBED1	ZBED1	Transcription factor		IP-W	[94]
KIAA1196	ZNF512B	Transcription factor		2-H	[95]
HDAC4	HDAC4	Histone deacetylase		2-H	[96]

* histone epigenetic code
** many histone coding genes

IP-MS: immunoprecipitation with mass spectrometry
IP-W: immunoprecipitation with western blot analysis
2-H: Yeast 2-hybrid assay
Crystal: X-ray crystal structure
ITC: isothermal titration calorimetry

1.3 Mouse models of ATR-X syndrome

The *ATRX* exonic structure across vertebrates is highly conserved as demonstrated by PhyloP basewise conservation mapping (**Figure 4A**). Furthermore, human and mouse ATRX amino acid sequences share 84.67% identity, with the majority of amino acid sequence incongruence arising outside of the conserved ADD and ATPase/Helicase domains (**Figure 4B**). Transgenic mouse lines are often used to model complex human genetic diseases. Unfortunately, the global ablation of ATRX expression is embryonic lethal in mice, so several mouse conditional deletions of ATRX expression have been generated to study the loss in isolated tissues relevant to ATR-X syndrome. These models have illuminated important clinical features of ATR-X syndrome, including muscle hypotonia, urogenital abnormalities, visual defects and complex neuronal deficits.

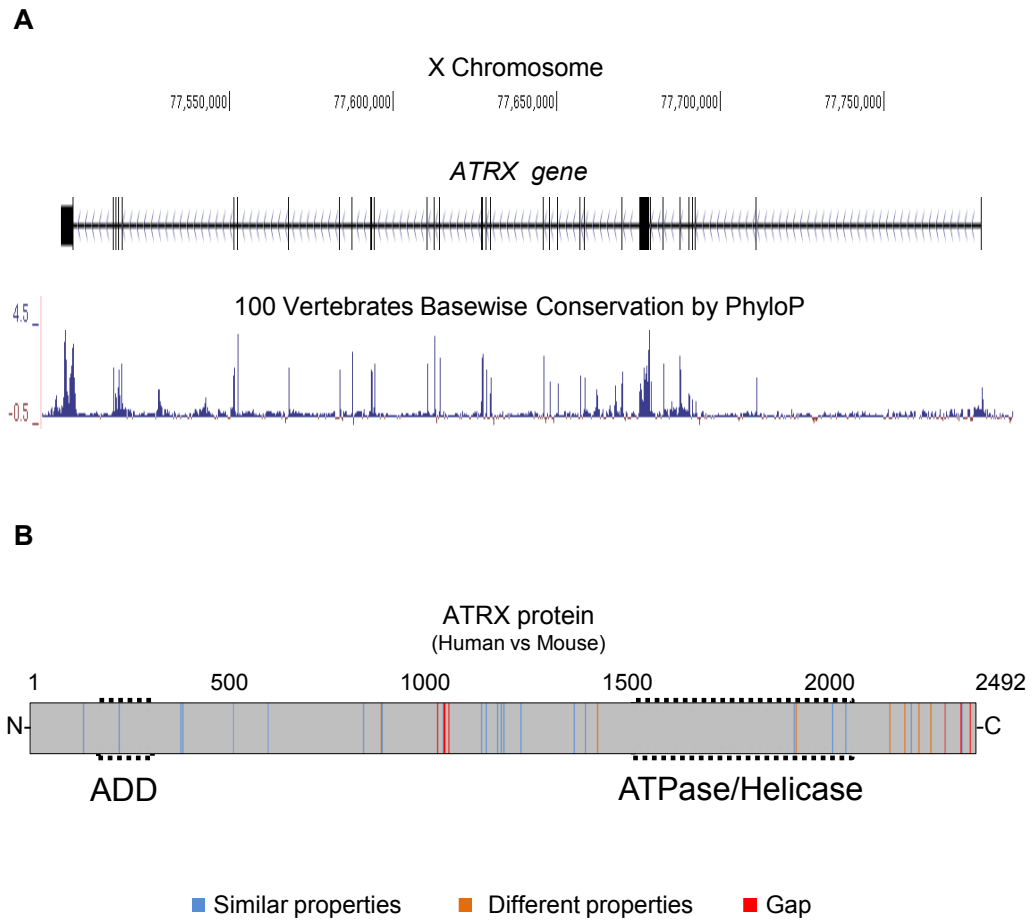

Figure 4. The conservation of the ATRX gene and protein

(A) The ATRX genomic locus on the human X-chromosome (UCSC Genome Browser, GRCh38/hg38 Assembly) depicts the 36 exons of the ATRX gene (vertical bars) with intronic sequences (block dashed line), directly aligned with the PhyloP per-base conservation plot of 100 closely related vertebrate species. y-axis is -log p value under hypothesis of neutrality. Positive scores suggest evolutionary constraint; negative scores suggest accelerated evolution.

(B) The human and mouse ATRX proteins share a 84.67% identity. Mouse ATRX amino acids were aligned to the human ATRX sequence with Clustal omega and amino acids scored with similar properties (blue lines), different properties (yellow lines) and gapped alignments (red lines) were highlighted. Identical ammino acids are grey. The ADD and ATPase/Helicase domains were shown for reference.

Hypotonia is a clinical hallmark of ATR-X syndrome that is typically diagnosed during infancy. Conditional loss of Atrx in skeletal muscle was examined using a Cre recombinase knockin (KI) mouse, specific to myogenic regulatory factor *Myf5*-expressing cells [11] [97]. These Atrx muscle specific cKO mice were consistently smaller in size during development and possessed muscle satellite cells, which exhibited compromised growth properties. Importantly, many of the aberrant myogenic properties were attributed to a genomic instability phenotype, associated with a reduced proliferative capacity [97]. Another common clinical characteristic of ATR-X syndrome is a range of urogenital abnormalities from undescended testes, hypospadias, underdeveloped testes and micropenis, and in its most severe form ambiguous or female genitalia in XY males [11] [98]. Conditional loss of Atrx in Sertoli cells was examined using a Cre recombinase KI mouse activated by anti-Müllerian hormone gene expression [99]. Atrx testis specific cKO mice possessed underdeveloped testis, with Sertoli cells showing a proliferation defect associated with a prolonged transit through G2/M phases, as well as elevated apoptosis [99]. While visual deficits are difficult to assess in ATR-X patients, at least 2 patients have presented with total blindness and ~23% are reported to have some visual abnormalities [11] [100]. Conditional loss of Atrx in the peripheral retina was examined using a Cre recombinase mouse activated by the Pax6 promotor [100]. These Atrx retinal specific cKO mice displayed interneuron abnormalities associated with compromised amacrine and horizontal cell survival [100]. Together, these mouse models suggest that the underlying consequence of Atrx-loss appears to be enhanced cellular death.

Profound mental retardation is the most often diagnosed feature of ATR-X syndrome, observed in ~95% of patients [11]. With respect to brain development, early studies in mice had identified that widespread Atrx expression during early embryogenesis seemed to become limited to actively proliferating cells. This suggested a role for Atrx during mitotic

proliferation in cells, such as neuronal progenitors during neurodevelopment [61] [101]. The first viable transgenic mouse model overexpressed the human ATRX protein in mice [102]. This often resulted in neural tube defects and embryonic lethality, while pups that survived birth often perished perinatally, or else suffered seizures and behavior abnormalities [102]. Although this model indicated that ATRX dosage was important and influenced pathways vital for normal neuronal development, it is important to note that ATR-X syndrome is caused by hypomorphic mutations that are associated with reduced protein expression levels. Unsurprisingly, the study which followed this work found that Atrx is important for neuronal survival during corticogenesis by examining Atrx ablation [103].

Microcephaly is a common feature of ATR-X syndrome and is a primary phenotype of a cortex-specific mouse model of ATR-X deficiency [11] [103]. In this regard, conditional loss of full length Atrx expression during telencephalon maturation has been examined using Foxg1 driven Cre expression [103]. Here, Atrx deficient male embryos were perinatal lethal, exhibiting cortical hypocellularity and increased neuron progenitor genomic instability with diminished neuronal migration to superficial cortical regions [103]. Two follow-up studies identified that the cell cycle checkpoint protein p53 induced the double strand DNA break (DSB) signalling kinase ATM and led to apoptosis within the Atrx-null telencephalon [104] [105]. Another recent study utilizing this model suggested that mitotic spindle defects in Atrx-null cortices may be associated with depletion of the neuron progenitor pool which supplies the later-born neuronal layers of the cortex [106].

Interestingly, a transgenic mouse line known as ATRX(ΔE2) has been developed, which mimics a known patient mutation [107]. By excising exon 2 of the mouse Atrx gene, the authors were able to mimic the R37X human mutation [20]. R37X is known to cause a milder manifestation of ATR-X syndrome wherein a near-full length, N-terminally truncated

protein possessing both the ADD and ATPase/Helicase domains is produced from an alternative transcript [20] [21]. These ΔE2 mice displayed impaired learning-memory and cognitive functions, which is accompanied by abnormal dendrite morphology concomitant with reduced Atrx protein expression [108] [107]. Although this model lacks any significant follow-up, the underlying implication of these findings remains true to the neuronal significance of ATR-X syndrome. A recurring finding from studies of Atrx-loss in the brain and other tissues seems to suggest that the developmental defects often arise from cell-loss, which is often proceeded by genomic instability [104] [105] [103] [97]. Therefore, it is essential to understand the developmental mechanisms associated with disease relevant tissues, such as the brain, in order to investigate the etiology of ATR-X syndrome.

1.4 A primer on cortical development

The cerebral cortex originates, along with the rest of the central nervous system (CNS), from a structure comprised of ectodermal stem cells which is known as the neural tube. During early embryonic development, the neural tube segregates into the prosencephalon (forebrain), the mesencephalon (midbrain) the rhombencephalon (hindbrain) and the spinal cord. The prosencephalon will develop into the diencephalon, as well as the precursor of the cerebrum, which is known as the telencephalon. The outer neuronal region of the cerebrum is known as the cerebral cortex, and it takes the form of a stratified neuronal structure with distinct laminar identities that are specified by particular neuronal lineages [109] (**Figure 5A**). Corticogenesis is the specific development of the cerebral cortex, from the dorsal region of the telencephalon.

The progenitor cells of the telencephalon are known as neural precursor cells (NPCs). At the beginning of corticogenesis, NPCs divide symmetrically as neuroepithelial stem cells

within a region known as the ventricular zone (VZ) and then begin to divide asymmetrically as radial glial cells, which both self-renew and generate neurons. These first post-mitotic neurons will project across the entire length of the developing cortex, while the subsequent neurons will migrate along their projections from the VZ and through the subventricular zone (SVZ) to form the cortical subplate (SP) and marginal zone (MZ). This process gives rise to the outer boundaries of the cerebral cortex (**Figures 5B and 5C**). A “bottom-up” sequence follows, wherein NPCs migrate from the VZ/SVZ, past the SP and towards the MZ, forming the cortical layers VI through II in successive fashion (**Figure 5B**) [110] [111] [112] [113] [114] [115]. Therefore, and with the exception of layer I (produced from the MZ), this ventral-to-dorsal neurogenic gradient requires that the uppermost neurons (i.e. comprising layers II and III) of the cerebral cortex form from the most proliferative NPCs in the VZ/SVZ [116] [117]. Importantly, this high replicative rate of NPCs during development has been associated with increased replication-induced DNA damage [118].

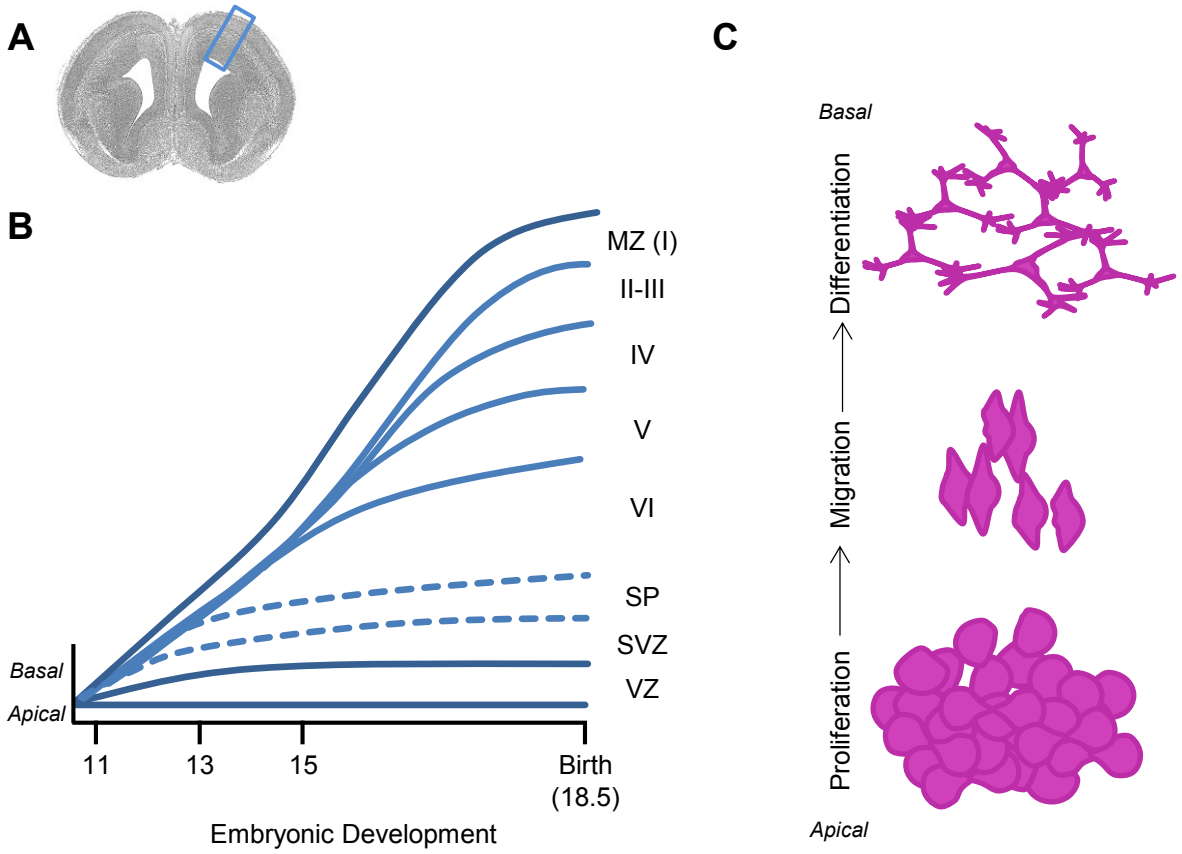

Figure 5. Stages of cortical development beside NPC proliferation, migration and differentiation.

(**A**) A coronal section of an adult mouse cortex highlighting (blue box) stratified neuronal layers from the apical (lateral ventricle) to basal (exterior lamina) regions.

(**B**) A developmental model of cortex development with neuronal layer stratification. The X-axis shows the developmental time and the Y-axis indicates the directions of the apical and basal regions. Neuronal progenitor cells migrate from the ventricular and subventricular zones (VZ and SVZ, respectively) to first form the medial zone (MZ), which becomes layer I. A bottom-up development follows with neurons migrating through the subplate (SP) into layer VI through to layer II, in successive order.

(**C**) Neuronal progenitor cells (NPC) proliferate through a series of symmetric and asymmetric divisions to generate additional NPCs and mature neurons, respectively. Asymmetric divisions give rise to maturing neurons which first adopt a migratory phenotype until they localize into the appropriate neuronal layer where terminal differentiation occurs.

1.5.1 ATRX and DNA damage

ATRX deficiency is unequivocally associated with DNA damage, as evidenced by models of ATR-X syndrome, as well as studies of ATRX-associated cancers [119] [120]. Activation of the ATM-p53 DSBR pathway in mouse models of ATR-X syndrome have specifically implicated dsDNA breakage as an adverse cellular consequence of ATRX deficiency [97] [104] [105]. Furthermore, ATRX deficient cells which sustain chemically or radiologically induced DNA damage succumb to p53-mediated cell death [121] [97] [122]. Therefore, it is imperative to understand this DNA damage signalling and repair pathways, with regards to ATRX.

1.5.2 A primer on DNA damage repair

In eukaryotes, nuclear DNA is organized into linear chromosomes, which each form from one continuous and highly organized strand of chromatin. Chromatin is a fiber of dsDNA (ranging from 49.5-247.2 mega base pairs [Mb] in humans) organized into nucleosomes consisting of 147 base pairs (bp) of DNA wrapped around an octamer of proteins known as histones [123]. The chromatin structure is highly organized and nucleosome placement and mobility is directly related to DNA damage repair kinetics [91] [124]. It has been estimated that a given mammalian cell may experience ~10^4 single stand DNA breaks (SSB) a day, which may lead to as many as 50-100 double strand DNA breaks (DSB) (**Figure 6**) by escaping the standard repair mechanisms [125] [126]. Typically, SSBs are recognized by Poly-(ADP)-ribose polymerase (PARP) enzymes, which undergo an auto-modification event known as PARylation to recruit SSB repair proteins such as XRCC1 (**Figure 6**). Cells signal the presence of SSBs through the ATR kinase enzyme, which in turn activates the CHK1 kinase and both the activated ATR and CHK1 kinases may then phosphorylate the histone

H2A variant, H2A.X, as well as the master cell-cycle checkpoint regulator known as p53 (**Figure 6**). This signalling cascade ensures proper repair of SSB, however in some instances SSBs may face a prolonged period of destabilization and develop into DSBs (**Figure 6**).

Due to the nature of the linear chromatin fiber comprising each chromosome, DSBs can be highly deleterious to the genomic integrity of a cell by enabling chromosome rearrangements, as well as mutagenic DSB repair products [127] [91]. DSBs can be invoked directly by ionizing radiation or by prolonged replication fork stalling events, as well as potentially evolving from unrepaired SSBs (**Figure 6**) [128] [125] [126]. Similar to SSBs, DSBs are signalled through the ATM kinase enzyme, which in turn activates the CHK2 kinase and both the activated ATM and CHK2 kinases may then phosphorylate the histone H2A variant, H2A.X, as well as the master cell-cycle checkpoint regulator known as p53 (**Figure 6**). At least 3 repair pathways can deal with DSBs [127] [91]. During G1-phase of the cell cycle, the only pathway available to deal with DSBs is the Nonhomologous end joining (NHEJ) pathway evolving the DNAPK DSB recognition and signalling complex, as well as the 53BP1 scaffolding protein and several other dsDNA ligating enzymes (**Figure 6**). NHEJ is considered a non-conservative form of DSB repair because indels will often occur during the repair process. During S and G2 phases of the cell cycle when a sister chromatid is available as a repair template, a conservative form of DSB repair called Homologous recombination (HR) can occur involving the MRN complex to recognize DSBs and expose ssDNA in a process called “resectioning”, then requiring the BRCA1, BRCA2, RAD51 and RAD54 proteins to signal and facilitate the ssDNA stand invasion into the homologous chromatid (**Figure 6**). An additional DSB repair pathway called Microhomology-mediated end joining (MMEJ), also known as Alternative nonhomologous end-joining (Alt-NHEJ), can occur when limited MRN resectioning enables stand invasion with minimal homology [127]

[129]. Because this process requires minimal homology, it is considered non-conservative and potentially mutagenic as it occurs during G1-phase and may facilitate dubious strand exchanges with nonhomologous chromosomes [129].

Regardless of the repair pathway selected when SSBs and DSBs are ameliorated, cell-cycle progression will become unrestrained and mitotic progression will then follow. However, when DNA damage cannot be dealt with in an appropriate manner, either due to an overabundance of lesions or faulty repair pathway activity, cells will undergo p53-mediated cell-cycle arrest, which can then lead to a cell-intrinsic apoptotic cascade causing cell death. Evading these mechanisms of cell death is a requisite of oncogenesis, thereby implicating the silencing of DSB and SSB repair pathways in cancer progression [130] [131] [132]. Additionally, a number of human neurodevelopmental diseases have been linked to mutations in DDR genes, perhaps due to the relatively high mitotic index associated with neuronal development [118] [126]. Accordingly, it is no surprise that compromised genome replication can in turn lead to DNA lesions.

The topic of DNA damage repair encompasses a wide and complex, yet well-studied field of research, which recently gained attention as the 2015 Nobel Prize in Chemistry was bestowed upon Tomas Lindahl, Paul Modrich and Aziz Sancar, for their contribution to the field [133]. Accordingly, several well cited reviews have been published on this topic in recent years, which explain the currently accepted models of DNA damage signalling and repair in great detail [127] [91] [124] [126] [134]. For brevity in highlighting the DDR pathways associated with ATRX, we have distilled the work in these reviews to encompass factors which we believe to be directly relevant to ATRX (**Figure 6**). For any further clarification, we recommend the previously cited reviews.

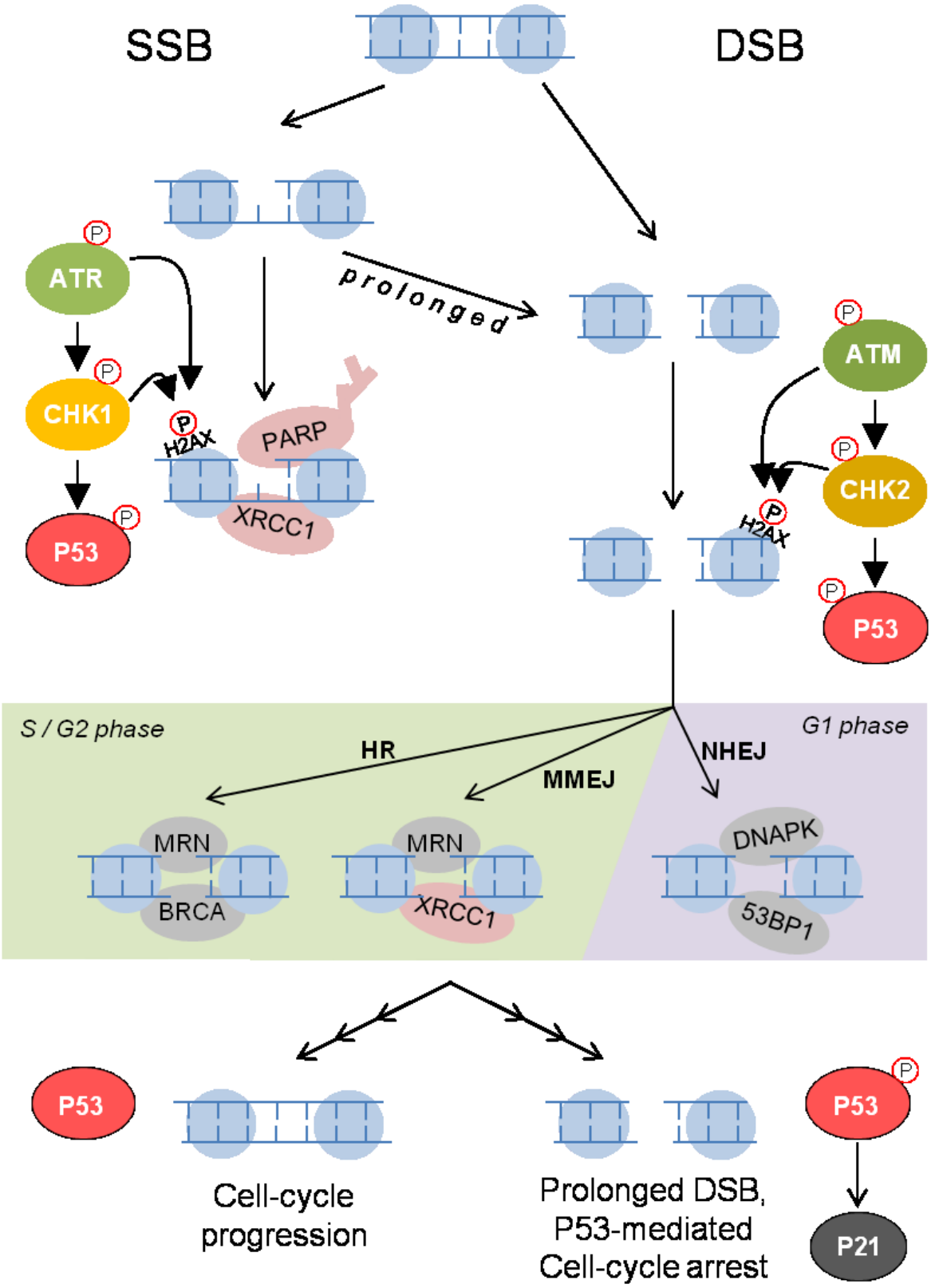
SSB
DSB
ATR
CHK1
P53
H2AX
PARP
XRCC1
prolonged
ATM
CHK2
P53
H2AX
S / G2 phase
G1 phase
HR
MMEJ
NHEJ
MRN
BRCA
MRN
XRCC1
DNAPK
53BP1
P53
Cell-cycle progression
Prolonged DSB, P53-mediated Cell-cycle arrest
P53
P21

Figure 6. DNA breakage signalling and repair pathways.
A model of ssDNA break (SSB) and dsDNA break (DSB) signalling cascade and repair pathways, specifically highlighting proteins relevant to ATRX. SSBs can arise from intracellular metabolites or spontaneous DNA decay. SSBs are recognized by PARP and XRCC1 enzymes. SSB signalling involves the automodification of PARP and the activation of the ATR kinase. ATR automodification and CHK1 kinase phosphorylation leads to H2A.X phosphorylation of serine 139 (known as γH2A.X) to mark DNA damage loci and phosphorylation of the cell-cycle master regulator p53 to arrest cell-cycle progression until the DNA damage has been fixed. Typically, DNA ligases will repair SSBs, however DSBs can develop from prolonged SSB, as well as ionizing radiation (e.g. X-rays). At DSBs the ATM kinase automodifies and phosphorylates the CHK2 kinase, which signal through γH2A.X and p53. DSBs can be repaired through 3 potential pathways. During G1 phase of the cell cycle, nonhomologous end joining (NHEJ) involves the DNAPK complex and 53BP1 to join the broken DNA ends. NHEJ can be deleterious to the flanking nucleotides at the DSB, with the potential to induce insertion/deletion mutations. During S/G2 phase of the cell cycle, there is the opportunity to utilize the identical sister chromatid as a error-free repair template in a process called homologous recombination (HR). HR is signalled by BRCA1 and requires the MRN complex to produce a ssDNA region, which is bound by RAD51 proteins in a BRCA2-dependent manner. The RAD51 nucleofilament undergoes template strand invasion in a RAD54-dependent manner, forming a D-loop structure, which is then polymerized and cleaved to separate the chromatids. An alternative form of DSB repair can occur involving MRN and XRCC1, called Microhomology-mediated end joining (MMEJ). MMEJ utilizes short homologous sequences (5-50nts) to produce stand invasion similar to HR, however because of the limited requirement for homologous sequences, MMEJ can be highly mutagenic and lead to large chromosomal rearrangements. When SSBs and DSBs are properly ameliorated, p54 becomes inactivated and the cell-cycle progresses, however prolonged DSBs and SSBs will lead to p53-mediated p21 induction and cell-cycle arrest/apoptosis.

1.6.1 ATRX and DNA replication

A growing body of evidence seems to suggest that the DNA damage associated with ATRX-deficiency results, at least in part, from DNA replication stress. Specifically, ATRX deficient cells experience a prolonged S-phase when DNA replication occurs, and display a hypersensitivity to replication stress factors such as cisplatin, hydroxyurea (HU) and ultraviolet (UV) radiation [135] [97] [121] [90] [84]. Furthermore, replication kinetics have been directly investigated in Atrx-null mouse embryonic stem cells (mESC) and in ATRX-deficient HCT116 cells, where elevated DNA replication fork stalling events and attenuated stalled replication fork restart was observed [90] [84]. In a reverse order, the re-introduction of ATRX expression into U2OS cells, which lack ATRX protein expression, reduced the occurrence of replication fork stalling events [136]. Finally, it is within reason to speculate that the physical association between ATRX and the DDR protein complex known as MRN, may be important for the replication defects associated with ATRX deficiency [90] [84]. Therefore, it raises the question, can genomic instability arise from arduous DNA replication in ATRX deficient cells?

1.6.2 A primer on DNA replication

Prior to a cell entering S-phase, replication start sites, called origins of replication, are licensed by origin recognition complexes (ORCs), which in turn load the minichromosome maintenance (MCM) 2–7 helicase complexes [137]. The order of origin firing is regulated by the epigenetic profile of the origin locus, wherein forks observed during the latter part of S-phase are located primarily in heterochromatin [138] [139]. Additionally, a large number of replication origins remain dormant during replication, unless initiated by replication stress [140] [141]. From each origin of replication fired, a bidirectional replication fork progresses in

an outward direction as a bubble-like structure known as the replisome (**Figure 7A**).

1.6.3 The replisome

The MCM complex is composed of the MCM2-7 proteins and functions as a helicase and scaffold to unwind dsDNA at the replication fork. The Proliferating cell nuclear antigen (PCNA) homotrimeric DNA clamp maintains a stable connection between DNA polymerases δ and ε with the lagging and leading ssDNA strands, respectively. Unlike the complement of the leading strand, which is polymerised continuously, the complement of the lagging strand is synthesized sequentially from RNA primers, ~150 nucleotide (nt) long, called Okazaki fragments [142]. DNA polymerization precedes as the replication fork progresses until the entire DNA fiber of each chromosome has been copied.

As the replication fork progresses forward, the FACT complex and histone chaperone ASF1, which physically associate with the MCM complex, function to recycle the modified parental histone proteins onto nascent dsDNA from the parental chromosomes. This histone recycling ensures the maintenance of histone epigenetic profile, which is only partially diluted by the incorporation of naïve, unmodified histone proteins that are exclusively generated during S-phase [143]. Furthermore, due to the nature of the replication fork intermediate structure, ssDNA waiting to be replicated is coated with the Replication protein A (RPA) heterotrimeric complex to maintain ssDNA stability. While, ssDNA is more susceptible to breakage than dsDNA, it may also fold into 2^{o} DNA structures, which can perturb replisome function.

1.6.4 Replication stress from 2^{o} DNA structures

Evidence suggests that HU-induced DNA replication stress can interfere with histone recycling, thereby inducing epigenetic instability [144] [145]. Interestingly, this epigenetic instability has been strongly associated with the formation of G4 2^{o} DNA structures [146] [147] [148] [149] [145]. G4 structures can form at a $G_{\geq 3}N_xG_{\geq 3}N_xG_{\geq 3}N_xG_{\geq 3}$ motif sequence when four guanines are held together by Hoogsteen bonds and intercalate a monovalent cation such as potassium (K^+) [150]. Specialized DNA helicases such as FANCJ, BLM and WRN unwind G4 DNA structures [147]. ATRX binds to these structures *in vitro* and preferentially localizes to their motif sequences *in vivo*, but does not possess this helicase activity [24] [90].

The function of ATRX with respect to G4 DNA is not well understood but some evidence seems to suggest that ATRX deficiency correlates to reduced genomic H3.3 incorporation and RNA polymerase II (RNA Pol II) stalling at some putative G4 motif intragenic loci. However, H3.3 deposition in gene bodies is more often attributed to the HIRA chaperone and not to the ATRX-DAXX chaperone complex [89] [151]. G4 structured DNA is thought to form a barrier that may impede DNA replication and G4-stabalizing ligands have been shown to impair replication fork progression through G-rich telomeric DNA [152] [153] [154]. A current model suggests that replication forks stalled at G4 DNA collapse to become DNA double strand breaks (DSB) [119] [155]. Here we explore that range of replication intermediate structures associated with G4-mediated replication fork stalling, with special focus on ATRX associated pathways.

1.6.5 G-quadruplex structures stall replication forks

For illustrative purposes, we examined a hypothetical scenario where a G4 structure forms on the leading strand of a replication fork, inducing a replication fork-stalling event (**Figure 7B**). The idea that G4 structures can form on the leading strand of the replication fork and cause replication fork stalling has been explored in recent studies [156] [157] [152]. Initial recognition of a stalled replication fork involves DNA topoisomerase 2-binding protein 1 (TOPBP1) recruitment of a PCNA-like DNA clamp known as the RAD9-HUS1-RAD1 (9-1-1) complex, along with RPA binding to ssDNA and activation of the ATR signalling kinase [158] [159] [127](**Figure 7B**). These G4 structures are recognized as DNA lesions, which would be ameliorated by specialized translesion DNA polymerase such as POL η and POL κ [160]. Recent evidence suggests that G4 DNA may inhibit translesion polymerase activity, thereby requiring an alternative method of amelioration [161]. The MRN complex member, MRE11, possesses a 3'-5' exonuclease activity, which typically functions upstream of the HR DSBR pathway [162] [127]. Additionally, MRE11 appears to function at stalled replication forks to promote replication fork restart via a homology directed repair (HDR) mechanism akin to HR [163] [164] [165]. In doing so, MRE11's exonuclease activity degrades the nascent DNA at a stalled replication fork. Unsurprisingly, unrestricted MRE11 activity at stalled replication forks can occur from deficiencies in the PARP, BRCA or Fanconi anemia pathways, leading to replication fork collapse and DSB induction along with ATM-mediated, p53 activation and cell-cycle checkpoint arrest [163] [166] [167].

Just as with the topic of DNA damage repair, several well-cited reviews have also been published in recent years to explain the currently accepted models of DNA replication stress [128] [168] [137] [127]. For brevity in highlighting the DNA replication stress pathways potentially associated with ATRX, we have distilled the work in these reviews to encompass

factors which we believe to be directly relevant to ATRX (**Figure 7**). As before, we recommend the previously cited reviews for any further clarification.

1.7 Addressing unanswered questions

Whether this highly dynamic pathway may relate to ATRX-associated genomic instability remains unclear. Loss of endogenous histone H3.3 sensitizes immortalized DT40 chicken cells to UV-induced replication stress causing attenuated replication fork progression [169]. Furthermore, ATRX's association with G4 structures and its involvement as an H3.3 chaperone may implicate a role for the deposition of H3.3 into nucleosomes at loci prone to G4 folding [24] [89] [170]. Interestingly, ATRX deficient cells are hypersensitive to G4 stabilizing ligands, thereby suggesting a role in G4 processing [136] [89] [105]. An alternative explanation may implicate ATRX's MRN interaction, as a means to prevent replication fork collapse [136]. As we take a step back, we may ask if replication-induced genomic instability associated with ATRX deficiency actually occurs in a primary manner directly related to ATRX's activity or perhaps in a secondary manner associated with a downstream gene dysregulation. Furthermore, we may ask in what way this could relate to the neurological symptoms of ATR-X syndrome? And ultimately, where might we find exploitable pathways that could benefit treatment development?

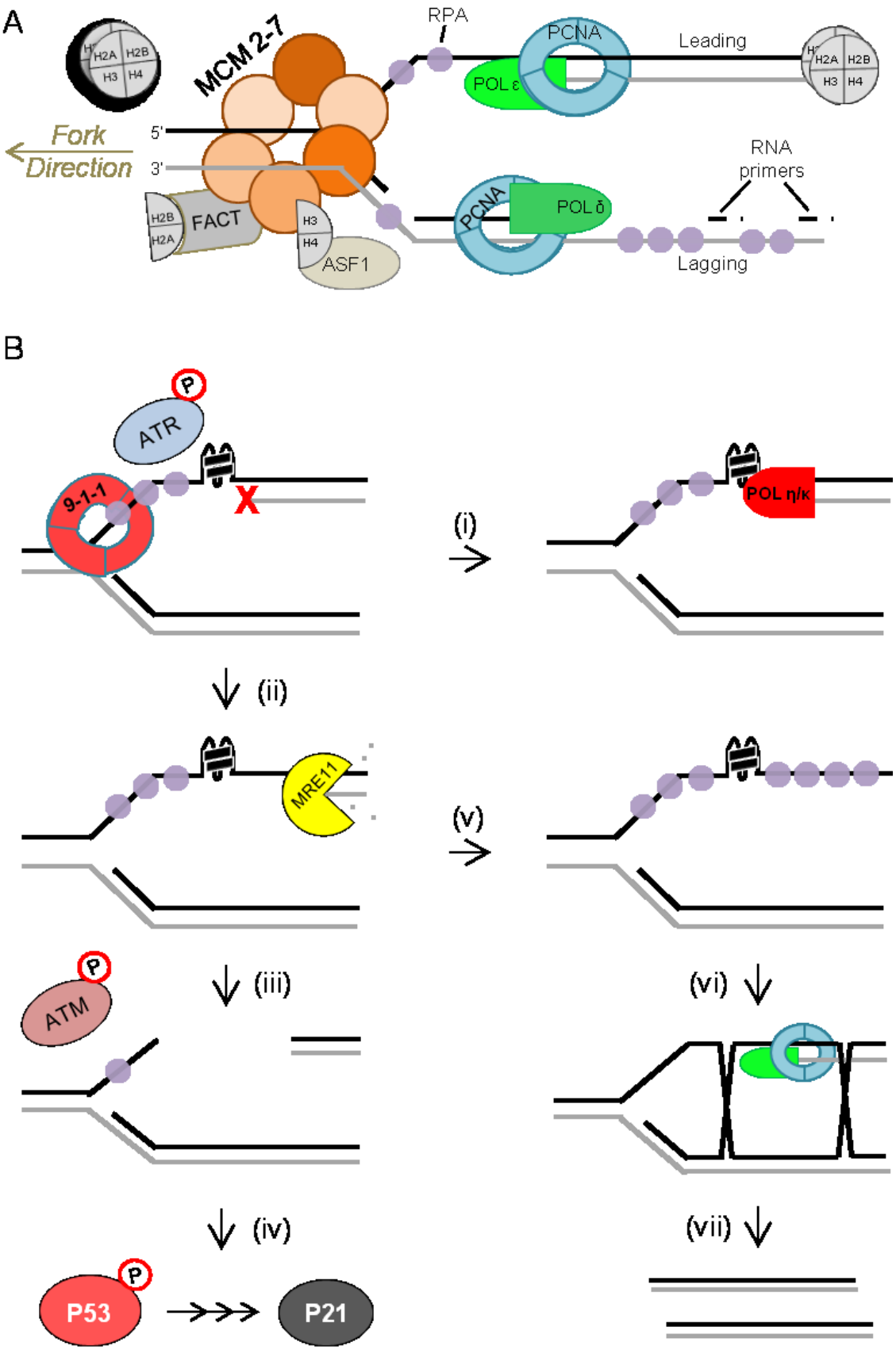
A
H3
H2A
H2B
H4
MCM 2-7
RPA
PCNA
Leading
POL ε
Fork
Direction
5'
3'
RNA
primers
PCNA
POL δ
H2B
H2A
FACT
H3
H4
ASF1
Lagging
B
P
ATR
9-1-1
X
(i)
POL η/κ
(ii)
MRE11
(v)
P
ATM
(iii)
(vi)
(iv)
(vii)
P
P53
P21

Figure 7. The replisome and G4-mediated replication fork stalling.
(**A**) A model of the replisome's structure at a DNA replication fork. The MCM complex sparates dsDNA into two ssDNA stands called the leading and lagging strands. The PCNA DNA clamp holds DNA polymerases onto the template strand. DNA synthesis occurs in a 5' to 3' direction by DNA Polymerase ε on the leading strand and DNA Polymerase δ on the lagging strand. While the leading strand is copied in a continuous manner, the lagging strand is copied in discontinuous sections known as Okazaki fragments, which start from RNA primers. The RPA complex coats ssDNA until it has been replicated, while the FACT complex and the ASF1 histone chaperone function to recycle modified parental histones at the replication fork, as newly synthesized histones are also incorporated.
(**B**) A model of G4 structured DNA inducing replication fork stalling (red X) on the leading strand of a replication fork. Early recognition of a stalled replication fork occurs when the PCNA-like DNA clamp known as the 9-1-1 complex binds. RPA loading onto exposed ssDNA and ATR activation begin the cascade of events leading to replication fork protection, repair and restart. (i) G4 DNA may be recognized as a DNA lesion, which can be replicated by specialized translesion polyermases known as POL η and POL κ. G4 structures may inhibit translesion synthesis requiring an alternative pathway. (ii) MRE11-dependent DNA resectioning exposes ssDNA for homology directed repair of the stalled fork. (iii) Overactive MRE11 activity can lead to a loss of replication fork protection and DSB formation, signalled by ATM activation. (iv) Prolonged DSBs from collapsed replication forks will lead to p53-mediated p21 induction and cell-cycle arrest. (v) When MRE11 is properly regulated, the expored ssDNA is bound by the RPA complex, which is replaced with RAD51 proteins in a BRCA2-dependent manner. (vi) Strand invasion is followed by template base polymerization leading to (vii) accurately replicated DNA.

1.8 Hypothesis and Specific Objectives

Investigating the causes of neurodevelopmental disorders greatly expands our understanding of brain development. Furthermore, investigating the genetic basis that underlines a disorder provides an essential perspective to understand the disease's etiology. Ultimately, we are seeking to build a foundation for treatment options tailored to specific genotypes. In this regard, by examining the chromatin-associated processes involving the ATRX protein, we are aiming to identify any relevant biological pathways that may ultimately be targeted by novel therapeutic strategies. To address this problem, we propose the following overarching hypothesis to direct our research.

We **hypothesize** that ATRX represses replication-induced genomic instability by re-enforcing heterochromatin replication dynamics. Specifically, ATRX prevents the formation of DNA lesions that arise during arduous DNA replication by localizing to replicating heterochromatin during S-phase and by the replication-independent deposition of histone H3.3 at repetitive DNA. Importantly, these functions facilitate the expansion of rapidly proliferating progenitor cells, such as neuronal precursor cells (NPCs) required for corticogenesis.

We propose the following 3 **objectives** to specifically address this hypothesis:

i. To determine if Atrx loss during cortical development produces a DNA damage response associated with microcephaly.

ii. To determine if ATRX prevents dsDNA breaks derived from S-phase progression.

iii. To determine if ATRX protects stalled replication forks from exonuclease-mediated degradation.

Our general approach will be to (**i.**) examine a cortex specific ablation of Atrx expression during corticogenesis. Here, the loss of Atrx protein expression in the mouse cortex will model the hypomorphic mutations that compromise brain development in patients with ATR-X syndrome. These embryonic cortices will be compared to wild-type (WT) controls by using immunofluorescent and western blot analysis. Next, we will model ATRX deficiency in rapidly proliferating human cell lines using an RNA interference (RNAi) strategy. These cells will be compared to ATRX-proficient control cells to assess (**ii.**) the development of DNA lesions associated with cell cycle progression and assess (**iii.**) the kinetics for replication fork procession and protection.

2. Materials and Methods

General Materials

General purpose chemicals: agarose, ethidium bromide, EDTA (ethylenediaminetetraacetic acid), glycerol, glycine, HEPES (4-(2-hydroxyethyl)-1-piperazineethanesulfonic acid), HCl, KCl, KH_2P0_4, NaCl, NaOH, Na_2HP0_4, Nonidet P-40 (octylphenoxypolyethoxyethanol), SDS (sodium dodecyl sulfate), TRIS (Tris(hydroxymethyl)aminomethane) and Tween 20 were obtained from either ThermoFisher Scientific (Ottawa, ON), Invitrogen (Burlington, ON), or Sigma-Aldrich (Oakville, ON). Solvents: anhydrous ethanol, denatured ethanol, anhydrous methanol, anhydrous isopropanol and HPLC-grade water were obtained from ThermoFisher Scientific (Ottawa, ON). Cell culture ware: sterile 10 cm and 6 cm polystyrene dishes and 6 and 12 well polystyrene plates; as well as sterile 50 mL and 15 mL conical centrifuge tubes and 1.5 mLmicrocentrifuge tubes were obtained from ThermoFisher Scientific (Ottawa, ON). Centrifugation was performed using either a table-top accuSpin Micro 17 ThermoFisher Scientific (Ottawa, ON), a Galaxy 20R Benchtop Microfuge Refrigerated Centrifuge (VWR, Ville Mont-Royal, QC) or a Heraeus Instruments Megafue 1.0, rotor #2740 (Hanau, Germany). Disposable pipettes and gloves were obtained from VWR (Mississauga, ON), and p1000, p200, p20, p10 and p2 micropipettes were obtained from Gilson (Guelph, ON).

Animal Husbandry

All mice were housed by the University of Ottawa's Animal Care and Veterinary Services. Mice were provided a diet of 18% Protein Rodent Diet pellets (Harlan Tekland Global Diets, Madison WI) and water *ad libitum*, while exposed to a regular bimodal light-dark cycle. Female mice were housed in pairs, while males were housed individually. Timed matings were arranged by the addition of female mice into a male's cage and removal from the cage the following morning. All animal experiments were approved by the University of Ottawa's

Animal Care ethics committee in accordance with the guidelines set out by the Canadian Council on Animal Care, licensed under the Ontario Animals for Research Act.

Generation of a telencephalon-specific Atrx conditional deletion mouse was performed as previously described [103]. Briefly, $Atrx^{flox/flox}$ females were bred with Forkhead box G1 (Foxg1) cre $^{+/-}$ males. Male offspring with $Atrx^{flox/y}$;$Foxg1^{-/-}$ and $Atrx^{KO/y}$;$Foxg1^{+/-}$ genotypes were generated, which provided the wildtype and Atrx conditional knockout embryos, respectively. All lines were maintained on a C57BL6 background to ensure genetic homogeneity.

Tissue Collection

Embryos from timed pregnant females at embryonic days 13.5 and 18.5 (E13.5 and E18.5) were surgically extracted. Briefly, dams were anaesthetized by carbon dioxide and sacrificed by cervical dislocation. The abdominal cavity was opened and the uterus was removed into a phosphate buffered saline solution (PBS; 137mM NaCl, 2.7 mM KCl, 10mM Na_2HPO4 and 1.8 mM KH_2PO4). Fetuses were dissected in ice-cold PBS using an inverted light microscope and the dorsal telencephalon was removed and snap-frozen on dry ice.

Embryo Genotyping

A piece of fetal tissue was collected from each embryo at the time of dissection. Genomic DNA (gDNA) was extracted in gDNA lysis buffer (100 mM Tris-HCl pH8, 5 mM EDTA, 200 mM NaCl and 1% SDS) containing 0.2 µg/µL proteinase K for 1 hour at 55^{o}C. The supernatant was isolated by centrifugation and DNA was precipitated in 1 volume of 100% isopropanol at room temperature for 10 minutes. Pelleted DNA was washed in 70% ethanol, which was then evaporated at 55^{o}C. Isolated gDNA was resuspended in HPLC-grade water. Polymerase chain reaction (PCR) was used to genotype fetal gDNA using primers specific

for sex-determining genes and transgenic identification (**Table 3**).

Table 3. Genotyping primers used for the determination of $Atrx^{flox/y}$;$Foxg1^{-/-}$ and $Atrx^{KO/y}$;$Foxg1^{+/-}$.

Target	Primer name	Sequence (5'-3')	Notes
Sry	Sry-F	ttgtctagagagcatggagggccatgtcaa	Only in males
	Sry-R	ccactcctctgtgacactttagccctccga	
Fabp1	Fabp1-F	tggacaggactggacctctgctttcctaga	Positive control band for female
	Fabp1-R	ctagagctttgccacatcacaggtcattcag	
Atrx	mAtrx-F	ggttttagatgaaaatgaagag	F and R1 give a band of ~1kb (wt) F and R2 give a band of ~1.5kb (floxed allele)
	mAtrx-R1	tgaacctggggacttctttg	
	mAtrx-R2	ccaccatgatattcggcaag	
Cre	Cre-F	atgcttctgtccgtttgccg	Only in $Foxg1Cre^{+/-}$
	Cre-R	gggcgtagacatctgggtag	

The PCR mixture contained 1X PCR buffer, 0.2 mM dNTPs, 1.5 mM $MgCl_2$, 0.1 mM primeran 0.3 ul of Taq polymerase (Invitrogen, Burlington ON) with 1.5 ul of gDNA (100-300ng/uL). Reactions were incubated at 95°C for 20 sec, 57°C for 30 sec, and 72°C for 90 sec for a total of 35 cycles. The PCR product was visualized after electrophoretic treatment on a 1.5% agarose gel with 0.5 ul /mL of ethidium bromide by ultraviolet (UV) illumination.

Cell Culture

HeLa, U2OS and MG63 cells were incubated at 37°C in 5% CO2 in Dulbecco's Modified Eagle Medium (DMEM) with 4.5 g/L glucose and L-glutamine (ThermoFisher Scientific Inc.) containing 10% Fetal Bovine Serum (FBS, ThermoFisher Scientific Inc.). Subconfluent cells

were dissociated from culture dishes in 0.125% trypsin (ThermoFisher Scientific Inc.) and split to avoid overgrowth.

Transient siRNA Transfection and Chemical Inhibition

Transient knockdown (KD) of ATRX, DAXX, PARP1 and BRCA1 was performed in HeLa cells with either siATRX RNA Smart Pool (ThermoFisher Scientific Inc.), siDAXX RNA (Sigma-Alderich), siPARP1 RNA (Sigma-Alderich), or a Scrambled RNA control (G.E. Healthcare, Amersham), while the siBRCA1 was a kind gift from Dr. Christine Pratt (University of Ottawa) (**Table 4**). HeLa cells that were 50% confluent were incubated with 0.72% (v/v) INTERFERin (Polyplus) in Opti-MEM® I Reduced Serum Medium (ThermoFisher Scientific Inc.) containing 100mM siRNA for 6 hours, as per the manufacturer's instructions. PARP was inhibited with 5.0 μM PARP Inhibitor VIII (PJ34; Santa Cruz Biotechnology Inc., Dallas, Texas, U.S.A, sc-204161A) in normal cell culture media.

Table 4. siRNA used to in vitro KD experiments.

mRNA	siRNA	Sequence / Product code
ATRX	siATRX Smartpool	M-006524-01-0005
DAXX	siDAXX	CCUGAUACCUUCCCUGACU
PARP1	siPARP1	GAUAGAGCGUGAAGGCGAA
BRCA1	siBRCA1	A gift from Dr. Christine Pratt
Control	siScramble non-targeting pool	D-001210-01-20

Protein Extraction

Cortical lysates were extracted by homogenization using a Tissue Tearor™ (Biospec Products, Inc.) in RIPA buffer (IX PBS, 1% NP-40, 0.1% SDS, 0.5% sodium deoxycholate, protease inhibitor Complete Mini EDTA-free in ddH_2O) and cell culture lysates were extracted in RIPA buffer (50 mM Tris-HCl pH 8.0, 150 mM NaCl, 1.0% Nonidet P-40, 0.5% sodium deoxycholate, 0.1% SDS (sodium dodecyl sulfate) and 1:500 protease inhibitor cocktail (Sigma-Alderich)) at 4^{o}C for 2 hours by gentle agitation. Supernatants were isolated by centrifugation at $2x10^4$ x g at 4^{o}C and relative protein concentrations were spectroscopically quantified using the Bio-Rad Protein Assay reagent (Bio-Rad, Mississauga, ON), as per the manufacturer's instructions with an Eppendorf BioPhotometer.

Protein Expression

Western blot analysis was used to detect relative protein expression levels. Briefly, proteins in NuPage® SDS Loading buffer (Invitrogen, Burlington, ON) were separated by molecular weight by sodium-dodecylsulfide polyacrylamide gel electrophoresis (SDS-PAGE) on either a 3-8% pre-cast Tris-Acetate gel or a 4-12% pre-cast Bis-Tris gel (Life Technologies) and transferred to a PVDF Immobilon-P Transfer Membrane (Millipore, Billerica, MA) in transfer buffer (50mM Tris base, 40mM Glycine, 20% MeOH). Membranes were incubated in blocking buffer (5% powered milk in TBST (20 mM Tris-HCl pH 7.5, 150 mM NaCl and 0.1% Tween 20)), before incubation at 4^{o}C, overnight, with gentle agitation in primary antibody (**Table 5**) diluted in blocking buffer. Membranes were washed in TBST and incubated in secondary antibody conjugated to horse-radish peroxidise (HRP) diluted in blocking buffer (**Table 5**) and washed again in TBST. Proteins were detected by enzymatic chemiluminescence using either the SuperSignal™ West Femto Maximum Sensitivity Substrate (ThermoFisher Scientific Inc.) or the Clarity™ Western ECL Blotting Substrate (Bio-rad) and developed in the Konica-Minolta SRX-101A Tabletop film processor.

Image Densitometry

Autoradiographic film was developed after chemiluminescent and digitally imaged using a table top scanner. ImageJ software (National Institutes of Health, Bethesda, Maryland, USA, version 1.46r) was used to densitometrically quantify protein expression levels. Briefly, bands corresponding to specific proteins were binned within equal areas and the total signal intensity was plotted. The background signal was subtracted by integrating the signal intensity above the baseline reading.

Table 5. Antibodies used in studies for western blot analysis.

Antibody target	Species	Company/product no.	Notes & concentration
ATRX (F39)	mouse	Gift from D. Higgs	Unpurified ascites, 1:6
β-actin	mouse	Sigma/A1978	1:50000
γ-H2A.X (20E3)	rabbit	Cell Signaling/9718S	1:2000
pATM (Ser1981ph)	mouse	Millipore; MAB3806	1:1000
BRCA1	mouse	Santa Cruz; sc-6954	1:2000
DAXX	mouse	Santa Cruz; sc8043	1:2000
53BP1	rabbit	Novus/NB100-304	1:2000
PAR	rabbit	BD Pharmingen/ 551813	1:2000
PARP1	mouse	BD Pharmingen/556362	1:2000
MRE11	mouse	Abcam/ab214	1:2000
RAD50	rabbit	Abcam/ ab124682	1:2000

Protein-Protein Interactions

Co-immunoprecipitation was used to identify specific ATRX-protein interactions in HeLa cells. Briefly, ~$9x10^6$ cells were collected by trypsinization and washed in PBS. Nuclei were isolated in hypotonic lysis buffer (10 mM HEPES pH 7.4, 1.5 mM $MgCl_2$, 10 mM KCl, 0.5 mM dithiothreitol (DTT, Sigma-Aldrich) and 1:500 protease inhibitor cocktail (Sigma-Aldrich, P8340)) containing 0.01% (v/v) Nonidet P40 after a 4^oC incubation for 10 minutes by centrifugation at 550 x g at 4^oC for 15 minutes. Nuclei were ruptured in nuclear lysis buffer

(20 mM HEPES pH 7.4, 1% Nonidet P40, 150 mM NaCl, 2 mM EDTA and 1:500 protease inhibitor cocktail) with a Vibra Cell sonicator (Sonics & Materials Inc) used at 30% amplitude for two 10 second pulses. Supernatant containing soluble protein complexes was clarified by centrifugation at 13,000 x g at 4^{o}C for 20 minutes. ATRX-protein complexes in nuclear lysate from ~10^{7} cells were captured with 1 µg of Sheep anti ATRX (Fxnp5) custom manufactured polyclonal antibody overnight at 4^{o}C with gentle rotation. Antibody-bound complexes were collected on Gamma bind G Sepharose beads (GE Biosciences) and proteins were eluted in 2X NuPAGE® Lithium dodecyl sulfate sample buffer (Invitrogen) 90°C for 10 mins. Proteins were identified by western blot analysis, as described.

Immunofluorescence (Tissue Sections)

Embryonic cortical sections were collected from heads and placed in 4% paraformaldehyde (PFA) 0.1M phosphate buffered saline (PBS) (0.14 M NaCl, 2.5 mM KC1, 0.2 M Na2HP04 and 0.2 M KH2HPO4 at pH 7.4) for fixation overnight at 4°C. The heads were washed in PBS, cryoprotected in a 30% sucrose/PBS solution overnight at 4°C, embedded in a 1:1 solution of 30% sucrose and O.C.T. Compound (Tissue-Tek®, Japan) and flash frozen on liquid nitrogen. Tissue was then sectioned in 12 µm increments at below -20°C, in a Leica 1850 cryostat and mounted onto Superfrost Plus coated slides (ThermoFisher Scientific, USA). Tissues were air dried for 3 hours at room temperature, dehydrated in 70% ethanol for 5 minutes at 4^{o}C and permeablized with TBS-T (0.1 M Tris-HCl pH 8.8 and 0.1% Tween-20). Tissues were washed in PBS and blocked in 20% goat serum and 0.3% Triton-X in PBS for 1 hour at room temperature. The slides were incubated overnight at 4°C with relevant primary antibodies diluted in blocking buffer, washed in PBS, incubated with secondary antibody diluted in PBS for 1 hour at room temperature (**Table 6**). Slides were washed in PBS and then incubated with10 ug/mL DAPI. Slides were washed with PBS and

mounted with fluorescent mounting medium (DakoCytomation, Carpinteria, CA).

Table 6. Antibodies used in studies for immunofluorescent staining of cells and tissue sections.

Antibody target	Species	Company/product no.	Notes, concentration
ATRX (H-300)	rabbit	Santa Cruz/sc-15408	1:500
HP1α	Mouse	Upstate; 05-689	1:500
HP1β	Mouse	Active Motif; 39980	1:500
HP1γ	mouse	Active Motif; 39982	1:500
53BP1	Rabbit	Abcam; ab36823	1:500
CyclinA (H-432)	Rabbit	Santa cruz; sc-596	1:1000
pATM (Ser1981ph)	Mouse	Millipore; MAB3806	1:500
BrdU	mouse	BD Pharmingen/347580	1:500
Nurr1	rabbit	Santa Cruz/sc-990	1:200
Tbr1	rabbit	Abcam/ab31940	1:200
Ctip2	rat	Abcam/18465	1:200
Satb2	mouse	Abcam/ab51502	1:200
Brn2	rabbit	Santa Cruz/sc-28594	1:200
Cux1	rabbit	Santa Cruz/sc-13024	1:200
Mouse IgG	Donkey	ThermoFisher Scientific Inc.	Alexa Fluor® 488, 1:4000
Rabbit IgG	Donkey	ThermoFisher Scientific Inc.	Alexa Fluor® 594, 1:4000

Immunofluorescence (Cultured Cells)

Cells were either gown directly on glass overslips (ThermoFisher Scientific Inc) or were spotted onto Superfrost Plus coated slides with a Cytospin™ 4 Cytocentrifuge (ThermoFisher Scientific Inc) at 500 x g for 5 minutes. Slides were first fixed with 2% paraformaldehyde (PFA, Sigma-Aldrich) for 10 minutes at room temperature and then rehydrated in PBS for 5 minutes. Cells we made permeable with 0.3% Triton-X in PBS, washed in PBS and blocked in blocking buffer (20% goat serum, 0.5% fetal bovine serum).

The slides were incubated overnight at 4°C with primary antibody (**Table 6**) diluted in blocking buffer, washed in PBS, incubated with secondary antibody (**Table 6**) diluted in PBS for 30 minutes are room temperatutre, washed in PBS and then incubated with 10 ug/mL DAPI. Slides were washed and mounted with fluorescent mounting medium (DakoCytomation, Carpinteria, CA). To identify DNA lesions in cells, TUNEL (terminal uridine deoxynucleotidyl transferase dUTP nick end labeling) was performed using the In Situ Cell Death Detection Kit (Roche Applied Science, Laval, QC) according to the manufacturer's instructions. After TUNEL labeling the cells were DAPI stained for 2min in 10 ug/ml DAPI solution and washed in PBS for 10 minutes before being mounted with a drop of fluorescent mounting medium (DakoCytomation, Carpinteria, CA). A positive control slide was created by digesting the DNA with DNAsel incubated in a DNAsel solution (50mM Tris-HCl pH7.5, lmg/ml BSA, DNAsel 15U/ml; Sigma, Oakville, ON) at room temperature for 10min.

DNA Fiber Assay

Nascent DNA was labeled with a 20 or 30 minute 50 μM BrdU pulse in unsynchronized HeLa cells, while replication forks were stalled with 4.0 mM hydroxyurea for 5 hours. DNA fibers were spread as previously described [171]. Briefly, 10^5 cells / 2 μL were spotted onto Superfrost Plus coated slides (ThermoFisher Scientific, USA) and lysed with 10 μl of fiber lysis solution (50 mM EDTA, 0.5% SDS and 200 mM Tris-HCl) for 5 minutes at RT. Slides were tilted 15° from horizontal to spread DNA across the length of the slide, then air dried and fixed in methanol/acetic acid (3:1). Slides were rinsed in ddH_2O and then immersed in 2.5 N HCl for 80 minutes, washed in PBS and blocked in 5% BSA. Primary staining with a BrdU specific antibody was carried out at room temperature for 2 hours, followed by three PBS washes and staining with the appropriate secondary antibody for 1 hour at room temperature (**Table 6**). Between 250 and 700 nascent DNA fibers were measured from 3

independent experiments per treatment condition. Fluorescently labeled DNA fibers were imaged (Zeiss Axio Imager M1 microscope) and measured using ImageJ software (National Institutes of Health, Bethesda, Maryland, USA).

Microscopy Image Acquisition

Images were taken with an Axio Imager M1 (Zeiss) microscope with an axioCam HRm camera, through 40X, 63X and 100X oil objectives with numerical apertures of 1.3, 1.4 and 1.46, respectively.

Cell Viability Quantification

HeLa cells treated with either siATRX or siScramble control RNA, as well as ATRX-null U2OS osteosarcoma cells and ATRX-expressing MG63 osteosarcoma cells were counted in a ViCell Counter (Beckman Coulter, Montréal, QC). Briefly, cells were plated at 12.5% confluency in a 12 well dish and allowed to settle during an overnight incubation. Cells were incubated in 750 µL of culture media and 5.0 µM PJ34 was added to half the samples and allowed to incubate for 48 hours. Each well was treated as an independent replicate. For each well, the individual media was collected, the cells were washed with 250 µL of PBS and pooled with the collected media. Cells were dislodged with 250 µL of trypsin and pooled with media-PBS. A second PBS wash was also pooled to collect any remaining cells. Supernatant containing all cells and debris was loaded into a ViCell counter. Trypan blue was used to distinguish non-viable cells with membrane damage from live cells based on the manufactures parameters. At least 3 replicates were read per experimental condition.

Statistical Analysis

Specific data was deemed to be statistically significant given a p-value of less than 0.05.

Data analyses were carried out using R (version 3.2.4) statistical software. The ‘t.test’ function was used to perform 2-tailed, Student’s t-tests to compare the means of 2 sets of data. The ‘var.test’ function was used to perform an F-test to assess for equality of 2 variances specified in the Student’s t-tests. The ‘z.test’ function from the ‘PASWR’ package was used to perform 2-tailed, Z-tests to compare 2 population proportions. The ‘std.error’ function from the ‘plotrix’ package was used to calculate the standard error of mean used to approximate ‘sigma.x’ and ‘sigma.y’ values specified in the ‘z-test’. The ‘wilcox.exact’ function from the ‘exactRankTests’ package was used to perform 2 sided, Mann-Whitney U-tests to compare the means of 2 sample populations with possibly tied observations.

3. Results

3.1.1 *In silico* analysis of the ATRX protein interactome

We analyzed the ontological features of the ATRX protein interactome with regards to “Cell component”, “Molecular function” and “Biological process” (**Table 7**). As expected, terms grouped under “Cell component” were described as nuclear and chromosomal. Additionally, we found that terms grouped under “Molecular function” were described as DNA/chromatin binding, including a small set of “damaged DNA binding” proteins. Finally, terms grouped under “Biological process” were described as chromosome and DNA regulating, as well as DNA repair and processing. All together, these data suggest a definitive role for ATRX at the junction of a protein interaction network linking chromatin maintenance and genomic stability.

Table 7. Gene ontology of ATRX protein interactome.
The genes encoding ATRX-interacting proteins were analyzed using the Clusters of Orthologous Groups software, which was accessed through the STRING Database (v10.0). The number of observed genes per category are indicated (31 total; histone genes were counted once each), while the False discovery rate (F.D.R) is reported as an estimate of the proportion of the expected number of false discoveries NFD among all discoveries.

	G.O. I.D.	Pathway description	Observed	F.D.R.
Biological Process	GO.0051276	chromosome organization	21	2.76×10^{-16}
	GO.0071103	DNA conformation change	12	7.17×10^{-12}
	GO.0006259	DNA metabolic process	16	1.64×10^{-11}
	GO.0006281	DNA repair	14	1.64×10^{-11}
	GO.0006974	response to DNA damage stimulus	16	1.64×10^{-11}
	GO.0000723	telomere maintenance	8	1.45×10^{-9}
Molecular Function	GO.0003682	chromatin binding	16	7.31×10^{-14}
	GO.0043566	structure-specific DNA binding	13	7.31×10^{-14}
	GO.0003677	DNA binding	22	9.51×10^{-10}
	GO.0003690	double-stranded DNA binding	7	4.34×10^{-7}
	GO.0003684	damaged DNA binding	6	5.08×10^{-7}
	GO.0031490	chromatin DNA binding	6	5.08×10^{-7}
Cell Component	GO.0000228	nuclear chromosome	22	9.54×10^{-26}
	GO.0044454	nuclear chromosome part	19	1.23×10^{-21}
	GO.0005694	chromosome	22	9.15×10^{-21}
	GO.0044427	chromosomal part	19	4.82×10^{-17}
	GO.0005654	nucleoplasm	27	3.74×10^{-14}

3.1.2 Neurological features of the ATRX interactome

We interrogated the ATRX interactome using the Online Mendelian Inheritance in Man (OMIM) database to determine if any genes encoding the ATRX interacting proteins were also causative for genetic diseases with neurological features. We found that mutations in *PRKDC* (causing Immunodeficiency 26), *MRE11A* (causing Ataxia Telangiectasia-like disorder), *NBN* (causing Nijmegen Breakage Syndrome), *RAD50* (causing NBS-like disorder), *EZH2* (causing Weaver's syndrome), *MeCP2* (causing Rett syndrome), *SMC1A* and *SMC3* (both causing Cornelia de Lange syndrome), all shared at least one neurological feature with ATR-X syndrome (**Table 8**). We assembled this ATRX interactome subgroup and found that ATRX links these proteins at the biochemical level by connecting the DSBR and heterochromatin maintenance pathways (**Figure 8**). Interestingly, the biomolecular pathways where these proteins overlap may be an invaluable topic to expose the etiologies of their associated conditions.

Table 8. ATRX interacting proteins are also encoded by genes mutated in neurological disorders.

Genes encoding ATRX interacting proteins which appear in the Online Mendelian Inheritance in Man (OMIM) database for genetic diseases were presented. All diseases were associated with ≥1 neurological feature(s) that were observed in ATR-X syndrome.

Mutated gene	Genetic Disorder (OMIM#)	Neurological feature(s)	Refs
ATRX	ATR-X syndrome (301040)	ID, microcephaly, seizures	[2] [172]
PRKDC	Immunodeficiency 26 (615966)	ID, microcephaly, seizures	[173]
MRE11A	Ataxia Telangiectasia-like disorder (604391)	ID, microcephaly	[174]
NBN	Nijmegen Breakage Syndrome (251260)	ID, microcephaly	[175] [176]
RAD50	NBS-like disorder (613078)	ID, microcephaly	[177] [178]
EZH2	Weaver's syndrome (277590)	ID	[179]
MeCP2	Rett syndrome (312750)	ID, microcephaly, seizures	[180]
SMC1A	Cornelia de Lange syndrome 2 (300590)	ID, microcephaly, seizures	[181]
SMC3	Cornelia de Lange syndrome 3 (610759)	ID	[182]

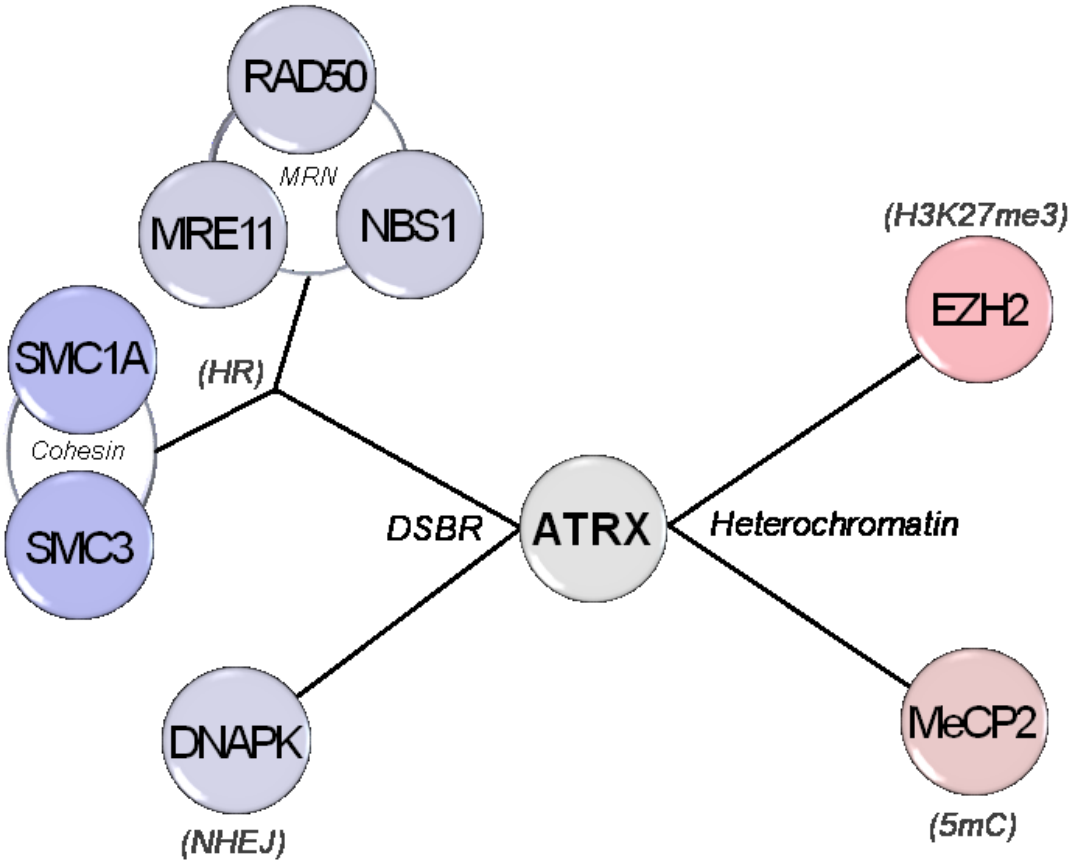

Figure 8. ATRX and interactome for brain development and genomic stability. A subgroup of the ATRX protein interaction network, only containing proteins encoded by causal genes in diseases with neurological phenotypes. On the dsDNA break response (DSBR) side, the MRE11-RAD50-NBS1 (MRN complex) proteins and the SMC1A and SMC3 (Cohesin complex) proteins are involved in homologous recombination (HR), while DNAPK is involved in nonhomologous end joining (NHEJ). On the heterochromatin side EZH2 is the catalytic subunit of the PRC2 complex with writes the histone 3, lysine 27, trimethylation mark (H3K27me3) important for heterochromatin signaling, while MeCP2, which binds 5-methylated cytosine (5mC) in DNA, is important for heterochromatin organization.

3.2 *In vivo* analysis of Atrx

i. Atrx loss in during cortical development produces a DNA damage response associated with microcephaly

Conditional loss of full length Atrx expression during telencephalon maturation was examined using male, $Atrx^{flox/y}$;Foxg1Cre knock in (KI) heterozygous-positive embryos (referred to as Atrx cKO; [183]. Previous examination of this genetic model had identified that a reduction in cortical size was the result of a decrease in neuronal progenitor cell (NPC) expansion and reduced migration towards the superficial cerebral cortical layers [103]. In this section, we have examined the circumstances surrounding these missing late-born pyramidal neurons of the upper cortical layers. Specifically, we explored the idea that late-born neurons are in fact depleted at the NPC-stage due to genomic instability. This logic echoed a similar paradigm used to explain Atrx's importance in myogenic precursor cells (MPCs). Conditional Atrx loss in MPCs, specifically hampered expansion of myoblast cells, which exhibited a delayed progression through late S-phase of the cell cycle that was directly associated with genomic instability [97].

To begin our analysis, we first examined the cerebral cortices of perinatal mice at embryonic day 18.5 (E18.5) (**Figure 9A**). At this point radial glial NPCs have completed terminal differentiation and have finished integrating into the superficial cortical layers [184] [185]. Quantification of DAPI labeled nuclei indicated that Atrx cKO cortices were significantly smaller that their wild-type (WT) littermates (p-value=0.013, Student's t-test: 2-tailed, unequal variance) (**Figure 9B**). Indeed, Atrx cKO cortices were calculated to contain ~20% fewer cells than that of the WT embryos consistent with previous findings [103]. Given this observation, we next examined whether or not the proportions of specific neuronal

populations were altered, relative to the total number of nuclei spanning the apical to basal surface of the cortex.

Neuronal heterogeneity is exemplified in the stratification of the cerebral cortex [109]. Importantly, corticogenesis follows a tightly regulated sequence of proliferation, migration and terminal differentiation events, to populate specific neuronal strata with distinct neuronal cell types. A “bottom-up” developmental process produces the cortical layers VI through to II in successive fashion [110] [111] [112] [113] [114]. Accordingly, this implies that the uppermost neurons (i.e. comprising layers II and III) of the cerebral cortex differentiate from NPCs that underwent the greatest number of cell cycles within the VZ/SVZ [116] [117]. We sought to determine if the cortices of Atrx cKO mice exhibited a neuronal depletion that was biased towards a particular lineage or identity, specifically focusing on the distinction between early-born, lower-layer (V-VI) and later-born, upper-layer (II-IV) neuronal populations.

We compared the proportion of neurons within the deep and upper cortical layers, at E18.5 between *Atrx* cKO and WT embryos. Positively stained cells, which were labeled for specific layer markers were imaged by immunofluorescent microscopy. Labeled neurons corresponding to specific layer markers were binned and quantified relative to the total number of DAPI cells equivalently framed across the entire cortical plate. Examination of the deeper cortical layer markers indicated a significant increase in the proportion of neurons compared to cells across the cortex (**Figure 10A**). Quantification of Nurr1+ neurons indicated that Atrx cKO cortices contained ~27% more SP neurons than WT (p-value=0.016, Z-test: 2-tailed, 2-proportions). We did not observe a statistically significant difference between Tbr1+ neurons labelling the SP and layer VI (p-value=0.14, Z-test: 2-tailed, 2-proportions) or Ctip2+ neurons labeling layer V (p-value=0.89, Z-test: 2-tailed, 2-

proportions) in Atrx cKO cortices compared to WT. In contrast, the examination of the upper cortical layer markers indicated a significant decrease in the proportion of neurons compared to cells across the cortex (**Figure 10B**). Quantification of Cux1+ neurons that reside in layers II and III indicated that Atrx cKO cortices contained ~52% fewer cells than WT (p-value=0.0012, Z-test: 2-tailed, 2-proportions). Brn2+ neurons also labelling the layers II and III were decreased by ~33% (p-value=0.16, Z-test: 2-tailed, 2-proportions) and Satb2+ neurons labeling layer II to IV neurons were decreased by ~8% (p-value=0.67, Z-test: 2-tailed, 2-proportions) in Atrx cKO cortices compared to WT, although these comparisons were not statistically significant.

Microcephaly is a common clinical feature of ATR-X syndrome, which is also reflected in Atrx cKO mice (**Figure 9**). Some genetic bases of developmental microcephalies are known to include genes encoding genomic instability repressors and chromatin modifiers [118] [186] [187]. Interestingly, Atrx loss during skeletal muscle development has been associated with increased genomic instability, identified by elevated phosphorylation of the ATM kinase on serine 1981 (pATM) and phosphorylation of the histone H2A variant H2A.X on serine 139 (γH2A.X); [97]. Some previous evidence had also suggested that Atrx cKO mice may experience elevated levels of genomic instability during corticogenesis, as evidenced by increased γH2A.X signalling, as well as increased poly (ADP-ribose) (PAR) signalling [188] [188] [188]. Notably, PAR signaling was observed to be highly elevated in Atrx cKO mice compared to WT by western blot analysis of cortical extracts at E12.5. Furthermore, the PAR signal gradually decreased bellow detection limits by E17.5, yet always remained higher in the Atrx cKO mice.

Next we explored the idea that NPCs succumb to genomic instability that preferentially depletes the genesis of later-born neurons. To accomplish this we analyzed protein

expression levels during a stage of early corticogenesis by harvesting the dorsal telencephalon (DT) from WT and (n=3) and Atrx cKO (n=4) embryos at E13.5 for western blot analysis (**Figure 11A**). Within the DT of Atrx cKO embryos, Atrx protein was detected at ~2% compared to WT (p-value=0.0025, Student's t-test: 2-tailed, unequal variance). Strikingly, pATM signalling in the DT of Atrx cKO embryos was elevated to a level ~251% relative to WT (p-value=0.026, Student's t-test: 2-tailed, unequal variance) and γH2A.X was elevated to ~197% (p-value=0.0097, Student's t-test: 2-tailed, unequal variance). Most notably, PAR levels were ~326% relative to WT (p-value=0.012, Student's t-test: 2-tailed, unequal variance), while there were no significant differences between Parp1 or Mre11 expression levels (**Figure 11B**).

PAR signaling is a product of poly (ADP-ribose) polymerases (PARPs). The PARP family consists of at least 17 members with either demonstrated or putative PARP activity and are demarcated by a conserved ADP-ribosyl transferase (ART) domain adjoined to one or more interaction domains [189]. PARP1 belongs to a minority subset of PARPs with the ability to produce PAR in a DNA damage-dependent manner [190] [191]. PARP1 automodification occurs upon sensing DNA damage, followed by the modification of several other protein targets, thereby inducing an increase of ~558 Daltons (Da) per polymerized residue [192]. Interestingly, upon western blot analysis of the DT from Atrx cKO and WT embryos, we observed a reproducible shift in Parp1 migration, suggesting a post-translational modification resulting in a higher molecular weight of Parp1 (**Figure 11C**).

Conclusion

In this section we examined Atrx cKO mice to determine if Atrx loss during cortical development produces a DNA damage response associated with microcephaly. We observed that Atrx cKO perinates possess significantly smaller cortices at E18.5, due to the loss of later-born, upper-layer neurons (**Figures 9 and 10**). Evidently, Atrx loss during cortical development in mice is positively correlated with microcephaly. Additionally, we observed that Atrx cKO embryos exhibit distinct characteristics of genomic instability in the developing cortex at E13.5. Specifically, normal Atrx expression during cortex development is negatively correlated with pATM, γH2A.X and PAR signalling and positively correlated with an increased molecular weight of Parp1 in the DT of E13.5 Atrx cKO embryos (**Figure 11**). Together, this data suggests that Atrx prevents DNA damage during cortical development and facilitates NPC expansion, driving the genesis of upper-layer, later born cortical neurons.

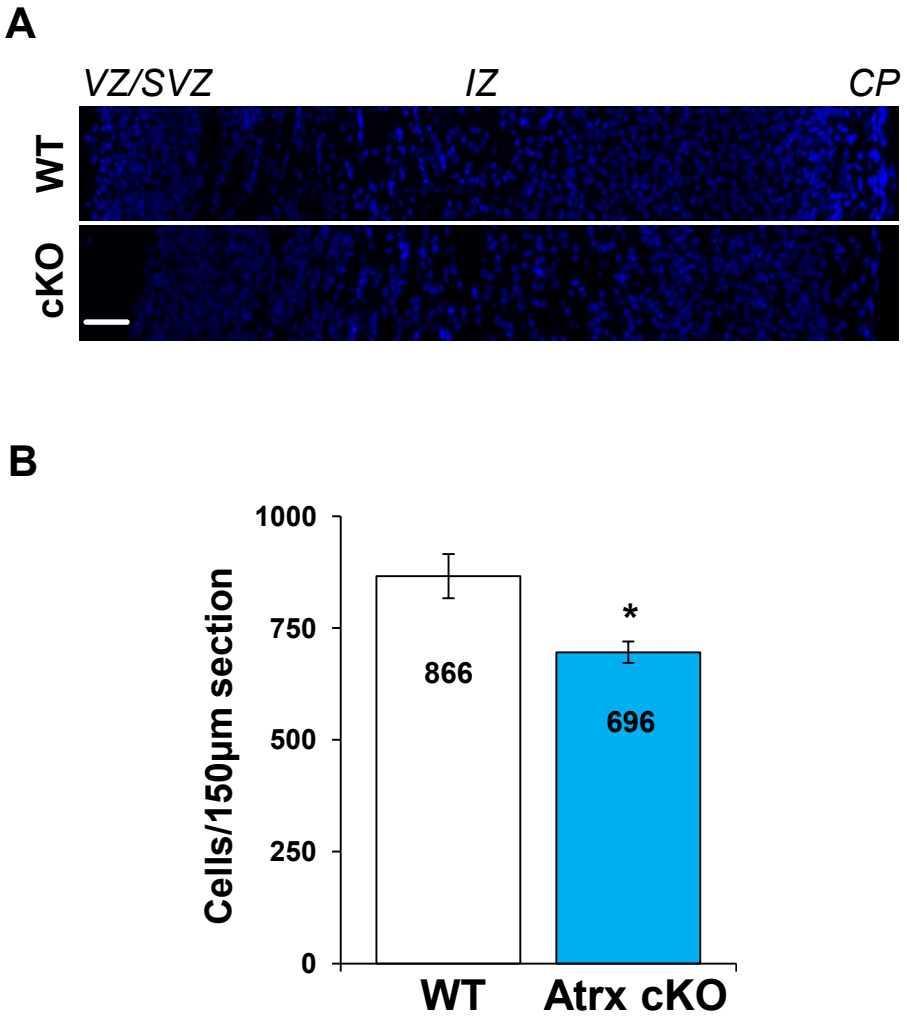

Figure 9. Telencephalon-specific loss of Atrx results in diminished cortical neuronal density in perinatal mice. (A) Average cell density counts across cortical sections were compared between WT (n=6) and Atrx cKO (n=6) mouse embryos at E18.5. Images of sections spanning from the ventricular zone and subventricular zone (VZ/SVZ; apical direction) through the intermediate zone (IZ) to the cortical plate (CP; basal direction) were stained with DAPI to visualize the total number of nuclei. (B) Quantification of the average number of DAPI staining across 150µm wide segments of cortical sections. Scale bar, 50 µm. Values represent proportional mean ± S.E.M. *p-value<0.05 calculated by unpaired Student's t-test with unequal variance. 200x magnification.

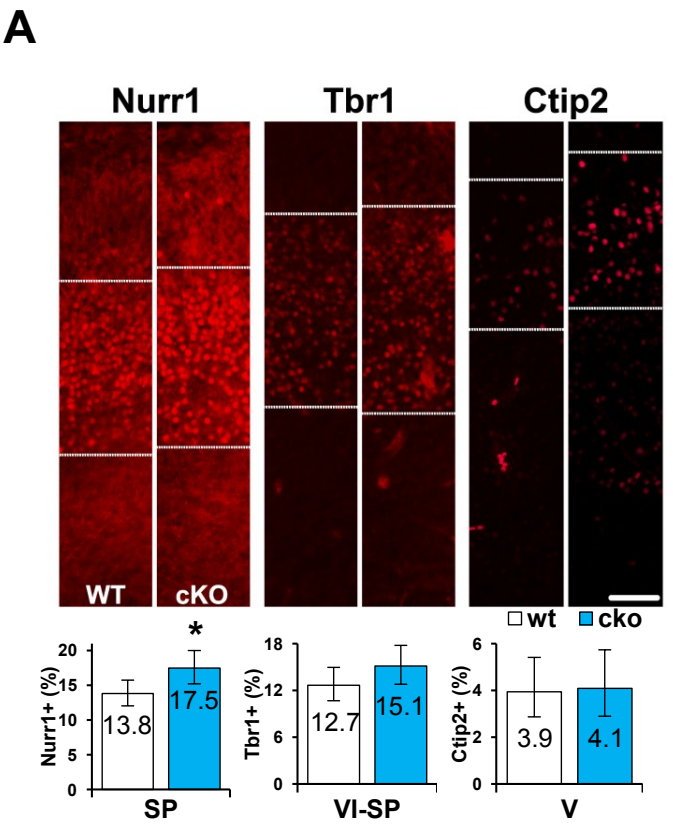
A
Nurr1
Tbr1
Ctip2
WT
cKO
wt
cko
Nurr1+ (%)
13.8
17.5
*
SP
Tbr1+ (%)
12.7
15.1
VI-SP
Ctip2+ (%)
3.9
4.1
V

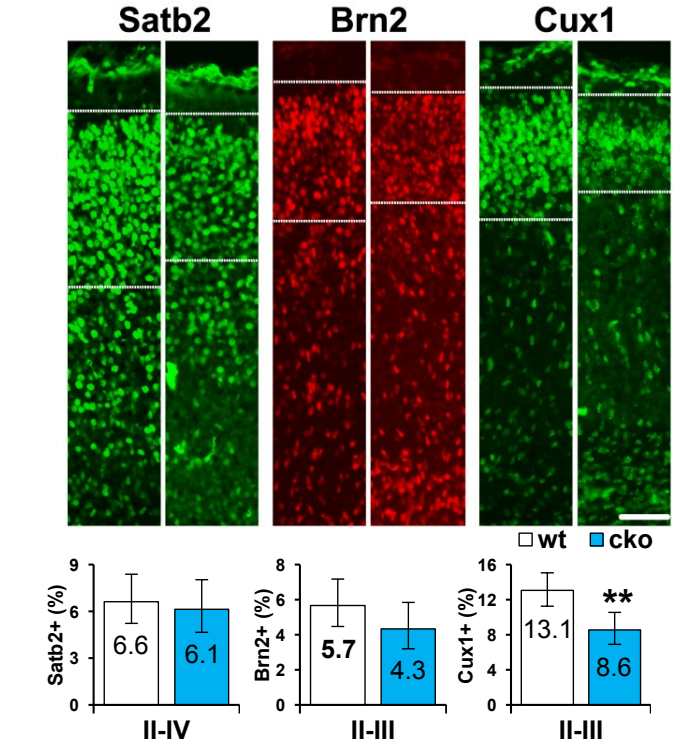
B
Satb2
Brn2
Cux1
wt
cko
Satb2+ (%)
6.6
6.1
II-IV
Brn2+ (%)
5.7
4.3
II-III
Cux1+ (%)
13.1
8.6
**
II-III

Figure 10. Upper- layer neurogenesis is specifically diminished in the cortex upon conditional loss of Atrx in the telencephalon.
Representative immunofluorescent images with quantification of the average number of positively stained neurons located in the deep (A) or upper (B) neocortical layers from E18.5 Atrx cKO and WT embryos. Positively stained cells were counted from within 150μm wide coronal brain sections. Sections were probed with antibodies that specifically labeled the subplate (SP; Nurr1), layer VI-SP (Tbr1), and layer V (Ctip2), layers II–IV (Satb2), and layers II/III (Brn2 and Cux1). Labeled neurons within bounded areas were quantified as a percent of the total nuclei within the 150μm wide neocortical section. Values represent percent total ± 95% confidence interval. *p-value<0.05 and **p-value<0.01 caluclated by z-score; 200x magnification. Scale bar, 100 μm.

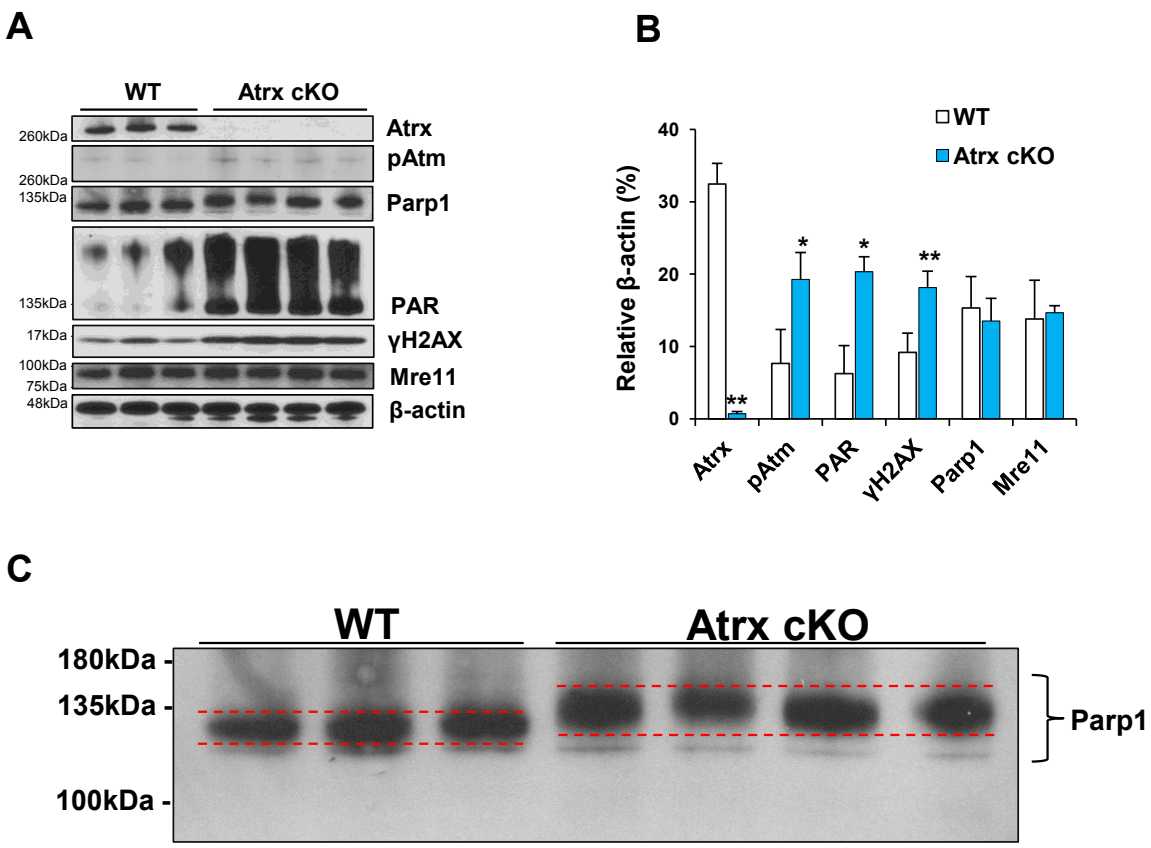

Figure 11. DNA damage occurs in the dorsal telencephalon upon conditional Atrx loss in mice.

(A) Western blot analysis for DNA-damage signaling in E13.5 cortices extracted from WT (n=3) and Atrx cKO (n=4) embryos. (B) Densitometry quantification of blot shown in (A). Values are the mean ± S.E.M. *p-value<0.05; **p-value<0.01, calculated by unpaired Student's t-test with uneqal variance. (C) Extracts from Atrx cKO brains display a shift in Parp1 migration. Mouse Parp1 (113kDa) was resolved on a 4-12% gradient gel from E13.5 wild type (n=3) and Atrx cKO (n=4) cortical extracts. The shift in Parp1 migration in the mutant lanes compared to WT lanes is indicative of auto PARylation or, alternatively, some other post-translational modification

3.3 *In vitro* analysis of ATRX

ii. ATRX prevents dsDNA breaks derived from S-phase progression

Primary cortical cultures and cortical extracts from Atrx KO embryos were previously demonstrated to exhibit increased intrinsic apoptosis, as marked by elevated levels of TUNEL staining, and increased caspase 3 and caspase 9 activation [103] [193]. Furthermore, Atrx KO myoblasts were shown to exhibit a reduced replicative capacity associated with a prolonged progression through the latter half of S phase during the cell cycle [97]. These findings demonstrate that Atrx KO primary cells possess a diminished ability for proliferation *in vitro*. Therefore, HeLa cells were selected to investigate a role for ATRX during cellular proliferation. While HeLa cells possess an abnormal karyotype associated with their oncogenic transformation, they express important cell cycle and DDR proteins (e.g. p53, ATM and ATR) which contributes to their long standing history as a reproducable model of DNA damage-associated phenotypes and genotypes [194] [195]. Previously, ATRX deficent HeLa cells were examined using siRNA and shRNA knockdown (KD) strategies. This model accurately recapitulated the proliferation and apoptosis phenotypes observed in primary cells, while additionally maintaining their capacity for unlimited replication [135].

Depletion of ATRX was carried out by transfecting a pool of siRNA oligonucleotides specific to the ATRX mRNA transcript into HeLa cells (ATRX KD). At 48 hours post-transfection and until 120 hours post-transfection, the expression of the ATRX and ATRXt (truncated ATRX) proteins was diminished below detection levels by western blot analysis, relative to control cells treated with scrambled siRNA (siScramble) (**Figure 12A**). Simultaneuously, γH2A.X was elevated above control levels between 72 and 120 hours post-transfection (**Figure**

12A). Next, we investigated if the elevated levels of γH2A.X observed in ATRX KD cells was due to increased dsDNA breaks (DSBs) associated with cell cycle progression. By co-immunofluorescent staining of cyclin A (CcnA) to track cell cycle progression and phosphorylation of the ATM kinase on Serine 1981 (pATM) to track DSBs, we examined ATRX KD HeLa cells at 72 and 96 hour post-transfection compared to controls (**Figures 12B-E**). CcnA marked cells specifically transiting S and G2 phases of the cell cycle, thereby coinciding with a period of DNA replication prior to mitosis [196]. Cells were scored positive for pATM if they contained >5 foci per nucleus (**white arrows; Figure 12B**). Cells with Dispersed cytoplasmic staining were excluded from our analysis of pATM as they mark mitotic spindles and not damage foci [197] (**Figure 12B**).

In total, ATRX KD HeLa cells had a significantly greater proportion of pATM positive cells compared to siSCRAMBLE control cells at both the 72 and 96 hour time points (72 hours: p-value=0.00318, Z-test: 2-tailed, 2-proportions; 96 hours: p-value<0.00001, Z-test: 2-tailed, 2-proportions) (**Figure 12C**). ATRX KD cells and siScramble control cells were binned as either CcnA positive or CcnA negative and analyzed for pATM status to assess any potential linkage of dsDNA breakage to cell cycle progression. When examining CcnA positive cells, ATRX KD cells had a significantly greater proportion of pATM positive cells compared to control cells at both the 72 and 96 hour time points (72 hours: p-value=0.000580, Z-test: 2-tailed, 2-proportions; 96 hours: p-value=0.00496, Z-test: 2-tailed, 2-proportions) (**Figure 12D**). Interestingly, when examining CcnA negative cells, ATRX KD cells only had a significantly greater proportion of pATM positive cells compared to control cells at the 96 hour time point, but not the 72 hour time point (72 hours: p-value=0.453, Z-test: 2-tailed, 2-proportions; 96 hours: p-value<0.00001, Z-test: 2-tailed, 2-proportions) (**Figure 12E**). This line of evidence suggested that the dsDNA damage associated with ATRX deficiency is associated with mitotic progression following DNA replication.

Within the PARP family, PARP 1, 2 and 3 are known to become active upon DNA damage [198]. Relevent to this study, PARP1 and 3 are directly tied to dsDNA break repair (DSBR) pathways, although PARP1 activity has been attributed for the majority of PARylation, compared to all PARPs [191] [199] [200] [201]. Additionally, PARP1 has been specifically associated with a homology-directed repair (HDR) mechanism at stalled or collapsed replication forks [163], as well as preferential recruitment to DSBs with heterochromatin over euchromatin [202]. Given our evidence for elevated PARylation and potential Parp1 automodification in the DT of Atrx cKO mice (**Figure 11**), we chose to investigate PARP1's contribution in further detail.

HeLa cells were treated with siRNAs targeting either ATRX or PARP1 (siPARP1) or ATRX and PARP1 simultaneously and protein levels were examined by Western blot (**Figure 13A**). As expected, when ATRX KD cells were compared to control cells, elevated PAR and γH2A.X was detected, without any discernable difference in PARP1 expression (**Figure 13A, lanes 1 and 2**). When siATRX and siScramble treated cells were additionally transfected with siPARP1, the PARP1 expression levels were dramatically decreased. Furthermore, the elevated PAR and γH2A.X levels that were detected upon ATRX KD became ameliorated (**Figure 13A, lanes 3 and 4**). Together, this data indicates that PARP1 expression contributes to the elevated PARylation observed upon ATRX deficiency.

PJ34 is a potent ($0.01<K_d<2.0$ μM), small molecule inhibitor of PARP (PARPi) that is broadly specific to multiple members of the PARP enzyme family [203]. Binding affinities are ~50 fold greater for PARP1 or PARP2 compared to PARP3 or PARP5A (also known as Tankyrase-1) [203]. We utilized PJ34 to examine PARP contributions to the ATRX KD phenotype in HeLa cells by western blot analysis. As with siPARP1 treatment, elevated PAR

levels observed in ATRX KD cells was ameliorated by the addition of PJ34, but in this case PARP1 expression was unaltered compared to controls (**Figure 13B**). Additionally, the expression of 53BP1 became elevated when siATRX treated cells were incubated with PJ34 (**Figure 13B, lane 4**).

Next, we performed an immunoflorescent analysis of ATRX KD HeLa cells treated with PJ34, focusing specifically on DSBs (**Figure 14**). The protein 53BP1 protein is recruited to DSBs where it serves as a scaffold for several other DSBR enzymes involved in NHEJ [204]. Given that 53BP1 becomes upregulated when ATRX KD is combined with PJ34 treatment (**Figure 13B, lane 4**), we quantified 53BP1 foci formation in cells treated with siATRX or siSCRAMBLE mRNA, with or without PJ34. Punctate foci, which totaled >5 foci per DAPI stained nucleus was set as a positive threshold for 53BP1 identification.

When we compared cells that were not treated with PJ34, we observed a ~60.5% greater proportion of ATRX KD cells that were 53BP1 positive compared to control cells (p-value<0.00001, Z-test: 2-tailed, 2-proportions). Additionally, when we compared cells that were treated with PJ34 for 24 hours, we observed a ~82.6% greater proportion of ATRX KD cells that were 53BP1 positive compared to control cells (p-value<0.00001, Z-test: 2-tailed, 2-proportions) (**Figure 14A**). We also observed that PJ34 treatment in siScramble control HeLa cells increased the proportion of 53BP1 positive cells by ~38.0%, indicating the genotoxic properties of PJ34 treatment in the HeLa cell model. However, the proportion of 53BP1 positive siATRX treated cells was ~57.0% greater upon PJ34 treatment, thereby associating ATRX deficiency with hypersensitivity to PARPi, and increased activation of NHEJ.

Terminal deoxynucleotidyl transferase dUTP nick end labeling (TUNEL) is a technique for

detecting DSBs and single strand DNA breaks (SSDBs) in fixed cells, by ligating the exposed 3'-OH terminal end with a fluorescently modified nucleotide. We quantified the proportion of TUNEL positive cells relative to DAPI stained nuclei in HeLa cells treated with siATRX or siScramble mRNA, and with or without PJ34. When we compared cells that were not treated with PJ34, we observed a ~360% greater proportion of ATRX KD cells that were TUNEL positive compared to control cells (p-value<0.00001, Z-test: 2-tailed, 2-proportions). When cells were treated with PJ34 for 24 hours, we observed a 140% greater proportion of ATRX KD cells that were TUNEL positive compared to control cells (p-value<0.00001, Z-test: 2-tailed, 2-proportions) (**Figure 14B**). As with 53BP1 staining, we observed that PJ34 treatment in siScramble control HeLa cells increased the proportion of TUNEL positive cells relative to DAPI by ~280%, indicating the genotoxic properties of PJ34 treatment in the HeLa cell model. Unlike our observation with 53BP1 staining, the proportion of TUNEL positive siATRX treated cells was only ~100% greater upon PJ34 treatment.

Given PJ34's genotoxicity and the evidence suggesting that ATRX deficient cells were hypersensitive to PARP inhibitors (PARPi), we next examined whether or not PJ34 treatment affected cellular proliferation in ATRX deficient cells. Interestingly, synthetic lethality has been previously described in BRCA1/2 deficient cells treated with PARPi [205]. We quantified cell proliferation and viability using an automated cell counting platform in conjunction with trypan blue detection as an indicator of cell death (**Figure 15**). HeLa cells were treated with siATRX or siScramble siRNA for 72 hours followed by 48 hours in media containing 5.0 μM PJ34 before analysis. Additionally, two osteosarcoma-derived cell lines were similarly examined. U2OS cells, which do not express the ATRX protein served as a model of ATRX-deficiency, while MG63 cells do express ATRX and served as a control group. First, we examined the difference in proliferation after PJ34 treatment (**Figure 15A**). In HeLa cells, ATRX KD with PJ34 treatment reduced the total cell count to ~53.7% relative

to untreated ATRX KD cells (p-value=0.00096, Student's t-test: 2-tailed, unequal variance). In siScramble control cells, we did not observe a significant difference resulting from PJ34 treatment (p-value=0.69, Student's t-test: 2-tailed, unequal variance). Similarly, U2OS cells treated with PJ34 did not proliferate as well as untreated cells (~76% relative to untreated U2OS cells; p-value=0.034, Student's t-test: 2-tailed, unequal variance). Furthermore, we did not observe a significant difference resulting from PJ34 treatment in ATRX expressing MG63 cells (p-value=0.38, Student's t-test: 2-tailed, unequal variance). Trypan blue cell staining was used to assess whether decreased cell number resulted from loss of cell viability, but no differences were observed (**Figure 15B**).

Conclusion

In this section we examined the DNA damage and proliferation defects associated with ATRX deficiency in HeLa cells to determine if ATRX prevents dsDNA breaks derived from S-phase progression. Data generated for the transient KD of ATRX with siRNA suggested an association between ATRX deficiency and elevated γH2A.X and pATM signalling, which appeared to be dependent on DNA replication. Following the increased PAR signalling observed *in vivo* in the previous section, ATRX KD cells treated with either siPARP1 or PJ34, displayed reduced PAR signalling comparable to WT cells. Furthermore, the data related to PJ34 treatment in ATRX deficient cells suggested that while 24 to 48 hours of exposure to 5.0μM PJ34 was sufficient to induce elevated genotoxicity and decreased cellular proliferation, it was not sufficient to induce detectable levels of cell death.

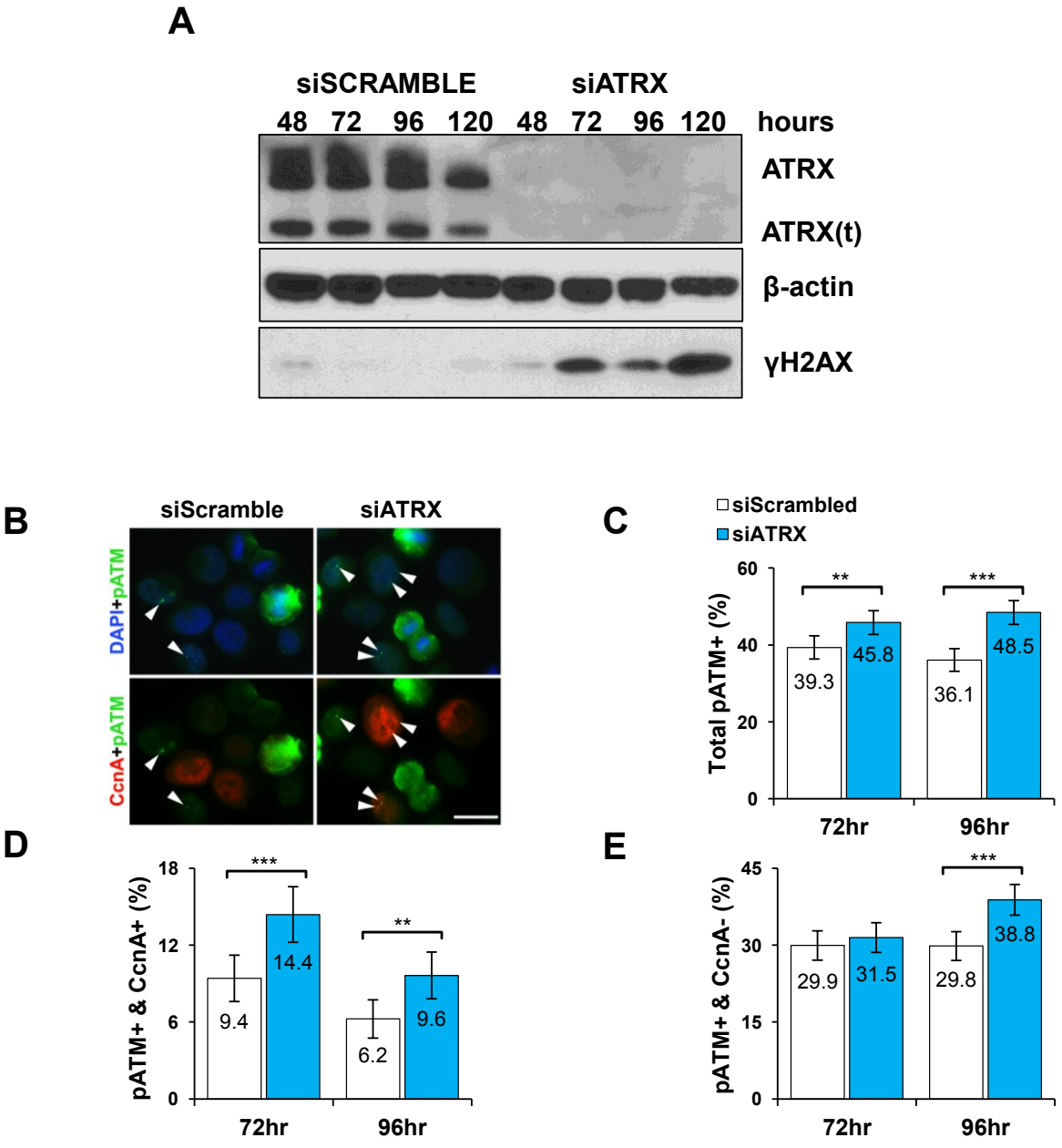
A
siSCRAMBLE
siATRX
48 72 96 120 48 72 96 120 hours
ATRX
ATRX(t)
β-actin
γH2AX
B
siScramble
siATRX
DAPI+pATM
CcnA+pATM
C
siScrambled
siATRX
Total pATM+ (%)
60
40
20
0
**
***
39.3
45.8
36.1
48.5
72hr
96hr
D
pATM+ & CcnA+ (%)
18
12
6
0
***
**
9.4
14.4
6.2
9.6
72hr
96hr
E
pATM+ & CcnA- (%)
45
30
15
0
***
29.9
31.5
29.8
38.8
72hr
96hr

Figure 12. ATRX depletion induces cell cycle-dependent DNA damage accumulation. (A) ATRX expression in HeLa cells after siRNA treatment. Western blot analysis of siRNA mediated knockdown of ATRX examined at 48, 72, 96 and 120 hours post transfection relative to scramble siRNA control cells. A progressive increase of γH2AX expression was evident in KD cells. B-actin served as a loading control. (B) Representative immunoflourescent images of phosphorylated ATMSer1981 (pATM; green) and cyclin A (CcnA; red) double IF staining of siScram- and siATRX-transfected HeLa cells at 96 h post-transfection. Arrowheads point to cells with DNA-damage foci. (C) Percentage of total interphase nuclei containing pATM foci in siATRX- versus siScram-transfected HeLa cells at 72 and 96 h post-transfection. siATRX: 72 h, n=1001; 96 h, n=1007. siScram: 72 h, n=999; 96 h, n=1009. (D) Percentage of S-G2 (CcnA+) nuclei containing pATM foci at 72 and 96 h post-transfection. siATRX: 72 h, n=365; 96 h, n=366. siScram: 72 h, n=342; 96 h, n=308. (E) Percentage of G1 (CcnA−) nuclei containing pATM foci at 72 and 96 h post-transfection. siATRX: 72 h, n=636; 96 h, n=641. siScram: 72 h, n=657; 96 h, n=701. Values represent percent total ± 95% confidence interval,; **P<0.01; ***P<0.001 calculated from *z*-scores. ×630 magnification with scale bar = 20 μm.

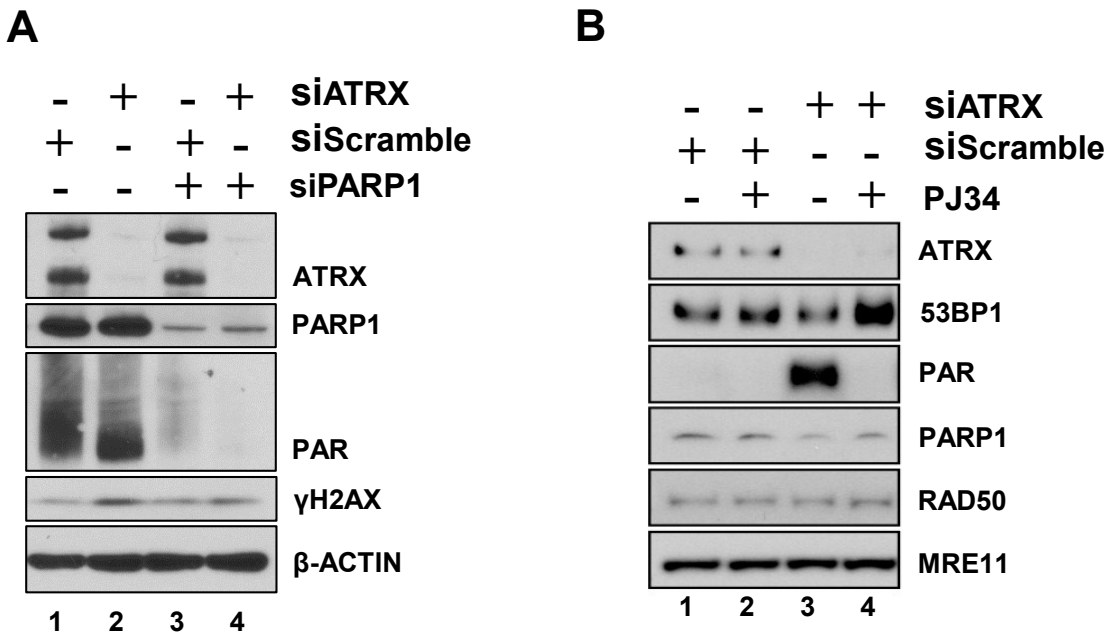

Figure 13. PARP1 contributes to elevated PARylation in ATRX depleted cells.
(A) Western blot analysis for PARP activation in HeLa cells following treatment with siATRX alone or combined with siPARP1. Whole cell protein lysates were harvested at 72 hours post-transfection for immunoblots of Atrx, Parp1, PAR, and γH2AX. ß-actin serves as a loading control. (B) Western blot analysis of PARP1 inhibition by PJ34 in ATRX KD HeLa cells. As indicated, HeLa cells were transfected with siScram and siATRX. At 48 h after transfection, cells were treated with 5 μM of PARP-1 inhibitor PJ34 (+) or untreated (−) for another 24 h. Whole-cell extracts were harvested 72 h post-transfection.

A

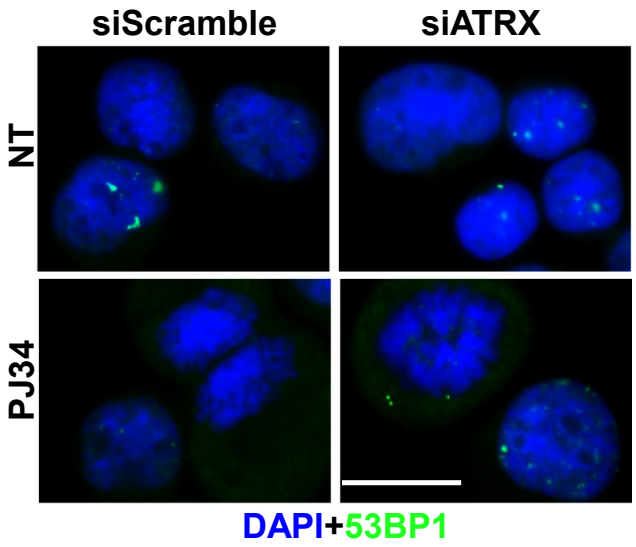
siScramble
siATRX
NT
PJ34
DAPI+53BP1

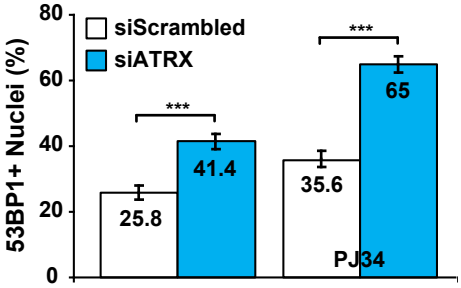
80
60
40
20
0
53BP1+ Nuclei (%)
siScrambled
siATRX
***
***
25.8
41.4
35.6
65
PJ34

B

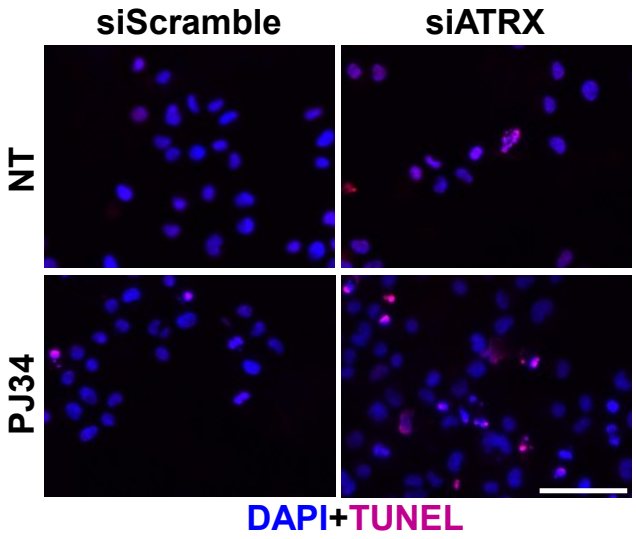
siScramble
siATRX
NT
PJ34
DAPI+TUNEL

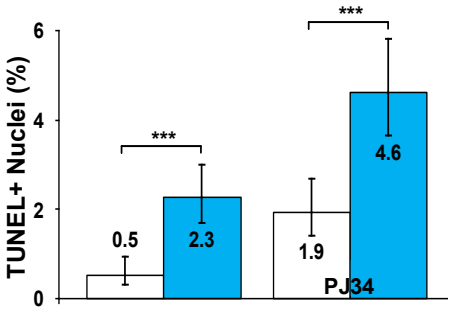
6
4
2
0
TUNEL+ Nuclei (%)
***
***
0.5
2.3
1.9
4.6
PJ34

Figure 14. ATRX depleted cells experience increased DNA damage upon poly-(ADP)-ribose polymerase inhibition.
(A) Representative immunofluorescent images of 53BP1 staining in siATRX and siScrambled transfected HeLa cells. Cells were treated with the PARP inhibitor PJ34 (+PJ34) for 24 hours prior to fixation in PFA and compared to no-treatment controls (NT). 630x magnification. Scale bar represents 20 μm. Graphs displaying the percentage of total nuclei containing greater than or equal to5 bright 53BP1 foci in siScram- versus siATRX-transfected HeLa cells at 96 h post-transfection. At 72 h after transfection, cells were treated with 5 μM of PARP-1 inhibitor PJ34 (right) or untreated for another 24 h (left). Cells were fixed 96 h post-transfection and stained for 53BP1. Values represent percent total±95% CI. siScram (n=1420); siATRX (n=1607); siScram+PJ34 (n=1473); siATRX+PJ34 (n=1492). ***p-value<0.001 calculated by z-scores.
(B) Representative immunofluorescent images of TUNEL staining in siATRX and siScrambled transfected HeLa cells. Cells were treated with the PARP inhibitor PJ34 (+PJ34) for 24 hours prior to fixation in PFA and compared to no-treatment controls (NT). 200x magnification. Scale bar represents 100 μm. Graphs displaying the percentage of total nuclei containing TUNEL+ apoptotic nuclei in siScram- versus siATRX-transfected HeLa cells at 72 h post-transfection. At 48 h after transfection, cells were treated with 5 μM of PARP-1 inhibitor PJ34 (right) or untreated for another 24 h (left). Cells were fixed 72 h post-transfection and TUNEL stained. Values represent percent total±95% CI. siScram (n=2251); siATRX (n=2031); siScram+PJ34 (n=1802); siATRX+PJ34 (n=1455). ***p-value<0.001 calculated by z-scores.

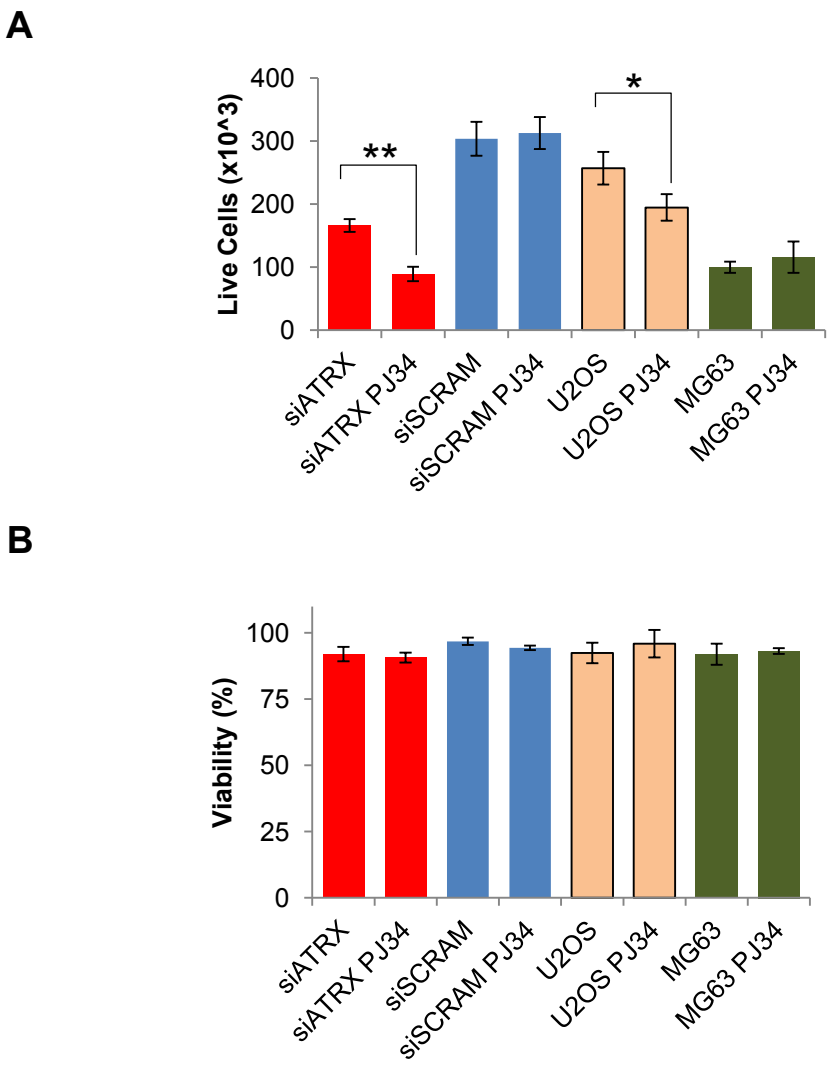

Figure 15. PARP inhibition in ATRX deficient cells results in decreased proliferation, without immediate detectable cell death.

ATRX deficient cells (siATRX treated HeLa cells starting at 48 hour post transfection and U2OS cells) were compared to control ATRX proficient cells (siScramble treated HeLa cells and MG63 cells) and counted for (A) total number of live cells, as well as (B) live cells relative to the total number of cells including those stained with trypan blue to mark dead or dying cells. n = $2X10^5$ cells per condition in triplicate, ** denotes p-value<0.001, * denotes p-values<0.05. Cells were counted in a ViCell Counter (Beckman Coulter). Values represent average total ± S.E.M.

iii. ATRX protects stalled replication forks from MRE11-dependent degradation

A role for Atrx in facilitating DNA replication was first highlighted when Atrx was identified to co-localize specifically with late-replicating regions of the genome in myogenic progenitor cells [97]. Subsequently, loss of Atrx resulted in genomic instability associated with telomeric defects, increased γH2AX signalling and DSBR pathway activation involving p53 and the ATM kinase [97]. The evidence that the genomic instability associated with ATRX deficiency was dependent on DNA replication fork defects came from a study in mouse embryonic stem cells (mESC). Here, Atrx loss increased the frequency of replication fork stalling events, exacerbated the restart efficiency of chemically stalled replication forks, and decreased replication fork processivity [90]. Additionally, an examination of ATRX deficiency in the immortalized HCT116 cell lines had originally demonstrated that dNTP depletion with hydroxyurea (HU) impaired replication fork restart and highlighted ATRX's physical interaction with the DNA damage response (DDR) complex MRN [84]. Conversely, re-introduction of ATRX into U2OS cells, a sarcoma cell line whose immortalization involved the loss of ATRX expression, diminished the occurrence of replication fork stalling events [136].

Given our previous data, which also suggested ATRX's involvement in the facilitation of genome replication (See: previous two sections), we sought to examine ATRX's role specifically during DNA replication in further detail. We returned to the HeLa cell model to validate ATRX's co-localization with late-replicating regions of the genome. Actively replicating regions of DNA were labeled in asynchronous WT HeLa cells with the thymidine analogue, ethynyl deoxyuridine (EdU) [206]. A 20 minute pulse of 20μM EdU was followed by chemical fixation with paraformaldehyde (PFA), effectively locking all cellular macromolecules in place. EdU was fluorescently labeled via a "click chemistry" reaction

[207] followed by immunofluorescent labeling of ATRX and the human Heterochromatin Protein 1 (HP1) paralogs HP1α, HP1β and HP1γ (**Figure16**). ATRX and HP1 co-immunoprecipitate, as well as co-localize at telomeric regions [68] [76]. We did not observe any distinct co-localization occurrences between EdU, ATRX or any HP1 homologs in cells with EdU staining reminiscent of early S-phase DNA labeling [97] (**Figure 16A**). Larger, punctate EdU foci indicated late-replicating chromatin, and this was where we observed that ATRX and the HP1 homologs co-localized (**Figure 16B, white arrows**). This data validated previous findings that ATRX co-localizes to late-replicating heterochromatin.

From the evidence that ATRX localized to late replicating heterochromatin (**Figure 16B**), as well as the evidence that ATRX facilitated DNA replication by preventing replication fork stalling and assisted in replication fork restart [84] [90]. We sought to investigate whether or not ATRX played a role in the protection of stalled replication forks. Just as ATRX deficient cells become hypersensitive to PARPi (**Figures 14 and 15**), so too do cells deficient for the BRCA1 and BRCA2 proteins [205]. BRCA1 and BRCA2 are involved in HR at DSBs resulting from prolonged replication fork stalling events and more recently, have each been demonstrated to contribute distinct functions for the protection of stalled forks prior to DSB formation [208] [167] [166]. Therefore, BRCA1 was selected from previously published literature as a positive control indicating replication fork protection defects [167].

We assessed whether or not ATRX deficiency genocopies BRCA1 deficiency. To do this we utilized an siRNA KD approach specific for BRCA1 (siBRCA1) and compared it to siATRX. Here we measured replication fork protection with the DNA fiber assay, which included chemically induced replication fork stalling. Methodologically, asynchronous HeLa cells were pulsed with the thymidine analog 5-bromo-2'-deoxyuridine (BrdU) to label nascent replicated DNA, followed by hydroxyurea (HU) treatment to chemically induce global DNA replication

fork stalling via deoxyribose nucleoside triphosphate (dNTP) depletion. After 5 hours of prolonged fork stalling, the cells were lysed and all genomic DNA was spread across glass microscope slides by gravitational force. The incorporated BrdU was immunofluorescently labeled and imaged to measure the length of the nascent DNA fibers (**Figure 17A**).

The fiber assay with HU-mediated replication fork stalling was carried out using siScramble control cells, siATRX treated cells and siBRCA1 treated cells, which all exhibited depleted levels of their siRNA-targeted protein product relative to the β-actin loading control (**Figure 17B**). Single-molecule DNA fiber lengths were measured with ImageJ software and binned in 2μm increments. A histogram indicating the proportional weight of each bin was overlaid with an approximate density distribution curve to visualize the distribution of each experimental condition. As expected from the literature [167], we saw that DNA fiber lengths were skewed towards smaller values in BRCA1 deficient cells compared to the siScramble treated control cells, with the average length 49% smaller than controls ($p<2.20x10^{-16}$, Mann-Whitney U-test) (**Figures 17C and D**). Intriguingly, ATRX KD cells also exhibited DNA fiber lengths that were skewed towards smaller values (**Figure 17C**). Quantitative analysis indicated that the mean nascent DNA fiber length after fork stalling in ATRX KD cells was not significantly different compared to fibers from BRCA1 KD cells ($p=0.104$, Mann-Whitney U-test). Furthermore, the average length of nascent DNA fibers from ATRX KD cells was ~45% smaller than siScramble control cells ($p<2.20x10^{-16}$, Mann-Whitney U-test) (Figure **17D**).

Oncogenesis can be driven by the dysreglation of either ATRX or BRCA1, and rarely are they found to be mutated simoltaneously in the same tumor [205] [255]. Interesting, we found that ATRX loss genocopies BRCA1 loss, but the mechanism for this observation warranted further examination. At least three possible outcomes could explain the shorter

DNA fibers following ATRX KD including (1) that ATRX deficient cells have a slower rate of BrdU incorporation, (2) that certain exonucleases might become hyperactive without ATRX present, and/or (3) that ATRX deficiency may alter the epigenetic chromatin landscape required for DNA synthesis.

(1) ATRX facilitates DNA replication

First, we assessed DNA replication processivity by measuring nascent DNA fibers of BrdU pulsed cells without HU treatment. Cells deficient for ATRX progress more slowly through late-S-phase compared to WT controls [135] [97]. Therefore, we expected that ATRX KD cells would produce shorter nascent DNA fibers compared to controls. Cells were treated with siATRX to deplete ATRX protein expression or siScramble RNA control and then pulsed with BrdU (**Figure 18A**). Here, instead of arresting fork progression with an HU treatment, the cells were harvested and their DNA fibers were spread, imaged and measured. Qualitatively, the distribution of DNA fiber lengths which came from the siScramble-treated cells adopted a more symmetrical form compared to the siATRX fibers which were skewed towards smaller lengths (**Figure 18B**). Quantitatively, ATRX KD cells produced BrdU-labeled nascent DNA fibers that were ~16% shorter than those from siScramble control cells ($p=2.42x10^{-15}$, Mann Whitney U test) (**Figure 18C**). Therefore, the ATRX KD cells produced significantly shorter nascent DNA fibers than the WT control cells, in a manner unrelated to chemically-induced replication fork stalling.

To examine the impact of chemically induced replication fork stalling events on nascent DNA fiber lengths, a cohort of siATRX and siScramble treated cells were exposed to HU immediately after the BrdU pulse labeling of nascent DNA. Qualitatively, the distribution of DNA fiber lengths which came from the siScramble cells treated with HU maintained a

symmetrical form similar to the untreated siScramble cells, while the fibers from siATRX cells treated with HU had a dramatically skewed distribution towards even smaller lengths compared to siATRX untreated cells (**Figure 18B**). Quantitatively, HU treatment in siScramble control cells resulted in nascent DNA fibers that were ~2.3% shorter, but not significantly different than untreated siScramble control cells (p=0.279, Mann-Whitney U test), while HU treatment in siATRX cells resulted in fibers that were ~38% shorter than untreated siATRX cells ($p<2.20x10^{-16}$, Mann Whitney U test). Additionally, HU treated siATRX cells were ~46% shorter than HU treated siScramble control cells ($p<2.20x10^{-16}$, Mann Whitney U test) (**Figure 18C**). Together, this data demonstrated that while ATRX KD cells incorporated BrdU significantly more slowly than WT cells, the chemical induction of stalled replication forks post-labeling resulted in a significant reduction in the length of BrdU-labeled nascent DNA fiber.

(2) ATRX attenuates MRE11 activity

Second, the exonuclease MRE11 is understood to expose ssDNA, which can then be bound by the RPA complex or RAD51 to ensure fork protection and repair in the event of a collapse-induced DSB [209]. We utilized the small molecule mirin, which specifically inhibits the 5'-3' exonuclease activity of MRE11 thereby blocking degradation of stalled replication forks [162]. ATRX deficiency *in vivo* (**Figure 11**) and *in vitro* (**Figure 12**) is directly associated with increased PARP1-mediated PAR signalling. Interestingly, PARP1 hyper-activation in BRCA2-deficient cells may protect stalled replication forks from degradation by MRE11 3'-5' exonuclease activity [163]. Indeed, several members of the Fanconi Anemia and BRCA protein families have been shown to protect nascent DNA fibers at stalled replication forks from degradation by MRE11 [210] [166] [167]. Since ATRX has been shown to physically interact with the MRE11-RAD50-NSB1 (MRN) complex [84] [90]. We

first tested whether this was also the case in HeLa cells. Indeed, two members of the MRN complex, MRE11 and NBS1, successfully co-immunoprecipitated with the ATRX protein (**Figure 19**). To define whether the interaction was dependent on DNA or not, we repeated the experiment in the presence of ethidium bromide. DNA-dependent protein interactions are specifically inhibited by 100 µg/ml ethidium bromide (EtBr) [211]. EtBr did not impede the co-immunoprecipitation of ATRX, nor did it impede the co- immunoprecipitation of MRE11, although we did observe an alteration between the signal intensities of a doublet associated with NBS1 (**Figure 19**). From this analysis, we observed that ATRX reliably associates with MRE11, independently of DNA.

To examine if hyper-activation of MRE11 contributed to the production of shorter DNA fibers in ATRX KD cells, we utilized the small molecule mirin, which specifically inhibits MRE11's exonuclease activity [162]. A cohort of siATRX and siScramble treated cells were exposed to HU and 50µM mirin immediately after the BrdU pulse labeling of nascent DNA in order to inhibit MRE11 while replication forks were stalled. As expected, the treatment with mirin did not alter the protein expression of MRE11 in ATRX KD or WT control cells compared to the untreated cells (**Figure 18A**). If MRE11 exonuclease activity contributed to the production of shorter DNA fibers in ATRX KD cells, then treatment with mirin would result in the production of nascent DNA fibers at similar lengths to the siScramble control cells. Indeed, while the distribution of DNA fiber lengths which came from the siScramble cells treated with HU+mirin maintained a symmetrical form similar to the untreated or HU treated siScramble cells, the fibers from siATRX cells treated with HU+mirin also exhibited a symmetrical distribution. Therefore, in ATRX KD cells, mirin ameliorated the skewed distribution of shorter nascent DNA fiber lengths in siATRX cells either treated with or without HU (**Figure 18B**). Quantitatively, HU+mirin treatment in siScramble control cells resulted in nascent DNA fibers that were approximately equal to HU treated siScramble control cells (p=0.229,

Mann-Whitney U test), while HU+mirin treatment in siATRX cells resulted in fibers that were ~74% longer than HU treated siATRX cells ($p<2.20x10^{-16}$, Mann Whitney U test). Additionally, HU+mirin treated siATRX cells were ~8.1% longer than siATRX cells that were not treated with HU ($p=4.39x10^{-5}$, Mann Whitney U test) (**Figure 18C**). Together, this data demonstrated that inhibition of MRE11 exonuclease activity in ATRX KD cells significantly rescued the shortened nascent DNA fibers in cells with and without chemically stalled replication forks.

(3) ATRX or DAXX deficiency

Finally, ATRX complexes with DAXX to chaperone a histone 3 variant know as H3.3 into nucleosomes within heterochromatin [77] [212]. By this association, DAXX may underlie ATRX's significance regarding DNA replication and this may potentially be associated with an H3.3-related epigenetic program. Therefore, to further define the mechanism by which ATRX deficiency genocopies BRCA1 deficiency, and to elucidate the replication dependent DNA damage associated therein, we explored these three potential influences. Replication-independent deposition of histone H3.3 by the ATRX-DAXX histone chaperone complex has been associated with the maintenance of heterochromatin involving the preservation of tri-methylation of lysine 9 on histone 3 (H3K9me3) [213]. In fact, the uncoupling of H3K9me3 epigenetic signalling in DAXX deficient cells has been linked to decreased chromatin compaction and loss of genomic structural integrity [214]. Furthermore, the presence of histone H3.3 in nucleosomes during S-phase has been demonstrated to support DNA replication fork progression in UV irradiated cells [169]. If ATRX deficiency alters the H3.3-mediated epigenetic landscape required for DNA synthesis, then loss of DAXX could result in similar replication defects observed upon ATRX loss, given their mutual role as an H3.3-chaperone.

We assessed DNA replication in HeLa cells treated with an siRNA specific for DAXX (siDAXX) using the DNA fiber assay, with and without HU-mediated replication fork stalling (**Figure 20**). DAXX KD was validated by western blot analysis. DAXX protein levels were reduced in siDAXX treated cells compared to siScramble control cells relative to the ß-actin loading control (**Figure 20A**). Importantly, DAXX KD did not have an effect on ATRX protein expression, while HU-treatment increased γH2A.X signalling in both the KD and control conditions (**Figure 20A**). As expected, the distribution of DNA fiber lengths which came from either the HU-treated or untreated siScramble control cells adopted a symmetrical form (**Figure 20B**). Conversely, the BrdU labeled fibers from untreated siDAXX cells were skewed towards smaller lengths (**Figure 20B**). Moreover, the distribution of labeled DNA fibers from siDAXX cells treated with HU was dramatically skewed towards even smaller lengths compared to untreated siDAXX cells (**Figure 20B**). Quantitatively, HU-treated siScramble control cells produced nascent DNA fibers that were ~2.7% longer than untreated siScramble control cells, but were not significantly different ($p=0.261$, Mann-Whitney U test), while HU-treated siDAXX cells were ~38% shorter than HU-treated siScramble control cells ($p<2.20\times10^{-16}$, Mann Whitney U test) (**Figure 20C**). Untreated DAXX KD cells produced BrdU-labeled nascent DNA fibers that were ~9.1% shorter than those from untreated siScramble control cells ($p=3.91\times10^{-5}$, Mann Whitney U test) (Figure 20C), while HU-treated siDAXX cells produced fibers that were ~30% shorter than untreated siDAXX cells ($p<2.20\times10^{-16}$, Mann Whitney U test) (**Figure 20C**). Therefore, in a similar manner to ATRX depletion, DAXX KD cells also incorporated BrdU significantly more slowly than WT cells and the chemical induction of stalled replication forks post-labeling resulted in a significant reduction in the length of BrdU-labeled nascent DNA fiber.

Conclusion

In this section we examined ATRX KD HeLa cells that were actively transiting S-phase to determine if ATRX protects stalled replication forks from exonuclease-mediated degradation. We observed that ATRX localizes to late replicating heterochromatin marked by a specific staining pattern of EdU and the HP1 paralogs. This protein behaviour suggested an active recruitment similar to the BRCA1/2 proteins. Indeed, ATRX deficiency genocopies BRCA1 deficiency, in that both conditions sensitize cells to HU-mediated replication fork stalling resulting in less nascent replicated DNA. We observed that ATRX deficiency alone reduces the length of nascent DNA compared to control cells, and that this condition is greatly exacerbated by the addition of HU for a prolonged period to stall replication forks. Interestingly, chemical inhibition of MRE11 exonuclease activity directly rescued this deficit, thereby suggesting a functional relevance for the ATRX-MRN interaction. Finally, DAXX KD HeLa cells also display a similar deficit for the protection of newly replicated DNA. Together, this data suggests that ATRX localizes to replicating DNA with a potential function being to restrict MRE11-mediated DNA resectioning at stalled replication forks. Furthermore, the ATRX binding partner DAXX appears to be integral for this function.

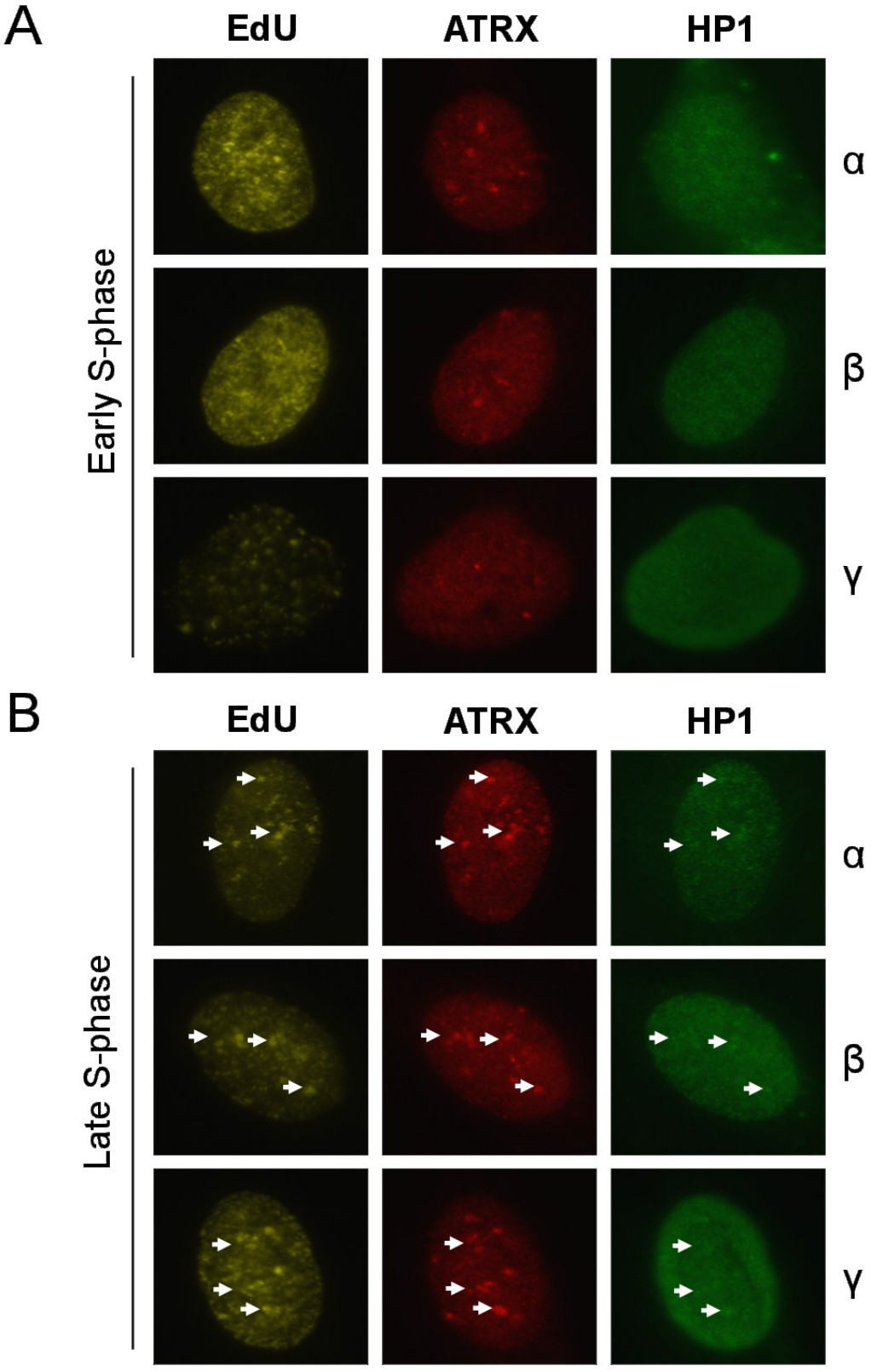
A
EdU
ATRX
HP1
Early S-phase
α
β
γ
B
EdU
ATRX
HP1
Late S-phase
α
β
γ

Figure 16. ATRX localizes to late-replicating heterochromatin.
Representative images of triple immunostaining for ATRX, EdU and each of the heterochromatin protein 1 (HP1) homologs and in unsynchronized WT HeLa cells. EdU+ cells were binned as transiting either (A) early or (B) late S-phase based on the staining pattern of the 20 minute EdU pulse. Fixed cells were stained with antibodies specific for ATRX (red) and HP1α, ß or γ (green) and BrdU (yellow). Co-localized foci of ATRX, HP1 and EdU were indicated by arrowheads. 1000X magnification. Scale bar, 10 μm.

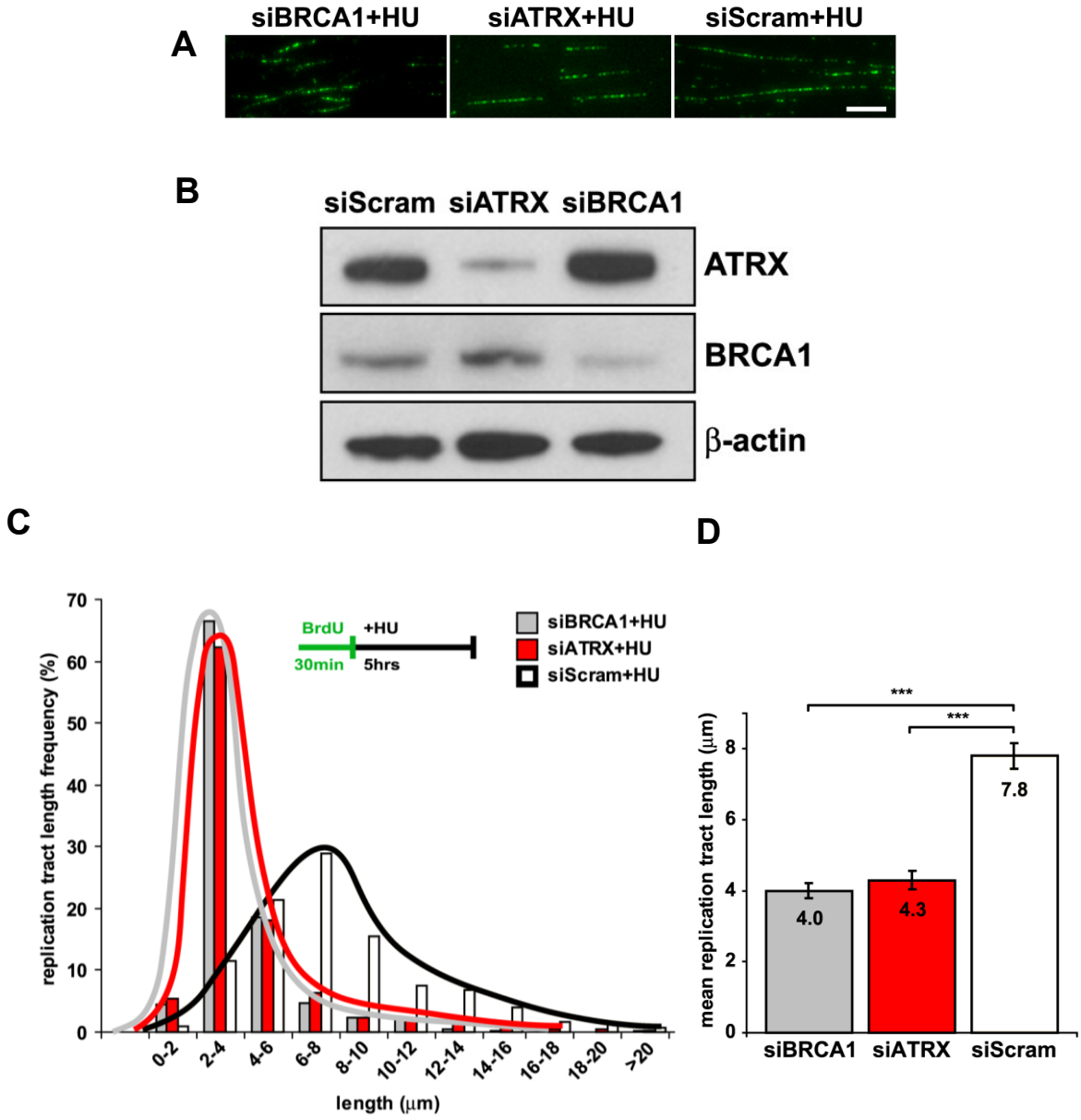

Figure 17. Hydroxyurea-induced replication fork stalling in BRCA1 or ATRX depleted cells reduces nascent DNA fiber length.

(A) Representative images of BrdU-labelled DNA fiber tracts. 630X magnification. Scale bar, 2 μm. (B) Western blot analysis demonstrating knockdown of ATRX and BRCA1. β-actin served as the loading control. (C) DNA fiber tract length distribution histogram of siBRCA1, siATRX, and siScram control transfected HeLa cells at 72 hr post transfection. Insert shows schematic of experimental paradigm. HU, hydroxyurea. Number of DNA fibers measured: siBRCA1 (n = 514); siATRX (n = 528); siScram (n = 502). (D) Mean DNA fiber tract length of siBRCA1, siATRX and siScram control treated HeLa cells. Values represent mean length ± 95% CI. (***) p-valye < 10^{-15} calculated by Mann-Whitney U test.

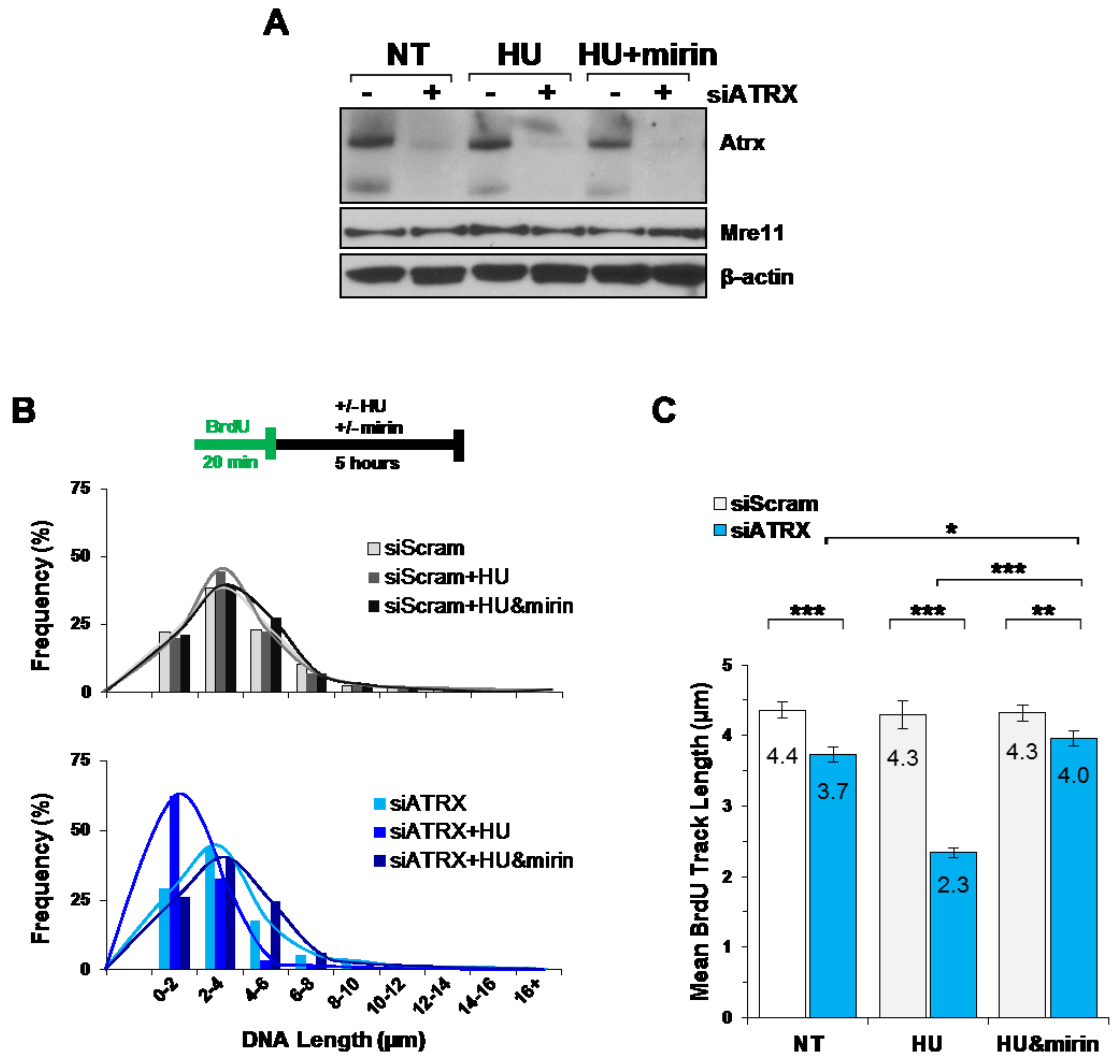

Figure 18. ATRX protects stalled DNA replication forks from degradation by MRE11 exonuclease activity.

(A) Representative western blot analysis demonstrating ATRX knockdown in HeLa cells after siATRX transfection alone (NT), or following hydroxyurea (HU), or HU and mirin treatments. Mre11 and β-actin were shown as loading controls.

(B) DNA fiber tract length distribution histogram of siScram- (top) and siATRX- (bottom) transfected HeLa cells at 72 h post-transfection. siRNA-treated cells were pulsed with BrdU and subsequently exposed to HU and mirin as indicated in the schematic. Total fibers counted for siScram experiment: no treatment, NT (n=1782); HU (n=1819); HU and mirin (n=1759). Total fibers counted for siATRX-treated cells: NT (n=1527); HU (n=1523); HU and mirin (n=1536). (C) Mean DNA fiber tract length ± 95% confidence intervals of experiments described in (A). **p-value<10^{-4} and ***p-value<10^{-15} calculated by Mann–Whitney U test.

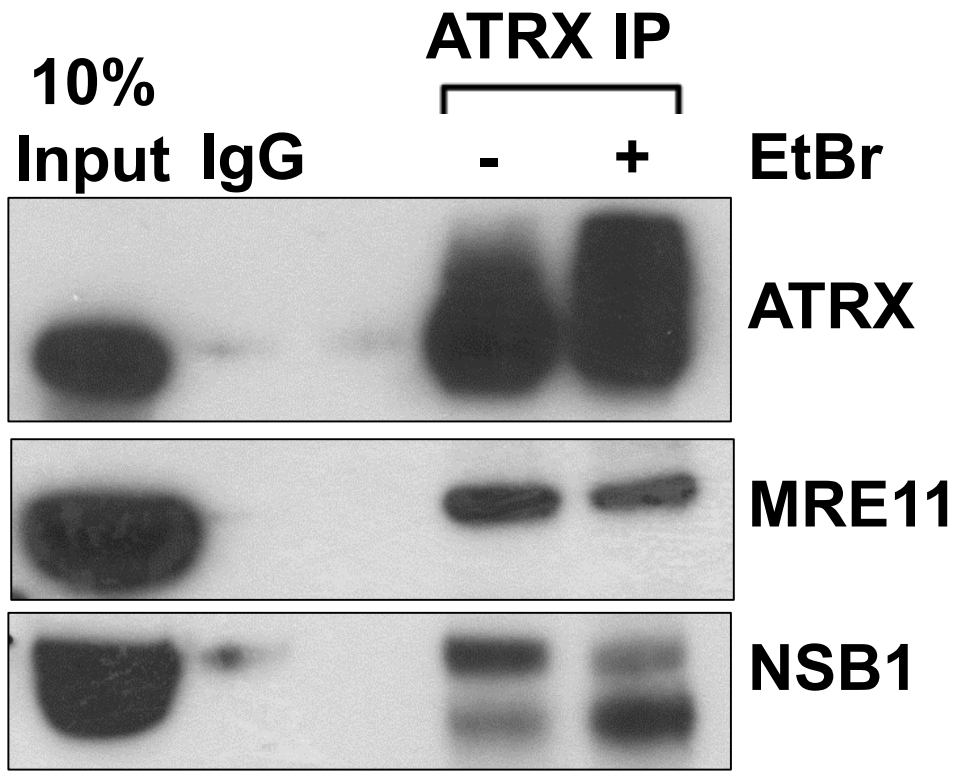

Figure 19. ATRX physically interacts with the MRN complex in a DNA-independent manner.

Co-immunoprecipitation of MRN with ATRX from HeLa cell nuclear lysates was resolved by western blot analysis and probed with antibodies specific for ATRX, as well as MRE11 and NBS1, two components of the MRN complex. Lysates were also treated with 100 µg/ml ethidium bromide (EtBr) to assess DNA dependent interactions. In, input; IgG, immunoprecipitates with rabbit IgG.

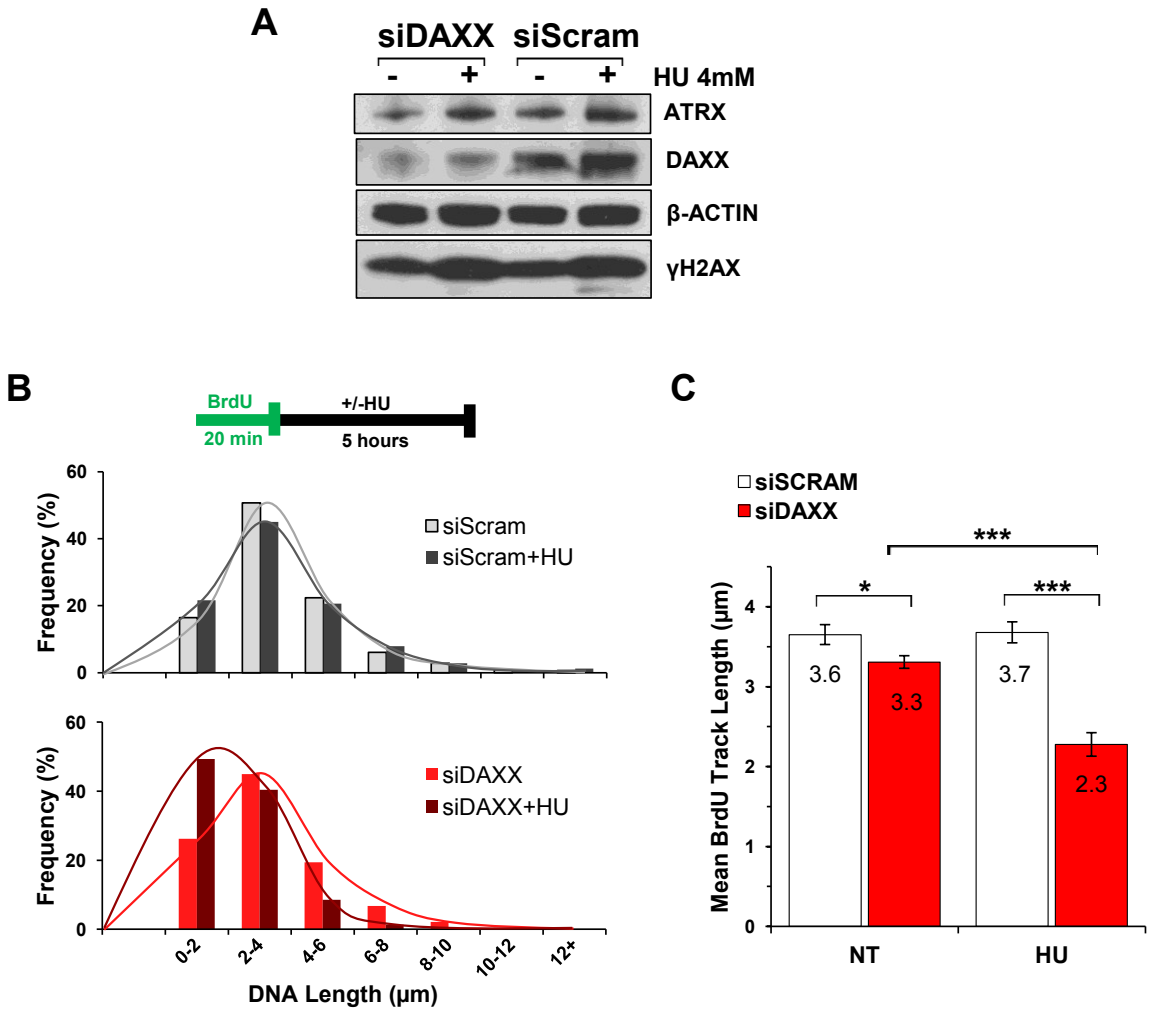

Figure 20. The ATRX-associated protein DAXX protects stalled DNA replication forks from degradation.

(A) Representative western blot analysis demonstrating DAXX knockdown in siDAXX treated cells compared to siScramble transfected cells, with (+) or without (-) HU treatment. ATRX expression appeared unaffected by siDAXX treatment and γH2AX appears to increase in expression upon HU treatment. β-actin was shown as a loading control. (B) DNA fiber tract length distribution histogram of siScram- (top) and siDAXX- (bottom) transfected HeLa cells at 72 h post-transfection. Fibers counted for siScram-treated cells were: NT (n=888); HU (n=998). Total fibers counted for siDAXX-treated cells were: NT (n=888) and HU (n=1171). (C) Mean DNA fiber tract length of experiments described in (B). For panels (b and d), the mean length±95% CI was plotted. *p-value<0.005 and ***p-value<10^{-15} calculated by Mann–Whitney U test.

4. Discussion

Intellectual disability may be the most important clinical manifestation of the ATR-X syndrome. While the features of the ATR-X syndrome are clinically heterogeneous and often range in severity, some individuals never develop the skills for communication, and are therefore ultimately unable to practice any significant form of self-determination. Consequently, while current treatments help manage the less severe symptoms, a further understanding of the neurodevelopmental deficits is required if a substantial treatment option is to be developed. In this study, we have explored the molecular mechanisms of the ATRX protein in the context of rapid cellular division, with a hypothesis that ATRX represses replication-induced genomic instability by reinforcing heterochromatin replication dynamics. We suggest that ATRX functions to facilitate the expansion of rapidly proliferating progenitor cells, such as NPCs required for corticogenesis. Accordingly, in the ATR-X syndrome, this molecular deficit propagates into a neurological deficit, encompassed by microcephaly and intellectual disability.

4.1.1 Neurological deficits of Atrx cKO mice

We examined the specific loss of Atrx during mouse telencephalon development and observed a positive correlation between Atrx loss and both microcephaly and increased DNA damage. Specifically, Atrx cKO perinates possessed significantly smaller cortices at E18.5, due to the loss of later-born, upper-layer neurons (**Figures 9 and 10**). Additionally, loss of Atrx expression during cortical development was correlated with hyperactive pATM, γH2A.X and Parp1 activity (**Figure 11**). In this regard, we propose a model to explain how the microcephaly associated with Atrx loss may be derived from replicative genomic instability (**Figure 21**). Neuronal progenitor cells proliferate and migrate from within the

VZ/SVZ and sequentially populate the distinct neuronal layers of the cortex starting in the DL and finishing with the UL (**Figure 21**). Each round of S-phase provides an opportunity for replication-induced DNA damage and because the NPCs that form the UL are also the most proliferative they will ultimately have the greatest potential to incur replication-induced DNA damage and subsequent genomic instability. While moderate levels of replicative genomic instability are present in the forebrains of healthy WT mouse embryos, the forebrains of Atrx cKO embryos experience elevated NPC genomic instability as early as E13.5, which specifically compromises the genesis of cells targeted for the upper neocortical layers (**Figure 21**).

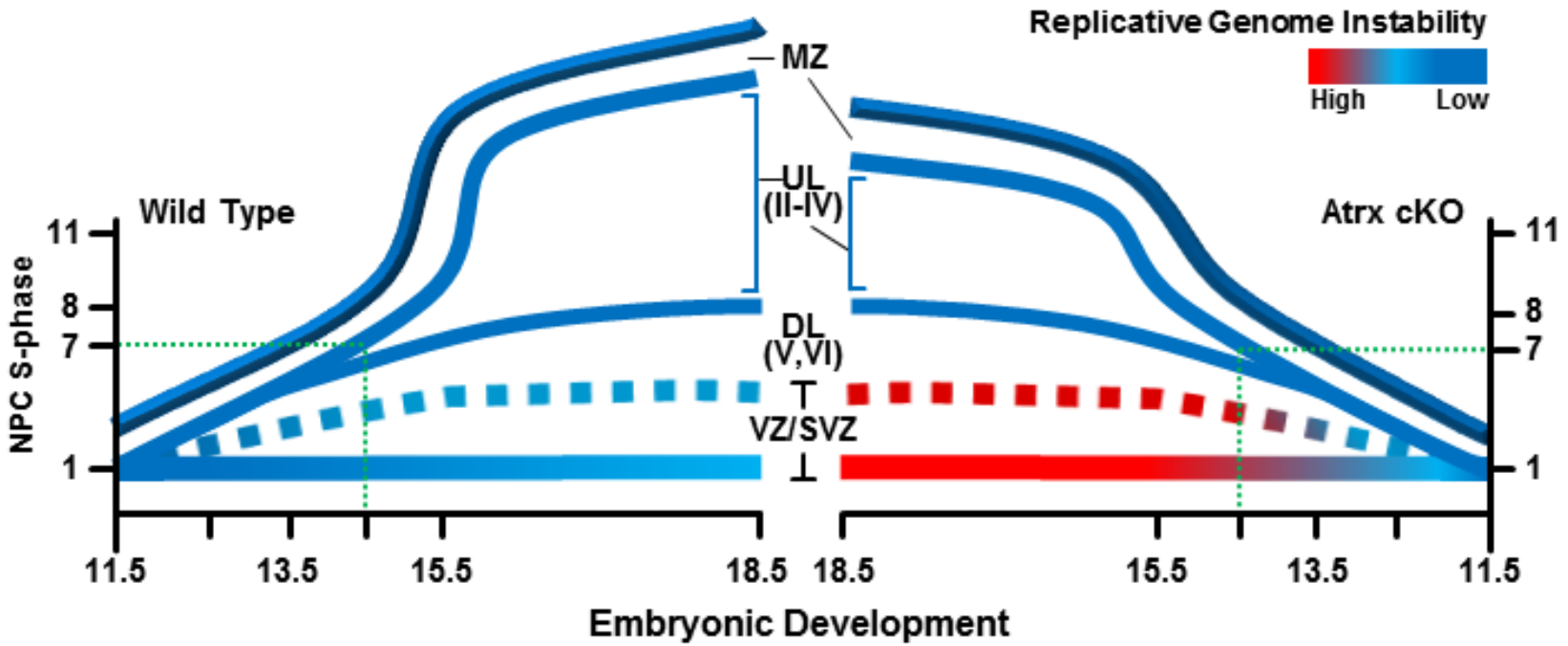

Figure 21. Developmental model of replication stress-induced loss of late-born neurons in the forebrains of Atrx cKO mice. The X axis shows the developmental time and the Y axis shows the number of cycles the NPCs have undergone. Dotted blue/red lines depict the subplate, while the solid blue lines indicate the boundaries of the deep (DL) and upper layer (UL) neurons. The blue/black line demarcates the marginal zone. Dotted green lines indicate the timing of progenitor cell loss. At this point, progenitors from Atrx cKO mice within the VZ/SVZ (red line) have high levels of genomic damage that compromise their survival, resulting in a smaller cortex by E18.5.

Previous studies have utilized the Foxg1Cre driver to examine Atrx ablation in NPCs of the developing cortex. The earliest study reported that cortical hypocellularity resulted from reduced neuronal migration into the superficial cortical layers, although normal embryonic neurogenesis was reported at up to E15.5 [103]. As we have reported, the neurogenic deficit observed in the Atrx cKO forebrains occurs in the latter-born, upper-layer neurons, which form after E15.5, thereby accounting for this discrepancy. Three additional follow-up studies have implicated the ATM-p53 DNA damage/cell-cycle checkpoint pathways with elevated cell-intrinsic apoptosis and neuronal loss in the Atrx cKO developing forebrain [104] [193] [105]. This directly supports our model and suggests that the genomic instability may lead to cell death. Alternatively, genomic instability could lead to premature cell-cycle exit and precarious differentiation, which would result in an increased population of early-born, lower-layer neurons.

A recent study has reported that Atrx cKO mice exhibit an expansion of cortical layer VI and depletion of cortical layers II–IV in the developed forebrain [106]. They propose that increased cell-cycle exit during early corticogenesis results in increased generation of Tbr1-labeled early-born neurons and deceased generation of later born Brn2-labeled upper layer neurons [106]. We had also observed an increase in Tbr1-labeled neurons and a decrease in Brn2-labeled neurons, although the quantification of these particular neuronal groups did not reach our threshold of statistical significance (p-values of 0.14 and 0.16, respectively) (**Figure 9**). Important for this matter, we also observed that Atrx cKO cortices contained ~20% fewer DAPI stained cells than their wild-type controls (**Figure 9**). In both studies, the quantification of labeled neurons was normalized to the total number of DAPI stained nuclei. Therefore, we interpreted the data as decreased proportion of later-born neurons, concurrently increases the proportion of earlier-born neurons, leading to their

overrepresentation. A neuronal birth-dating experiment would allow for the determination of layer-specific neurogenesis to further clarify this issue.

4.1.2 Caveats and considerations (*in vivo*)

In order to study Atrx ablation specifically in NPCs during telencephalon development, we utilized the Foxg1 promoter-driven Cre recombinase system [183]. The Foxg1Cre mouse line was generated by inserting the Cre-transgene into the Foxg1 locus, such that Cre recombinase was expressed under the promotor of Foxg1 [183]. This has the secondary consequence of disrupting Foxg1 expression from one allele, which has the potential to induce a haploinsufficiency phenotype. While this transgenic system has routinely been utilized for multiple transgenic mouse studies of forebrain development, it is important to note that mice homozygous for Foxg1Cre are embryonic lethal and the Foxg1Cre heterozygotes display a mild neurological phenotype [215] [216] [217] [183] [218]. Specifically, the superficial layers of the cortex are preferentially affected in adult Foxg1Cre mice [218]. We have reported a more severe deficit in the Atrx cKO mice, then what has been reported in the Foxg1Cre mice (**Figure 10**). Regardless, it is impossible to weigh the contribution of Foxg1 haploinsufficiency along with Atrx ablation in our transgenic system as we have reported thus far. Future studies must mitigate this unintended variable, to more accurately address Atrx's contribution to forebrain development.

An additional consideration must be addressed to highlight the differences between ATR-X syndrome and Atrx cKO mice. As stated, ATR-X syndrome is often caused by point mutations resulting in the lowered expression of a hypomorphic protein, while the Atrx cKO mice exhibit total ablation of the full length Atrx protein but maintain Atrx-t expression. This

fundamental difference is exemplified by the finding that total ablation of full length Atrx protein expression during mouse development is embryonic lethal, and although no longitudinal studies have been published, patients afflicted with ATR-X syndrome can survive well into adulthood [219] [14]. Atrx-t lacks the conserved ATPase/Helicase domain of the full-length Atrx protein and displays an altered, often lower, expression pattern compared to the full-length isoform (**Figure 2A**) [60]. Because Atrx-t cannot compensate for the lack of full-length Atrx expression during development, it suggests that the ATRXt protein is not required during early development or, that the ATPase/Helicase domain is a requisite for proper development. Evidently, it is unlikely that conditional ablation of Atrx in mice accurately mimics mutations in ATRX in humans, indicating a need for better transgenic models.

A requirement for an accurate transgenic mouse model is the equivalence between the mouse and human protein at the structural and functional levels. At least one line of evidence seems to suggest that the mouse and human ATRX proteins may have evolved different functions, implicating the nature of Atrx and ATRX target loci in mice and humans, respectively. ATRX and Atrx both bind to telomeres, centromeres and other repetitive DNA loci, with some of the highest reported enrichments at telomeres [24] [78] [80] [89]. Mouse telomeres are 5 to 10 times longer than human telomeres [220]. Therefore, we anticipate that the requirement for Atrx in mice may simply be greater than in humans, due to the genomic burden associated with more repetitive DNA at longer telomeres.

While the gross anatomical features of the mouse and human genomes may contribute to differences in their respective Atrx/ATRX functions, another line of evidence suggests a functional equivalence among placental mammals. Atrx appears to be indispensible for the development of the trophoblast in mice [219]. Unlike the embryonic genome, which is

heavily methylated, the trophoblast genomic DNA is hypomethylated, and Atrx has been directly implicated in the heterochromatinization of hypomethylated genomes at repetitive DNA [221] [80]. There have been no reports to suggest placental abnormalities with ATR-X syndrome, although ATR-X patients do display increased genomic hypomethylation [14] [222]. Perhaps the genomic stability requirements for both human and mouse trophoblast genomes are equivalent. Furthermore, the fact that patients with ATR-X syndrome produce some level of a hypomorphic protein may imply that the total absence of any Atrx in mice (or ATRX in humans) is incompatible with embryonic development.

4.1.3 Future directions (*in vivo*)

Due to the previously mentioned caveats regarding mouse models used to study ATR-X syndrome, we suggest two alternative approaches for future studies. First, a transgenic mouse line known as ATRX(ΔE2) has been developed, which phenocopies a known patient mutation [107]. By excising exon 2 of the mouse Atrx gene, the authors were able to mimic the R37X human mutation, which is known to cause a milder phenotype wherein a near-full length, N-terminally truncated protein possessing both the ADD and ATPase/Helicase domains is produced from an alternative transcript [20] [21]. These ΔE2 mice displayed impaired learning-memory and cognitive functions, which is accompanied by abnormal dendrite morphology concomitant with reduced Atrx protein expression [108] [107]. Only two studies have reported on these mice to date, perhaps due to their very mild phenotype which does not represent that typical form of the disease. However, their existence as the sole model of a patient mutation enforces a clinical relevance, which warrants further analysis. A second approach would be to develop additional models containing patient mutations, specifically targeting either the ADD or ATPase/Helicase domain. This approach could offer invaluable information regarding the significance of each structural domain, and

would more accurately model ATR-X syndrome in a clinically relevant fashion.

Additionally, we have characterized a DDR signaling pathway associated with ATRX deficiency that may offer valuable insight towards the development of a targeted therapy for ATR-X syndrome. Specifically, we have found that increased PARylation is associated with Parp1 automodification concomitant with Atrx loss during cortical development (**Figure 11**). We have further attributed this to PARP1 hyperactivation as response to replication-induced genomic instability, as per the findings of our *in vitro* experiments (**Figure 13**). Furthermore, our findings suggest that ATRX-deficient cells may be sensitive to PARP inhibition, which may reduce their proliferative velocity without inducing cell death (**Figure 15**). How this pathway relates to neurodevelopment in our Atrx cKO mice is a matter for further investigation.

Increased PARylation has a diverse range of functions in response to genotoxic stresses, including regulation of chromatin structure modulation, DNA repair, transcription, and cell death [223] [201]. Proteomic analysis has found that PARP1 activation is responsible for the majority PARylation in cells, with the next most productive polymerase, PARP2, only accounting for 15% [201]. Whether or not PARP1 hyperactivation, or any other form of increased PARylation, is actually relevant to ATR-X syndrome remains to be seen.

Some studies suggest that PARP1 inhibition may protect against various non-malignant, inflammatory neurological disorders [224]. Recent evidence has also demonstrated that neuronal death associated with perinatal hypoxia and axonal degeneration associated with neurotoxic chemical agents can be mitigated by PARP1 inhibition [225] [226]. Furthermore, rapidly proliferating cells are more sensitive to PARP activation than quiescent cells, due to the metabolic depletion of adenosine triphosphate (ATP) resulting from the increased

nicotinamide adenine dinucleotide (NAD) consumed through PARP activity [227] [228]. If this paradigm of PARP1-mediated neurotoxicity is consistent with Atrx cKO mice, then perhaps PARPi may offer an invaluable tool to develop treatments for ATR-X syndrome. However, other evidence suggests that it is entirely possible that increased PARylation may also be an indispensable compensatory mechanism required to maintain some level of genomic stability in DSBR-deficient cells [229] [230].Therefore, we propose that a further examination of this pathway is required *in vivo* to determine what role increased PARylation has during NPC replication in mouse models of ATR-X syndrome.

4.2.1 ATRX in heterochromatin biology

We examined the phenotype of ATRX-deficient HeLa cells to better understand how DNA-damage develops in our *in vivo* cortical model of Atrx loss. Just as with our *in vivo* analysis, we observed increased γH2A.X and pATM signalling in ATRX-deficient cells, which appeared to accumulate through DNA replication. To further dissect the elevated PAR signalling that we had observed *in vivo*, we utilized either a PARP1 KD approach or PARPi with PJ34, and found that the elevated PAR signalling in ATRX-deficient cells could be reduced. Furthermore, PJ34 treatment in ATRX deficient cells appeared to induce elevated genotoxicity and decreased cellular proliferation, compared to WT control cells. Next, we concentrated on ATRX's contributions specifically during DNA synthesis. We observed that ATRX localizes to late-replicating heterochromatin in proliferating HeLa cells. When we examined ATRX-deficient cells using the DNA fiber assay, we observed that ATRX-deficiency limits the production of nascent DNA fibers and chemical-induction of replication fork stalling results in the degradation of these nascent fibers in an MRE11-dependent manner. Finally, either siRNA-mediated BRCA1 or DAXX KD in HeLa cells produced similar results to ATRX deficiency by also producing a DNA replication fork protection insufficiency.

From our findings, we propose a model where ATRX functions throughout the cell cycle to ultimately facilitate DNA replication during S-phase and this function maintains the genomic stability during rapid cellular proliferation (**Figure 22**). The ATRX-DAXX histone chaperone complex deposits H3.3 at globally diffuse heterochromatic loci including telomeres, centromeres, differentially methylated regions (DMRs), CpG islands and endogenous retroviral elements (ERVs) in a replication-independent manner [77] [83] [82] [80]. While ATRX can recognize both the heterochromatin associated markers, HP1 and H3K9me3, its H3.3-chaperone function appears to be upstream of SUV39H and/or SETDB1-mediated H3K9 trimethylation [80] [81] [82] [83]. Additionally, ATRX's ability to bind to G4-structured DNA *in vitro*, as well as its high binding enrichment at G4-motif containing DNA sequences *in vivo* elicits the possibility that ATRX may recruit DAXX and H3.3 to G4 structured DNA for localized heterochromatinization [24] [89] [170].

Repetitive DNA, such as G4 motif DNA, is a poor substrate for nucleosome stability. Accordingly ATRX may maintain a compact heterochromatin state by ensuring histone occupancy, thereby preventing the formation of 2^{o} DNA structures, or activation of ERVs or imprinted genes [231] [232] [25] [82] [83]. Indeed, simple repeats such as G4 motifs represent regions of latent genomic instability as they are demonstrated to encumber the replication machinery [233] [146] [145] [149] [147]. Therefore, we propose that ATRX functions to maintain a condensed heterochromatin state, which is most important during G1-phase, in order to repress G4 DNA structures from inducing replication fork stalling events during S-phase (**Figures 22A and B**).

During S-phase we propose a mechanism wherein ATRX actively protects stalled replication forks within heterochromatin (**Figure 22B**). By adapting a previous model for ATRX

regarding telomere maintenance, we propose that ATRX physically sequesters MRE11 near replication forks to inhibit its exonuclease activity, thereby preventing fork degradation (**Figure 22B**) [136]. Accordingly, ATRX-deficiency leads to MRE11-mediated degradation of stalled replication forks, followed by loss of replication fork protection and attenuated replication fork restart (**Figure 22B**). Moreover, in the absence of ATRX, there is increased fork stalling due to the loss of heterochromatinization of repetitive sequences in other phases of the cell cycle that promotes non-B-DNA structures that impede the replisome during S-phase. Furthermore, MRE11-hyperactivity may induce a compensatory PARP1-mediated response (**Figure 22B**). This PARP1 activation has been suggested as a mechanism that engages at stalled replication forks to form a reversed fork or "chicken foot"-like structure to facilitate repair and restart [234]. Recent data has shown that ATRX-deficient cells are burdened by increased replication fork stalling events [84] [90]. Interestingly, our model suggests that ATRX-deficient cells consecutively encounter increased fork stalling events and then a deceased ability to appropriately process them. Ultimately, any unresolved replication intermediates may develop into DSBs during G2-phase, which can progress through mitosis and accumulate as genomic instability associated ATRX loss (**Figure 22C**).

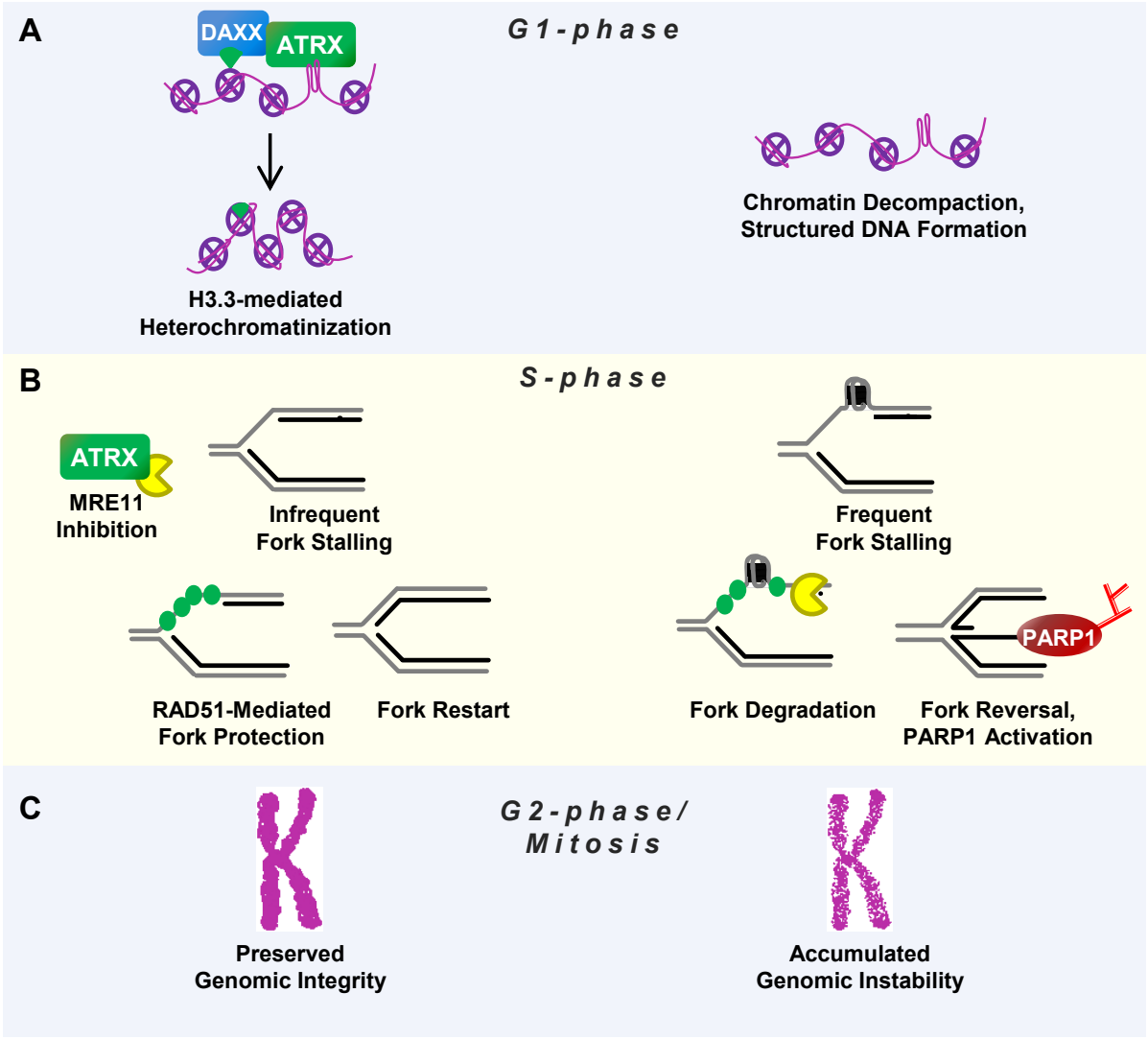

Figure 22. A model of how ATRX suppresses genomic instability during cellular proliferation. Relevant scenarios are shown during (a) G1 phase, (b) S phase and (C) G2/M phase in the presence (left) or absence (right) of ATRX. (a) During G1, ATRX localizes to decompacted and structured DNA (e.g. G4-DNA) along with DAXX to chaperone H3.3-H4 dimers that serve as a beacon for further heterochromatinization. When cells progress into the S phase (b), DNA replication forks experience more frequent stalling events when ATRX is absent owing to an increased incidence of structured DNA. ATRX physically interacts with MRE11 and inhibits excessive MRE11-mediated resectioning of stalled replication forks, which subsequently require RAD51-mediated protection of nascent DNA. In the absence of ATRX, PARP-1 activation is upregulated in an attempt to reverse stalled replication forks and protect against further MRE11 resectioning. Cells with frequent fork stalling that progress into the G2 phase and mitosis (c) are more prone to DSBs resulting in genomic instability.

4.2.2 Caveats and considerations (in vitro)

The defective growth properties of Atrx primary mouse cells has proven prohibitive for *in vitro* cultures, while immortalized cells that stably express shRNA specific for ATRX evolve means to re-express ATRX [97] [135] [219]. For this reason, we have chosen to examine the acute loss of ATRX expression mediated by siRNAs. While RNAi is an invaluable tool to study the loss of a particular gene's expression, it has several drawbacks including the potential for non-specific interactions with other mRNAs, as well as cellular toxicity to the transfection reagents or the exogenous RNA molecule itself. These drawbacks have been addressed in a thorough manner by carefully selecting specific siRNA sequences, as well as by using non-specific siRNAs for control WT cells. Furthermore, we have attempted to present our *in vitro* data as a complement to our *in vivo* data, when we lack the tools to adequately pursue a specific aim.

4.2.3 Future directions (in vitro)

Further experimentation is required to validate a role for ATRX at replication forks. How ATRX localizes to sites of active DNA replication and for what specific function, remain as open questions for future research. A clue may come from the SNF2-family member RAD54, which is an ATPase/Helicase domain paralog of ATRX. RAD54 functions during HR at DSBs and during HDR at stalled replication forks by facilitating stand invasion of the RAD51-coated ssDNA into the homologous dsDNA sequence [235] [236]. Recently, NEK1-mediated phosphorylation of RAD54 has been shown to be imperative for replication fork processing during S-phase and DSBR during late-G2 phase [237]. The NEK1 phosphorylation consensus site is a serine or threonine residue with phenylalanine 3 amino acids upstream [93]. Interestingly, ATRX shares this consensus site with RAD54 (**Figure**

23). Therefore, Ser2166 phosphorylation on ATRX may offer an avenue to study ATRX's function at replication forks, as well as at DSBs.

Figure 23. Amino acid sequence alignment of ATRX and RAD54 highlight a putative NEK1 phosphorylation site on ATRX. The ATRX paralog RAD54 is phosphorylated by NEK1 at Ser572 which is required for stalled replication fork processing. The homologous serine on ATRX at position 2166 may also be phosphorylated by NEK1 and this may regulate ATRX's function during replication. * implies a matched animo acid, : implies a similar amino acid and a blank space implies a dissimilar amino acid.

Evidence is mounting that ATRX may play a role during DSBR specifically within heterochromatin. Here, we suggest examining the fidelity and function of ATRX's interactions with the MRN, cohesin and DNAPK complexes, as it may relate to a role for ATRX during DSBR. Given the association of ATRX with repetitive DNA within heterochromatin, it is interestingly to speculate that ATRX may facilitate the DSBR pathway choice at these loci. Indeed, DSBR pathway choice is tightly regulated and dysregulation directly transmits into genomic instability [238]. For example, elevated HR and microhomology mediated end-joining (MMEJ) activation within repetitive DNA loci may increase the frequency of deleterious chromosome rearrangements arising from non-allelic homologous recombination (NAHR) events [239] [240] [241]. This would suggest that NHEJ would be the preferred DSBR pathway at repetitive DNA within heterochromatin, in order to suppress NAHR. However, some studies suggest that repetitive sequences in heterochromatin often rely on HR for their repair because NHEJ may result in inappropriate end-joining [238] [242] [243]. Interestingly, ATRX-null tumors may utilize NHEJ less frequently than tumors that express ATRX [244]. Furthermore, ATRX-null cancers appear to preferentially utilize a HR-like mechanism as a means to maintain telomere length, as discussed in the following sections.

Taken together, we suggest that further clarification on these matters regarding ATRX's role during DSBR, as well as DNA replication. *In vitro* analysis has found that patient mutations in the ATRX protein causes a nuclear mislocalization phenotype, while cell cycle-dependent phosphorylation events regulate its chromatin association [245] [68]. Using a molecular biology approach to create a phospho-mimic and an unphosphorylatable ATRX protein (Ser2166Glu and Ser2166Ala, respectively) would allow the investigation of whether or not this signalling event is required for ATRX's role during DSBR or at replication forks. Furthermore, utilizing the isolation of proteins on nascent DNA (iPOND) technique would

enable a proteomic analysis of the replisome in cells with or without ATRX protein [246]. Here we would anticipate the ATRX loss may lead to defective recruitment of protective machinery to the replication fork and increased recruitment of MRE11.

4.3.1 ATRX rises in notoriety

The first publication of ATRX with reference to ATR-X syndrome is dated to 1991 (**Figure 24**). Since that time, papers referring to ATR-X syndrome which make reference to the "mental retardation" associated with the syndrome have risen on average by a rate of ~1 publication (journal article or review) every 17 months (**Figure 24**). A topic that has gained recent attention quite rapidly in the ATRX field is cancer. This is thanks to the recent advances of Next-generation sequencing (NGS) technologies, which have been used to characterize the genomic diversity of different tumor types. The association of ATRX and cancer was first raised in 1997, when it was highlighted that ATRX's frequently mutated ATPase/Helicase domain bares a high degree of homology with the human RAD54 protein, which is often mutated in tumors [247]. This seemingly inconsequential observation became the harbinger of a rapidly developing field that would begin over a decade in the future. Since 2011, ATRX papers referencing "cancer" have risen at a rate of ~1 publication every month (**Figure 24**).

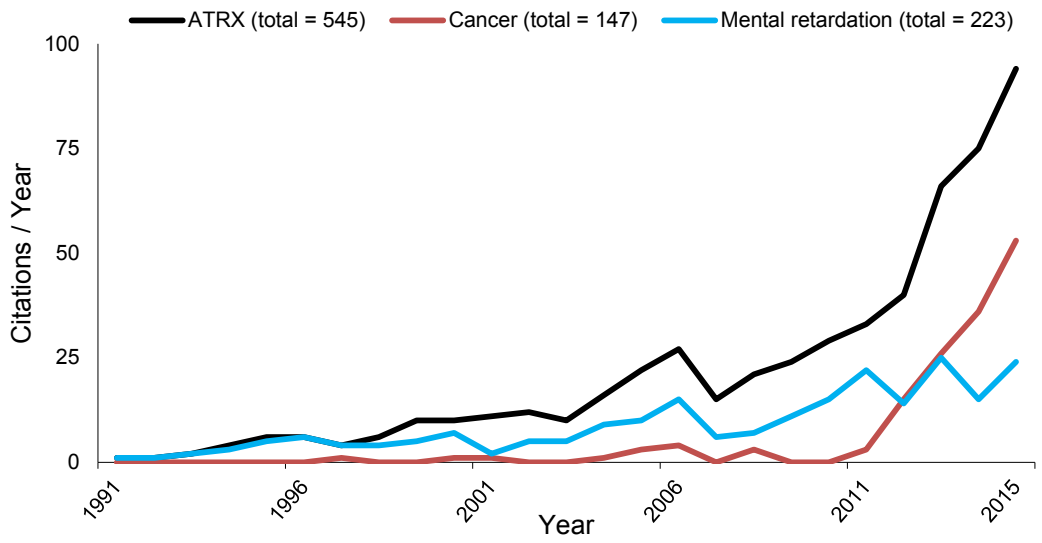

Figure 24. A timeline of ATRX in the literature.
Peer-reviewed articles and reviews with Titles, abstracts or keywords referring to "ATRX" and/or "ATR-X" (black line) and the subgroups including "Cancer" (red line) or "Mental retardation" (blue line) were gathered from the Scopus bibliographic database. The number of published articles and reviews per year were plot from the initial reference of ATRX/ATR-X, up to and including May 1st, 2016.

4.3.2 ATRX and the cancer connection

In their seminal reviews on the “Hallmarks of Cancer”, Hanahan and Weinberg emphasized “six biological capabilities acquired during the multistep development of human tumors … [including] sustaining proliferative signaling, evading growth suppressors, resisting cell death, enabling replicative immortality, inducing angiogenesis, and activating invasion and metastasis.” [130] [131]. Telomeres exist at the ends of linear chromosomes and shorten after each round of genome replication, unless a mechanism provides support to maintain telomere length. Their existence was proposed as a mechanism for a cell to maintain the integrity of its coding DNA from marginotomy, or the shortening of the replicon with respect to the template [248]. Cancer cells often acquire replicative immortality through the reactivation of the ribonucleoprotein enzyme known as telomerase to maintain telomere length [130]. At least 10% of cancers do not show any detectable levels of telomerase, but rather utilize a mechanism known as the Alternative Lengthening of Telomeres (ALT) when acquiring replicative immortality [249] [250].

Next-generation genome-wide sequencing has helped find mutations in the ATRX-DAXX-H3.3 chromatin remodeling pathway, which have been identified as drivers for the ALT phenotype and are often associated with p53 mutations and increased TERRA RNA expression [251] [252] [167] [253] [254] [255]. Significantly, ATRX localizes to telomeres with DAXX to deposit the histone 3 variant H3.3 into telomeric chromatin [76] [77] [78]. Conversely, reintroduction of ATRX into U2OS cells, which exhibit the ALT phenotype concomitant with loss of ATRX expression, resulted in H3.3 enrichment at telomeres followed by attenuated ALT characteristics [136].

Interestingly, in ATRX-negative ALT positive cancers, ATRX protein expression is

completely absent, either due to deletion or transcriptional repression of the *ATRX* gene [255]. This is in contrast to ATR-X syndrome, where afflicted patients present with hypomorphic mutations and only partially diminished protein expression [17] [15]. The requirement for some level of ATRX expression during development may be partially explained by the fact that in mice the total loss of Atrx expression results in embryonic lethality, owing to fatal defects in trophectoderm development [219]. This may explain that while total loss of ATRX expression is associated with the development of the ALT pathway in some cancers, patients with ATR-X syndrome are not reported to develop cancer at an increased frequency than normal individuals.

Another interesting feature of ALT is the apparent oncogenic bias for particular tissue lineages. Specifically, sarcomas, pancreatic neuroendocrine tumors and gliomas, but not carcinomas are biased towards the ALT pathway [256] [257] [253] [258] [259]. Whether this predisposition towards specific lineages over others is due to differences in the ease of telomerase activation or ATRX inactivation is yet to be fully uncovered, but this may provide an important avenue for oncological classification and targeted treatments in the future. In this regard, our findings that ATRX-null cells are sensitive to PARP1 inhibitors may offer further insight into mechanisms of ATRX function and highlight a potential treatment option for ALT+ cancers.

4.3.3 PARPi and ATRX-null cancers

ATRX loss in cancer facilitates the ALT pathway enabling an unlimited replicative capacity [255] [260]. In this regard, ATRX loss is believed to be a late oncogenic event, presumably after sufficient growth control checkpoints such as p53 have been eliminated. The instability of telomeric heterochromatin in the absence of ATRX facilitates telomere sister chromatid

exchange, which maintains telomere length in ALT. Thus, our finding that small molecule inhibition of PARP1 activity attenuated growth of ATRX deficient cells offers a potentially therapeutic avenue towards treatment of ALT positive cancers.

Targeting PARP in ATRX-deficient ALT positive cancers is analogous to PARPi treatment to eliminate BRCA1/2 deficient cancer cells [261] [262] [263]. BRCA deficiency has been attributed to the impaired homologous recombination characteristics of frequently occurring ovarian and breast cancers. PARPi treatments for these cancers are currently at Phases I, II and III clinical trials [264] [265] [266]. We propose that the increased PARP1 activity concomitant with elevated DNA damage and replication defects in ATRX-deficient cells, is a novel avenue to explore PARPi in ATRX-deficient ALT positive cancers.

4.4 Conclusion

ATRX dysregulation underlies the developmental disease known as ATR-X syndrome, as well as some cancers, which utilize the ALT pathway for replicative immortality. The neurological features of ATR-X syndrome include intellectual disability, often associated with microcephaly. We have posited that ATRX dysregulation impairs DNA replication fidelity, which ultimately results in DNA damage. The accumulation of unmitigated DNA damage in ATRX-deficient cells leads to genomic instability and cellular proliferation defects. Accordingly, when ATRX is lost in NPCs, a progressive defect ensues that preferentially affects progenitors undergoing the highest number of cycles. Therefore, during forebrain development, the later-born neurons of the upper cortical layers are most severely affected by ATRX loss, leading to microcephaly.

5. References

[1] D. Botstein, R. L. White, M. Skolnick and R. W. Davis, "Construction of a genetic linkage map in man using restriction fragment length polymorphisms," *Am. J. Hum. Genet.,* no. 32, pp. 314-31, 1980.

[2] D. Weatherall, D. Higgs, C. Bunch, J. Old, D. Hunt, L. Pressley, J. Clegg, N. Bethlenfalvay, S. Sjolin, R. Koler, E. Magenis, J. Francis and D. Bebbington, "Hemoglobin H disease and mental retardation: a new syndrome or a remarkable coincidence?," *N Engl J Med,* vol. 305, no. 11, pp. 607-12, 1981.

[3] A. Wilkie, H. Zeitlin, R. Lindenbaum, V. Buckle, N. Fischel-Ghodsian, D. Chui, D. Gardner-Medwin, M. MacGillivray, D. Weatherall and D. Higgs, "Clinical features and molecular analysis of the alpha thalassemia/mental retardation syndromes. II. Cases without detectable abnormality of the alpha globin complex.," *Am J Hum Genet.,* vol. 46, no. 6, pp. 1127-40, 1990.

[4] D. Higgs, M. Vickers, A. Wilkie, I. Pretorius, A. Jarman and D. Weatherall, "A review of the molecular genetics of the human alpha-globin gene cluster.," *Blood,* vol. 73, no. 5, pp. 1081-104, 1989.

[5] A. Wilkie, M. Pembrey, R. Gibbons, D. Higgs, M. Porteous, J. Burn and R. Winter, "The non-deletion type of alpha thalassaemia/mental retardation: a recognisable dysmorphic syndrome with X linked inheritance.," *J Med Genet,* vol. 28, no. 10, p. 724, 1991.

[6] R. Gibbons, A. Wilkie, D. Weatherall and D. Higgs, "A newly defined X linked mental retardation syndrome associated with alpha thalassaemia.," *J Med Genet,* vol. 28, no. 11, pp. 729-33, 1991.

[7] R. Gibbons, G. Suthers, A. Wilkie, V. Buckle and D. Higgs, "X-linked alpha-thalassemia/mental retardation (ATR-X) syndrome: localization to Xq12-q21.31 by X inactivation and linkage analysis.," *Am J Hum Genet.,* vol. 51, no. 5, pp. 1136-49, 1992.

[8] C. Houdayer, A. Toutain, N. Ronce, G. Lefort, P. Sarda, J. Taib, S. Briault, J. Lambert and C. Moraine, "X-linked alpha-thalassemia/mental retardation syndrome. Linkage analysis in a new family further supports localization in proximal Xq.," *Ann Genet.,* vol. 36, no. 4, pp. 194-9, 1993.

[9] L. Wang, A. Collins, S. Lawrence, B. Keats and N. Morton, "Integration of gene maps: chromosome X.," *Genomics.,* vol. 22, no. 3, pp. 590-604, 1994.

[10] R. Gibbons, D. Picketts, L. Villard and D. Higgs, "Mutations in a putative global transcriptional regulator cause X-linked mental retardation with alpha-thalassemia (ATR-X syndrome).," *Cell,* vol. 80, no. 6, pp. 837-45, 1995.

[11] R. Gibbons and D. Higgs, "Molecular-clinical spectrum of the ATR-X syndrome," *Am J Med Genet,* vol. 97, no. 3, pp. 204-12, 2000.

[12] R. Gibbons, T. Wada, C. Fisher, Malik, N, M. Mitson, D. Steensma, A. Fryer, D. Goudie, I. Krantz and J. Traeger-Synodinos, "Mutations in the chromatin-associated protein ATRX.," *Hum. Mutat.,* vol. 29, pp. 796-802, 2008.

[13] S. Moncini, M. Bedeschi, P. Castronovo, M. Crippa, M. Calvello, R. Garghentino, G. Scuvera, P. Finelli and M. Venturin, "ATRX mutation in two adult brothers with non-specific moderate intellectual disability identified by exome sequencing.," *Meta Gene,* vol. 29, no. 1, pp. 102-8, 2013.

[14] R. Gibbons, "Alpha thalassaemia-mental retardation, X linked.," *Orphanet J. Rare Dis.,* p. 15, 2006.

[15] R. Gibbons, T. Wada, C. Fisher, N. Malik, M. Mitson, D. Steensma, A. Fryer, D. Goudie, I. Krantz and J. Traeger-Synodinos, "Mutations in the chromatin-associated protein ATRX.," *Hum Mutat,* vol. 29, no. 6, pp. 769-802, 2008.

[16] S. Iwase, B. Xiang, S. Ghosh, T. Ren, P. Lewis, J. Cochrane, C. Allis, D. Picketts, D. Patel, H. Li and Y. Shi, "ATRX ADD domain links an atypical histone methylation recognition mechanism to human mental-retardation syndrome.," *Nat.Struct.Mol.Biol.,* vol. 18, pp. 769-76, 2011.

[17] M. Howard, N. Malik, C. Anderson, J. Voskuil, J. Atkins and R. Gibbons, "Attenuation of an amino-terminal premature stop codon mutation in the ATRX gene by an alternative mode of translational initiation.," *J Med Genet,* vol. 41, no. 12, pp. 951-6, 2004.

[18] C. Badens, C. Lacoste, N. Philip, N. Martini, S. Courrier, F. Giuliano, A. Verloes, A. Munnich, B. Leheup, L. Burglen, S. Odent, H. Van Esch and N. Levy, "Mutations in PHD-like domain of the ATRX gene correlate with severe psychomotor impairment and severe urogenital abnormalities in patients with ATRX syndrome.," *Clin Genet,* vol. 70, no. 1, pp. 57-62, 2006.

[19] A. Argentaro, J. Yang, L. Chapman, M. Kowalczyk, R. Gibbons, D. Higgs, D. Neuhaus and D. Rhodes, "Structural consequences of disease-causing mutations in the ATRX-DNMT3-DNMT3L (ADD) domain of the chromatin-associated protein ATRX.," *Proc.Natl.Acad.Sci.USA,* vol. 104, pp. 11939-44, 2007.

[20] F. Abidi, C. Cardoso, A. Lossi, R. Lowry, D. Depetris, M. Mattéi, H. Lubs, R. Stevenson, M. Fontes, A. Chudley and C. Schwartz, "Mutation in the 5' alternatively spliced region of the

XNP/ATR-X gene causes Chudley-Lowry syndrome.," *Eur J Hum Genet.,* vol. 13, no. 2, pp. 176-83, 2005.

[21] M. Basehore, R. Michaelson-Cohen, E. Levy-Lahad, C. Sismani, L. Bird, M. Friez, T. Walsh, F. Abidi, L. Holloway, C. Skinner, S. McGee, A. Alexandrou, M. Syrrou, P. Patsalis, G. Raymond, T. Wang, C. Schwartz, M. King and R. Stevenson, "Alpha-thalassemia intellectual disability: variable phenotypic expression among males with a recurrent nonsense mutation - c.109C>T (p.R37X).," *Clin Genet,* vol. 87, no. 5, pp. 461-6, 2015.

[22] M. Mitson, L. Kelley, M. Sternberg, D. Higgs and R. Gibbons, "Functional significance of mutations in the Snf2 domain of ATRX.," *Hum Mol Genet,* vol. 20, no. 13, pp. 2603-10, 2011.

[23] L. Villard, D. Lacombe and M. Fontés, "A point mutation in the XNP gene, associated with an ATR-X phenotype without alpha-thalassemia.," *Eur J Hum Genet,* vol. 4, no. 6, pp. 316-20, 1996.

[24] M. Law, K. Lower, H. Voon, J. Hughes, D. Garrick, V. Viprakasit, M. Mitson, M. De Gobbi, M. Marra, A. Morris, A. Abbott, S. Wilder, S. Taylor, G. Santos, J. Cross, H. Ayyub, S. Jones, J. Ragoussis, D. Rhodes, I. Dunham, D. Higgs and R. Gibbons, "ATR-X syndrome protein targets tandem repeats and influences allele-specific expression in a size-dependent manner.," *Cell,* vol. 143, no. 3, pp. 367-78, 2010.

[25] Y. Li, J. Syed, Y. Suzuki, S. Asamitsu, N. Shioda, T. Wada and H. Sugiyama, "Effect of ATRX and G-Quadruplex Formation by the VNTR Sequence on α-Globin Gene Expression.," *Chembiochem.,* vol. 17, no. 10, pp. 928-35, 2016.

[26] A. Ion, L. Telvi, J. Chaussain, F. Galacteros, J. Valayer, M. Fellous and K. McElreavey, "A novel mutation in the putative DNA helicase XH2 is responsible for male-to-female sex reversal associated with an atypical form of the ATR-X syndrome.," *Am J Hum Genet.,* vol. 58, no. 6, pp. 1185-91, 1996.

[27] D. Picketts, D. Higgs, S. Bachoo, D. Blake, O. Quarrell and R. Gibbons, "ATRX encodes a novel member of the SNF2 family of proteins: mutations point to a common mechanism underlying the ATR-X syndrome.," *Hum Mol Genet. ,* vol. 5, no. 12, pp. 1899-907, 1996.

[28] L. Villard, A. Toutain, A. Lossi, J. Gecz, C. Houdayer, C. Moraine and M. Fontès, "Splicing mutation in the ATR-X gene can lead to a dysmorphic mental retardation phenotype without alpha-thalassemia.," *Am J Hum Genet,* vol. 58, no. 3, pp. 499-505, 1996.

[29] L. Villard, J. Gecz, J. Mattéi, M. Fontés, P. Saugier-Veber, A. Munnich and S. Lyonnet, "XNP mutation in a large family with Juberg-Marsidi syndrome.," *Nat Genet.,* vol. 12, no. 4, pp. 359-60, 1996.

[30] R. Gibbons, S. Bachoo, D. Picketts, S. Aftimos, B. Asenbauer, J. Bergoffen, S. Berry, N. Dahl, A. Fryer, K. Keppler, K. Kurosawa, M. Levin, M. Masuno, G. Neri, M. Pierpont, S. Slaney and D. Higgs, "Mutations in transcriptional regulator ATRX establish the functional significance of a PHD-like domain.," *Nat Genet,* vol. 17, no. 2, pp. 146-8, 1997.

[31] M. Fichera, C. Romano, L. Castiglia, P. Failla, C. Ruberto, S. Amata, D. Greco, C. Cardoso, M. Fontés and A. Ragusa, "New mutations in XNP/ATR-X gene: a further contribution to genotype/phenotype relationship in ATR/X syndrome. Mutations in brief no. 176.," *Hum Mutat.,* vol. 12, no. 3, p. 214, 1998.

[32] F. Abidi, C. Schwartz, N. Carpenter, L. Villard, M. Fontés and M. Curtis, "Carpenter-Waziri syndrome results from a mutation in XNP.," *Am J Med Genet. ,* vol. 85, no. 3, pp. 249-51, 1999.

[33] A. Lossi, J. Millán, L. Villard, C. Orellana, C. Cardoso, F. Prieto, M. Fontés and F. Martínez, "Mutation of the XNP/ATR-X gene in a family with severe mental retardation, spastic paraplegia and skewed pattern of X inactivation: demonstration that the mutation is involved in the inactivation bias.," *Am J Hum Genet,* vol. 65, no. 2, pp. 558-62, 1999.

[34] L. Villard, M. Bonino, F. Abidi, A. Ragusa, J. Belougne, A. Lossi, L. Seaver, J. Bonnefont, C. Romano, M. Fichera, D. Lacombe, A. Hanauer, N. Philip, C. Schwartz and M. Fontés, "Evaluation of a mutation screening strategy for sporadic cases of ATR-X syndrome.," *J Med Genet,* vol. 36, no. 3, pp. 183-6, 1999.

[35] T. Wada, T. Kubota, Y. Fukushima and S. Saitoh, "Molecular genetic study of japanese patients with X-linked alpha-thalassemia/mental retardation syndrome (ATR-X).," *Am J Med Genet,* vol. 94, no. 3, pp. 242-8, 2000.

[36] L. Villard, M. Fontès, L. Adès and J. Gecz, "Identification of a mutation in the XNP/ATR-X gene in a family reported as Smith-Fineman-Myers syndrome.," *Am J Med Genet,* vol. 91, no. 1, pp. 83-5, 2000.

[37] R. Guerrini, J. Shanahan, R. Carrozzo, P. Bonanni, D. Higgs and R. Gibbons, "A nonsense mutation of the ATRX gene causing mild mental retardation and epilepsy.," *Ann Neurol,* vol. 47, no. 1, pp. 117-21, 2000.

[38] M. Fichera, M. Silengo, A. Spalletta, M. Giudice, C. Romano and A. Ragusa, "Prenatal diagnosis of ATR-X syndrome in a fetus with a new G>T splicing mutation in the XNP/ATR-X gene.," *Prenat Diagn.,* vol. 21, no. 9, pp. 747-51, 2001.

[39] H. Yntema, F. Poppelaars, E. Derksen, A. Oudakker, T. van Roosmalen, A. Jacobs, H. Obbema, H. Brunner, B. Hamel and H. van Bokhoven, "Expanding phenotype of XNP mutations: mild to moderate mental retardation.," *Am J Med Genet,* vol. 110, no. 3, pp. 243-7, 2002.

[40] E. Borgione, M. Sturnio, A. Spalletta, L. Angela, M. Giudice, L. Castiglia, O. Galesi, A. Ragusa and M. Fichera, "Mutational analysis of the ATRX gene by DGGE: a powerful diagnostic approach for the ATRX syndrome.," *Hum Mutat.,* vol. 21, no. 5, pp. 529-34, 2003.

[41] F. Giuliano, C. Badens, C. Richelme, N. Levy and J. Lambert, "[ATR-X syndrome: a new mutation in the XNP/ATRX gene near the helicase domain].," *Arch Pediatr. ,* vol. 12, no. 9, pp. 1372-5, 2005.

[42] I. Wieland, J. Sabathil, A. Ostendorf, O. Rittinger, A. Röpke, B. Winnepenninckx, F. Kooy, E. Holinski-Feder and P. Wieacker, "A missense mutation in the coiled-coil motif of the HP1-interacting domain of ATR-X in a family with X-linked mental retardation.," *Neurogenetics,* vol. 6, no. 1, pp. 45-7, 2005.

[43] R. Leahy, R. Philip, R. Gibbons, C. Fisher, M. Suri and W. Reardon, "Asplenia in ATR-X syndrome: a second report.," *Am J Med Genet A.,* vol. 139, no. 1, pp. 137-9, 2005.

[44] M. Falco, D. Luciano, M. Sturnio, A. Spalletta, D. Scionti, M. Lo Giudice, C. Romano and M. Fichera, "Denaturing HPLC-based assay for detection of ATRX gene mutations.," *Clin Chem,* vol. 51, no. 7, pp. 1314-5, 2005.

[45] C. Badens, C. Lacoste, N. Philip, N. Martini, S. Courrier, F. Giuliano, A. Verloes, A. Munnich, B. Leheup, L. Burglen, S. Odent, H. Van Esch and N. Levy, "Mutations in PHD-like domain of the ATRX gene correlate with severe psychomotor impairment and severe urogenital abnormalities in patients with ATRX syndrome.," *Clin Genet,* vol. 70, no. 1, pp. 57-62, 2006.

[46] T. Wada, M. Sakakibara, Y. Fukushima and S. Saitoh, "A novel splicing mutation of the ATRX gene in ATR-X syndrome.," *Brain Dev.,* vol. 28, no. 5, pp. 322-5, 2006.

[47] T. Wada, Y. Fukushima and S. Saitoh, "A new detection method for ATRX gene mutations using a mismatch-specific endonuclease.," *Am J Med Genet A,* vol. 140, no. 14., pp. 1519-23, 2006.

[48] B. Thienpont, T. de Ravel, H. Van Esch, D. Van Schoubroeck, P. Moerman, J. Vermeesch, J. Fryns, G. Froyen, C. Lacoste, C. Badens and K. Devriendt, "Partial duplications of the ATRX gene cause the ATR-X syndrome.," *Eur J Hum Genet,* vol. 15, no. 10, pp. 1094-7, 2007.

[49] D. Cohn, R. Pagon, L. Hudgins, C. Schwartz, R. Stevenson and M. Friez, "Partial ATRX gene duplication causes ATR-X syndrome.," *Am J Med Genet A.,* vol. 149A, no. 10, pp. 2317-20, 2009.

[50] L. Jensen, W. Chen, B. Moser, B. Lipkowitz, C. Schroeder, L. Musante, A. Tzschach, V. Kalscheuer, E. H. van, J. Chelly, A. de Brouwer, A. Hackett, S. van der Haar, W. Henn, J. Gecz, O. Riess, M. Bonin, R. Reinhardt, H. Ropers and A. Kuss, "Hybridisation-based resequencing of 17 X-linked intellectual disability genes in 135 patients reveals novel mutations in ATRX, SLC6A8

and PQBP1.," *Eur J Hum Genet.,* vol. 19, no. 6, pp. 717-20, 2011.

[51] K. Yun, S. Chae, J. Lee, S. Yun, B. Yoo, I. Lim, E. Choi and M. Lee, "The first case of X-linked Alpha-thalassemia/mental retardation (ATR-X) syndrome in Korea.," *J Korean Med Sci,* vol. 26, no. 1, pp. 146-9, 2011.

[52] S. Thakur, M. Ishrie, R. Saxena, S. Danda, R. Linda, A. Viswabandya and I. Verma, "ATR-X syndrome in two siblings with a novel mutation (c.6718C>T mutation in exon 31).," *Indian J Med Res,* vol. 134, pp. 483-6, 2011.

[53] S. Lin, H. Sun, X. Song, L. Chen, M. Du and Z. Chen, "[Mutation analysis for a Chinese family featuring X-linked alpha thalassemia/mental retardation syndrome].," *Zhonghua Yi Xue Yi Chuan Xue Za Zhi,* vol. 30, no. 6, pp. 654-8, 2013.

[54] T. Wada, H. Ban, M. Matsufuji, N. Okamoto, K. Enomoto, K. Kurosawa and N. Aida, "Neuroradiologic features in X-linked α-thalassemia/mental retardation syndrome.," *AJNR Am J Neuroradiol,* vol. 34, no. 10, pp. 2034-8, 2013.

[55] C. Lacoste, B. Leheup, I. Agouti, D. Mowat, F. Giuliano and C. Badens, "Mutations of codon 2085 in the helicase domain of ATRX are recurrent and cause ATRX syndrome.," *Clin Genet,* vol. 86, no. 5, pp. 502-3, 2014.

[56] H. Shimbo, S. Ninomiya, K. Kurosawa and T. Wada, "A case report of two brothers with ATR-X syndrome due to low maternal frequency of somatic mosaicism for an intragenic deletion in the ATRX.," *J Hum Genet,* vol. 59, no. 7, pp. 408-10, 2014.

[57] J. Lee, S. Lee, B. Lim, K. Kim, Y. Hwang, M. Choi and J. Chae, "Alpha-thalassemia X-linked intellectual disability syndrome identified by whole exome sequencing in two boys with white matter changes and developmental retardation.," *Gene,* vol. 569, no. 2, pp. 318-22, 2015.

[58] A. Al-Nafie, J. Borgio, S. AbdulAzeez, A. Al-Suliman, F. Qaw, Z. Naserullah, S. Al-Jarrash, M. Al-Madan, R. Al-Ali, M. AlKhalifah, F. Al-Muhanna, M. Steinberg and A. Al-Ali, "Co-inheritance of novel ATRX gene mutation and globin (α & β) gene mutations in transfusion dependent beta-thalassemia patients.," *Blood Cells Mol Dis,* vol. 55, no. 1, pp. 27-9, 2015.

[59] A. Hamzeh, P. Nair, M. Mohamed, F. Saif, N. Tawfiq, M. Al-Ali and F. Bastaki, "A novel missense mutation in ATRX uncovered in a Yemeni family leads to alpha-thalassemia/mental retardation syndrome without alpha-thalassemia.," *Ir J Med Sci,* pp. DOI 10.1007/s11845-016-1418-6, 2016.

[60] D. Garrick, V. Samara, T. McDowell, A. Smith, L. Dobbie, D. Higgs and R. Gibbons, "A conserved truncated isoform of the ATR-X syndrome protein lacking the SWI/SNF-homology domain.,"

Gene, vol. 326, pp. 23-34, 2004.

[61] C. Stayton, B. Dabovic, M. Gulisano, J. Gecz, V. Broccoli, S. Giovanazzi, M. Bossolasco, L. Monaco, S. Rastan, E. Boncinelli, M. Blanchil and G. Consalez, "Cloning and characterization of a new human Xq13 gene, encoding a putative helicase.," *Hum Mol Genet,* vol. 3, no. 11, pp. 1957-64, 1994.

[62] S. Eustermann, J. Yang, M. Law, R. Amos, L. Chapman, C. Jelinska, D. Garrick, D. Clynes, R. Gibbons, D. Rhodes, D. Higgs and D. Neuhaus, "Combinatorial readout of histone H3 modifications specifies localization of ATRX to heterochromatin.," *Nat Struct Mol Biol.,* vol. 18, no. 7, pp. 777-82, 2011.

[63] K. Noh, I. Maze, D. Zhao, B. Xiang, W. Wenderski, P. Lewis, L. Shen, H. Li and C. Allis, "ATRX tolerates activity-dependent histone H3 methyl/phos switching to maintain repetitive element silencing in neurons.," *Proc Natl Acad Sci U S A.,* 2014.

[64] J. Peng and J. Xu, "RaptorX: exploiting structure information for protein alignment by statistical inference.," *Proteins,* vol. 79, no. 10, pp. 161-71, 2011.

[65] M. Källberg, H. Wang, S. Wang, J. Peng, Z. Wang, H. Lu and J. Xu, "Template-based protein structure modeling using the RaptorX web server.," *Nat Protoc,* vol. 7, no. 8, pp. 1511-22, 2012.

[66] M. Wakamori, Y. Fujii, N. Suka, M. Shirouzu, K. Sakamoto, T. Umehara and S. Yokoyama, "Intra- and inter-nucleosomal interactions of the histone H4 tail revealed with a human nucleosome core particle with genetically-incorporated H4 tetra-acetylation.," *Sci Rep,* vol. 5, no. 17204, p. doi: 10.1038/srep17204, 2015.

[67] A. Dhayalan, R. Tamas, I. Bock, A. Tattermusch, E. Dimitrova, S. Kudithipudi, S. Ragozin and A. Jeltsch, "The ATRX-ADD domain binds to H3 tail peptides and reads the combined methylation state of K4 and K9.," *Hum Mol Genet.,* vol. 20, no. 11, pp. 2195-203, 2011.

[68] N. Bérubé, C. Smeenk and D. Picketts, "Cell cycle-dependent phosphorylation of the ATRX protein correlates with changes in nuclear matrix and chromatin association.," *Hum Mol Genet,* vol. 9, no. 4, pp. 539-47, 2000.

[69] K. Ratnakumar, L. Duarte, G. LeRoy, D. Hasson, D. Smeets, C. Vardabasso, C. Bönisch, T. Zeng, B. Xiang, D. Zhang, H. Li, X. Wang, S. Hake, L. Schermelleh, B. Garcia and E. Bernstein, "ATRX-mediated chromatin association of histone variant macroH2A1 regulates α-globin expression.," *Genes Dev.,* vol. 26, no. 5, pp. 433-8, 2012.

[70] M. Ramamoorthy and S. Smith, "Loss of ATRX Suppresses Resolution of Telomere Cohesion to

Control Recombination in ALT Cancer Cells.," *Cancer Cell. ,* vol. 28, no. 3, pp. 357-69, 2015.

[71] X. Nan, J. Hou, A. Maclean, J. Nasir, M. Lafuente, X. Shu, S. Kriaucionis and A. Bird, "Interaction between chromatin proteins MECP2 and ATRX is disrupted by mutations that cause inherited mental retardation.," *Proc Natl Acad Sci U S A,* vol. 104, no. 8, pp. 2709-14, 2007.

[72] M. Hein, N. Hubner, I. Poser, J. Cox, N. Nagaraj, Y. Toyoda, I. Gak, I. Weisswange, J. Mansfeld, F. Buchholz, A. Hyman and M. Mann, "A human interactome in three quantitative dimensions organized by stoichiometries and abundances.," *Cell,* vol. 163, no. 3, pp. 712-723, 2015.

[73] K. Kernohan, Y. Jiang, D. Tremblay, A. Bonvissuto, J. Eubanks, M. Mann and N. Bérubé, "ATRX partners with cohesin and MeCP2 and contributes to developmental silencing of imprinted genes in the brain.," *Dev Cell,* vol. 18, no. 2, pp. 191-202, 2010.

[74] Y. Xue, R. Gibbons, Z. Yan, D. Yang, T. McDowell, S. Sechi, J. Qin, S. Zhou, D. Higgs and W. Wang, "The ATRX syndrome protein forms a chromatin-remodeling complex with Daxx and localizes in promyelocytic leukemia nuclear bodies.," *Proc Natl Acad Sci U S A.,* vol. 100, no. 19, pp. 10635-40, 2003.

[75] J. Tang, S. Wu, H. Liu, R. Stratt, O. Barak, R. Shiekhattar, D. Picketts and X. Yang, "A novel transcription regulatory complex containing death domain-associated protein and the ATR-X syndrome protein.," *J Biol Chem,* vol. 279, no. 19, pp. 20369-77, 2004.

[76] L. Wong, J. McGhie, M. Sim, M. Anderson, S. Ahn, R. Hannan, A. George, K. Morgan, J. Mann and K. Choo, "ATRX interacts with H3.3 in maintaining telomere structural integrity in pluripotent embryonic stem cells.," *Genome Res,* vol. 20, no. 3, pp. 351-60, 2010.

[77] A. Goldberg, L. Banaszynski, K. Noh, P. Lewis, S. Elsaesser, S. Stadler, S. Dewell, M. Law, X. Guo, X. Li, D. Wen, A. Chapgier, R. DeKelver, J. Miller, Y. Lee, E. Boydston, R. ... Gibbons, D. Higgs, I. Cristea, F. Urnov, D. Zheng and C. Allis, "Distinct factors control histone variant H3.3 localization at specific genomic regions.," *Cell,* vol. 140, no. 5, pp. 678-91, 2010.

[78] P. Lewis, S. Elsaesser, K. Noh, S. Stadler and C. Allis, "Daxx is an H3.3-specific histone chaperone and cooperates with ATRX in replication-independent chromatin assembly at telomeres.," *Proc Natl Acad Sci U S A.,* vol. 107, no. 32, pp. 14075-80, 2010.

[79] S. Elsässer, H. Huang, P. Lewis, J. Chin, C. Allis and D. Patel, "DAXX envelops a histone H3.3-H4 dimer for H3.3-specific recognition.," *Nature,* vol. 491, no. 7425, pp. 560-5, 2012.

[80] Q. He, H. Kim, R. Huang, W. Lu, M. Tang, F. Shi, D. Yang, X. Zhang, J. Huang, D. Liu and Z. Songyang, "The Daxx/Atrx Complex Protects Tandem Repetitive Elements during DNA Hypomethylation by Promoting H3K9 Trimethylation.," *Cell Stem Cell,* vol. 17, no. 3, pp. 273-

86, 2015.

[81] M. Udugama, F. M Chang, F. Chan, M. Tang, H. Pickett, J. R McGhie, L. Mayne, P. Collas, J. Mann and L. Wong, "Histone variant H3.3 provides the heterochromatic H3 lysine 9 tri-methylation mark at telomeres.," *Nucleic Acids Res.,* vol. 43, no. 21, pp. 10227-37, 2015.

[82] S. Elsässer, K. Noh, N. Diaz, C. Allis and L. Banaszynski, "Histone H3.3 is required for endogenous retroviral element silencing in embryonic stem cells.," *Nature,* vol. 522, no. 7555, pp. 240-4, 2015.

[83] H. Voon, J. Hughes, C. Rode, I. De La Rosa-Velázquez, T. Jenuwein, R. Feil, D. Higgs and R. Gibbons, "ATRX Plays a Key Role in Maintaining Silencing at Interstitial Heterochromatic Loci and Imprinted Genes.," *Cell Rep.,* vol. 11, no. 3, pp. 405-18, 2015.

[84] J. Leung, G. Ghosal, W. Wang, X. Shen, J. Wang, L. Li and J. Chen, "Alpha thalassemia/mental retardation syndrome X-linked gene product ATRX is required for proper replication restart and cellular resistance to replication stress.," *J Biol Chem,* vol. 228, no. 9, pp. 6342-50, 2013.

[85] C. Cardoso, S. Timsit, L. Villard, M. Khrestchatisky, M. Fontès and L. Colleaux, "Specific interaction between the XNP/ATR-X gene product and the SET domain of the human EZH2 protein.," *Hum Mol Genet.,* vol. 7, no. 4, pp. 679-84, 1998.

[86] A. Kuzmichev, K. Nishioka, H. Erdjument-Bromage, P. Tempst and D. Reinberg, "Histone methyltransferase activity associated with a human multiprotein complex containing the Enhancer of Zeste protein.," *Genes Dev,* vol. 16, no. 22, pp. 2893-905, 2002.

[87] K. Sarma, C. Cifuentes-Rojas, A. Ergun, A. Del Rosario, Y. Jeon, F. White, R. Sadreyev and J. Lee, "ATRX directs binding of PRC2 to Xist RNA and Polycomb targets.," *Cell,* vol. 159, no. 4, pp. 869-83, 2014.

[88] D. Sadic, K. Schmidt, S. Groh, I. Kondofersky, J. Ellwart, C. Fuchs, F. Theis and G. Schotta, "Atrx promotes heterochromatin formation at retrotransposons.," *EMBO Rep,* vol. 16, no. 7, pp. 836-50, 2015.

[89] M. Levy, K. Kernohan, Y. Jiang and N. Bérubé, "ATRX promotes gene expression by facilitating transcriptional elongation through guanine-rich coding regions.," *Hum Mol Genet. ,* vol. 24, no. 7, pp. 1824-35, 2015.

[90] D. Clynes, C. Jelinska, B. Xella, H. Ayyub, S. Taylor, M. Mitson, C. Bachrati, D. Higgs and R. Gibbons, "ATRX dysfunction induces replication defects in primary mouse cells.," *PLoS One,* vol. 9, no. 3, p. e92915, 2014.

[91] J. Chapman, M. Taylor and S. Boulton, "Playing the end game: DNA double-strand break repair

pathway choice.," *Mol Cell.,* vol. 47, no. 4, pp. 497-510, 2012.

[92] E. Delbarre, K. Ivanauskiene, T. Küntziger and P. Collas, "DAXX-dependent supply of soluble (H3.3-H4) dimers to PML bodies pending deposition into chromatin.," *Genome Res.,* vol. 23, no. 3, pp. 440-51, 2013.

[93] M. Surpili, T. Delben and J. Kobarg, "Identification of proteins that interact with the central coiled-coil region of the human protein kinase NEK1.," *Biochemistry,* vol. 42, no. 51, pp. 15369-76, 2003.

[94] V. Valadez-Graham, Y. Yoshioka, O. Velazquez, A. Kawamori, M. Vázquez, A. Neumann, M. Yamaguchi and M. Zurita, "XNP/dATRX interacts with DREF in the chromatin to regulate gene expression.," *Nucleic Acids Res.,* vol. 40, no. 4, pp. 1460-74, 2012.

[95] F. Colland, X. Jacq, V. Trouplin, C. Mougin, C. Groizeleau, A. Hamburger, A. Meil, J. Wojcik, P. Legrain and J. Gauthier, "Functional proteomics mapping of a human signaling pathway.," *Genome Res.,* vol. 14, no. 7, pp. 1324-32, 2004.

[96] A. Wang, S. Grégoire, E. Zika, L. Xiao, C. Li, H. Li, K. Wright, J. Ting and X. Yang, "Identification of the ankyrin repeat proteins ANKRA and RFXANK as novel partners of class IIa histone deacetylases.," *J Biol Chem.,* vol. 280, no. 32, pp. 29117-27, 2005.

[97] M. Huh, T. Price O'Dea, D. Ouazia, B. McKay, G. Parise, R. Parks, M. Rudnicki and D. Picketts, "Compromised genomic integrity impedes muscle growth after Atrx inactivation.," *J Clin INvest,* vol. 122, no. 12, pp. 4412-23, 2012.

[98] P. Tang, A. Argentaro, A. Pask, L. O'Donnell, J. Marshall-Graves, M. Familari and V. Harley, "Localization of the chromatin remodelling protein, ATRX in the adult testis.," *J Reprod Dev,* vol. 57, no. 3, pp. 317-21, 2009.

[99] S. Bagheri-Fam, A. Argentaro, T. Svingen, A. Combes, A. Sinclair, P. Koopman and V. Harley, "Defective survival of proliferating Sertoli cells and androgen receptor function in a mouse model of the ATR-X syndrome.," *Hum Mol Genet,* vol. 20, no. 11, pp. 2213-24, 2011.

[100] C. Medina, C. Mazerolle, Y. Wang, N. Bérubé, S. Coupland, R. Gibbons, V. Wallace and D. Picketts, "Altered visual function and interneuron survival in Atrx knockout mice: inference for the human syndrome.," *Hum Mol Genet.,* vol. 18, no. 5, pp. 966-77, 2009.

[101] J. Gecz, H. Pollard, G. Consalez, L. Villard, C. Stayton, P. Millasseau, M. Khrestchatisky and M. Fontes, "Cloning and expression of the murine homologue of a putative human X-linked nuclear protein gene closely linked to PGK1 in Xq13.3.," *Hum Mol Genet. ,* vol. 3, no. 1, pp. 39-44, 1994.

[102] N. Bérubé, M. Jagla, C. Smeenk, Y. De Repentigny, R. Kothary and D. Picketts, "Neurodevelopmental defects resulting from ATRX overexpression in transgenic mice.," *Hum Mol Genet,* vol. 11, no. 3, pp. 253-61, 2002.

[103] N. Bérubé, M. Mangelsdorf, M. Jagla, J. Vanderluit, D. Garrick, R. Gibbons, D. Higgs, R. Slack and D. Picketts, "The chromatin-remodeling protein ATRX is critical for neuronal survival during corticogenesis.," *J Clin Invest,* vol. 115, no. 2, pp. 258-67, 2005.

[104] C. Seah, M. Levy, Y. Jiang, S. Mokhtarzada, D. Higgs, R. Gibbons and N. Bérubé, "Neuronal death resulting from targeted disruption of the Snf2 protein ATRX is mediated by p53.," *J Neurosci.,* vol. 28, no. 47, pp. 12570-80, 2008.

[105] L. Watson, L. Solomon, J. Li, Y. Jiang, M. Edwards, K. Shin-ya, F. Beier and N. Bérubé, "Atrx deficiency induces telomere dysfunction, endocrine defects, and reduced life span.," *J Clin Invest.,* vol. 123, no. 5, pp. 2049-63, 2013.

[106] K. Ritchie, L. Watson, B. Davidson, Y. Jiang and N. Bérubé, "ATRX is required for maintenance of the neuroprogenitor cell pool in the embryonic mouse brain.," *Biol Open,* vol. 3, no. 12, pp. 1158-63, 2014.

[107] T. Nogami, H. Beppu, T. Tokoro, S. Moriguchi, N. Shioda, K. Fukunaga, T. Ohtsuka, Y. Ishii, M. Sasahara, Y. Shimada, H. Nishijo, E. Li and I. Kitajima, "Reduced expression of the ATRX gene, a chromatin-remodeling factor, causes hippocampal dysfunction in mice.," *Hippocampus.,* vol. 21, no. 6, pp. 678-87, 2011.

[108] N. Shioda, H. Beppu, T. Fukuda, E. Li, I. Kitajima and K. Fukunaga, "Aberrant calcium/calmodulin-dependent protein kinase II (CaMKII) activity is associated with abnormal dendritic spine morphology in the ATRX mutant mouse brain.," *J Neurosci.,* vol. 31, no. 1, pp. 346-58, 2011.

[109] N. Germain, E. Banda and L. Grabel, "Embryonic stem cell neurogenesis and neural specification.," *J Cell Biochem,* vol. 111, no. 3, pp. 535-42, 2010.

[110] G. Frantz and S. McConnell, "Restriction of late cerebral cortical progenitors to an upper-layer fate.," *Neuron,* vol. 17, no. 1, pp. 55-61, 1996.

[111] A. Desai and S. McConnell, "Progressive restriction in fate potential by neural progenitors during cerebral cortical development.," *Development,* vol. 127, no. 13, pp. 2863-72, 2000.

[112] Q. Shen, Y. Wang, J. Dimos, C. Fasano, T. Phoenix, I. Lemischka, N. Ivanova, S. Stifani, E. Morrisey and S. Temple, "The timing of cortical neurogenesis is encoded within lineages of individual progenitor cells.," *Nat Neurosci,* vol. 9, no. 6, pp. 743-51, 2006.

[113] G. Miyoshi and G. Fishell, "Dynamic FoxG1 expression coordinates the integration of multipolar pyramidal neuron precursors into the cortical plate.," *Neuron,* vol. 74, no. 6, pp. 1045-58, 2012.

[114] E. Stancik, I. Navarro-Quiroga, R. Sellke and T. Haydar, "Heterogeneity in ventricular zone neural precursors contributes to neuronal fate diversity in the postnatal neocortex.," *J Neurosci,* vol. 30, no. 20, pp. 7028-36, 2010.

[115] M. Woodworth, L. Custo Greig, A. Kriegstein and J. Macklis, "SnapShot: cortical development.," *Cell,* vol. 151, no. 4, pp. 918-918, 2012.

[116] T. Mitsuhashi and T. Takahashi, "Genetic regulation of proliferation/differentiation characteristics of neural progenitor cells in the developing neocortex.," *Brain Dev,* vol. 31, no. 7, pp. 553-7, 2009.

[117] C. MuhChyi, B. Juliandi, T. Matsuda and K. Nakashima, "Epigenetic regulation of neural stem cell fate during corticogenesis.," *Int J Dev Neurosci,* vol. 31, no. 6, pp. 424-33, 2013.

[118] P. McKinnon, "Maintaining genome stability in the nervous system.," *Nat Neurosci,* vol. 16, no. 11, pp. 1523-9, 2013.

[119] D. Clynes, D. Higgs and R. Gibbons, "The chromatin remodeller ATRX: a repeat offender in human disease.," *Trends Biochem Sci.,* vol. 38, no. 9, pp. 461-6, 2013.

[120] H. Pickett and R. Reddel, "Molecular mechanisms of activity and derepression of alternative lengthening of telomeres.," *Nat Struct Mol Biol,* vol. 22, no. 11, pp. 875-80, 2015.

[121] D. Conte, M. Huh, E. Goodall, M. Delorme, R. Parks and D. Picketts, "Loss of Atrx sensitizes cells to DNA damaging agents through p53-mediated death pathways.," *PLoS One.,* vol. 7, no. 12, p. E52167, 2012.

[122] R. Flynn, K. Cox, M. Jeitany, H. Wakimoto, A. Bryll, N. Ganem, F. Bersani, J. Pineda, M. Suvà, C. Benes, D. Haber, F. Boussin and L. Zou, "Alternative lengthening of telomeres renders cancer cells hypersensitive to ATR inhibitors.," *Science,* vol. 347, no. 6219, pp. 273-7, 2015.

[123] E. Campos and D. Reinberg, "Histones: annotating chromatin.," *Annu Rev Genet.,* vol. 43, pp. 559-99, 2009.

[124] B. Price and A. D'Andrea, "Chromatin remodeling at DNA double-strand breaks.," *Cell,* vol. 152, no. 6, pp. 1344-54, 2013.

[125] M. Vilenchik and A. Knudson, "Endogenous DNA double-strand breaks: production, fidelity of repair, and induction of cancer.," *Proc Natl Acad Sci U S A.,* vol. 100, no. 22, pp. 12871-6, 2003.

[126] R. Madabhushi, L. Pan and L. Tsai, "DNA damage and its links to neurodegeneration.," *Neuron,* vol. 83, no. 2, pp. 266-82, 2014.

[127] A. Ciccia and S. Elledge, "The DNA damage response: making it safe to play with knives.," *Mol Cell,* vol. 40, no. 2, pp. 179-204, 2010.

[128] D. Cortez, "Preventing replication fork collapse to maintain genome integrity.," *DNA Repair (Amst).,* vol. 32, pp. 149-57, 2015.

[129] M. McVey and S. Lee, "MMEJ repair of double-strand breaks (director's cut): deleted sequences and alternative endings.," *Trends Genet. ,* vol. 24, no. 11, pp. 529-38, 2008.

[130] D. Hanahan and R. Weinberg, "The hallmarks of cancer.," *Cell,* vol. 100, no. 1, pp. 57-70, 2000.

[131] D. Hanahan and R. Weinberg, "Hallmarks of cancer: the next generation.," *Cell,* vol. 144, no. 5, pp. 646-74, 2011.

[132] S. Negrini, V. Gorgoulis and T. Halazonetis, "Genomic instability--an evolving hallmark of cancer.," *Nat Rev Mol Cell Biol.,* vol. 11, no. 3, pp. 220-8, 2010.

[133] T. Lindahl, P. Modrich and A. Sancar, "The 2015 Nobel Prize in Chemistry The Discovery of Essential Mechanisms that Repair DNA Damage.," *J Assoc Genet Technol.,* vol. 42, no. 1, pp. 37-41, 2016.

[134] M. De Vos, V. Schreiber and F. Dantzer, "The diverse roles and clinical relevance of PARPs in DNA damage repair: current state of the art.," *Biochem Pharmacol. ,* vol. 84, no. 2, pp. 137-46, 2012.

[135] M. Delorme, Downregulation of ATRX disrupts cell proliferation and cell cycle progression, Master's Thesis ed., Ottawa: University of Ottawa, 2008.

[136] D. Clynes, C. Jelinska, B. Xella, H. Ayyub, C. Scott, M. Mitson, S. Taylor, D. Higgs and R. Gibbons, "Suppression of the alternative lengthening of telomere pathway by the chromatin remodelling factor ATRX.," *Nat Commun,* vol. 6, no. 7538, p. 10.1038/ncomms8538, 2015.

[137] M. Musiałek and D. Rybaczek, "Behavior of replication origins in Eukaryota - spatio-temporal dynamics of licensing and firing.," *Cell Cycle.,* vol. 14, no. 14, pp. 2251-64, 2015.

[138] D. Löb, N. Lengert, V. Chagin, M. Reinhart, C. Casas-Delucchi, M. Cardoso and B. Drossel, "3D replicon distributions arise from stochastic initiation and domino-like DNA replication progression.," *Nat Commun.,* vol. 7, no. 11207, p. doi: 10.1038/ncomms11207, 2016.

[139] C. Casas-Delucchi, J. van Bemmel, S. Haase, H. Herce, D. Nowak, D. Meilinger, J. Stear, H.

Leonhardt and M. Cardoso, "Histone hypoacetylation is required to maintain late replication timing of constitutive heterochromatin.," *Nucleic Acids Res.,* vol. 40, no. 1, pp. 159-69, 2012.

[140] L. Toledo, M. Altmeyer, M. Rask, C. Lukas, D. Larsen, L. Povlsen, S. Bekker-Jensen, N. Mailand, J. Bartek and J. Lukas, "ATR prohibits replication catastrophe by preventing global exhaustion of RPA.," *Cell,* vol. 155, no. 5, pp. 1088-103, 2013.

[141] J. Blow, X. Ge and D. Jackson, "How dormant origins promote complete genome replication.," *Trends Biochem Sci.,* vol. 36, no. 8, pp. 405-14, 2011.

[142] K. Sakabe and R. Okazaki, "A unique property of the replicating region of chromosomal DNA.," *Biochim Biophys Acta.,* vol. 129, no. 3, pp. 651-4, 1966.

[143] C. Alabert and A. Groth, "Chromatin replication and epigenome maintenance.," *Nat Rev Mol Cell Biol.,* vol. 13, no. 3, pp. 153-67, 2012.

[144] Z. Jasencakova, A. Scharf, K. Ask, A. Corpet, A. Imhof, G. Almouzni and A. Groth, "Replication stress interferes with histone recycling and predeposition marking of new histones.," *Mol Cell,* vol. 37, no. 5, pp. 736-43, 2010.

[145] C. Papadopoulou, G. Guilbaud, D. Schiavone and J. Sale, "Nucleotide Pool Depletion Induces G-Quadruplex-Dependent Perturbation of Gene Expression.," *Cell Rep,* vol. 13, no. 11, pp. 2491-503, 2015.

[146] P. Sarkies, C. Reams, L. Simpson and J. Sale, "Epigenetic instability due to defective replication of structured DNA.," *Mol Cell.,* vol. 40, no. 5, pp. 703-13, 2010.

[147] P. Sarkies, P. Murat, L. Phillips, K. Patel, S. Balasubramanian and J. Sale, "FANCJ coordinates two pathways that maintain epigenetic stability at G-quadruplex DNA.," *Nucleic Acids Res.,* vol. 40, no. 4, pp. 1485-98, 2012.

[148] C. Wickramasinghe, H. Arzouk, A. Frey, A. Maiter and J. Sale, "Contributions of the specialised DNA polymerases to replication of structured DNA.," *DNA Repair (Amst).,* vol. 29, pp. 83-90, 2015.

[149] D. Schiavone, G. Guilbaud, P. Murat, C. Papadopoulou, P. Sarkies, M. Prioleau, S. Balasubramanian and J. Sale, "Determinants of G quadruplex-induced epigenetic instability in REV1-deficient cells.," *EMBO J.,* vol. 33, no. 21, pp. 2507-20, 2014.

[150] P. Murat and S. Balasubramanian, "Existence and consequences of G-quadruplex structures in DNA," *Curr Opin Genet Dev. ,* vol. 25, pp. 22-9, 2014.

[151] K. Ivanauskiene, E. Delbarre, J. McGhie, T. Küntziger, L. Wong and P. Collas, "The PML-

associated protein DEK regulates the balance of H3.3 loading on chromatin and is important for telomere integrity.," *Genome Res,* vol. 24, no. 10, pp. 1584-94, 2014.

[152] K. Paeschke, J. Capra and V. Zakian, "DNA replication through G-quadruplex motifs is promoted by the Saccharomyces cerevisiae Pif1 DNA helicase.," *Cell,* vol. 145, no. 5, pp. 678-91, 2011.

[153] A. Rizzo, E. Salvati, M. Porru, C. D'Angelo, M. Stevens, M. D'Incalci, C. Leonetti, E. Gilson, Zupi and A. Biroccio, "Stabilization of quadruplex DNA perturbs telomere replication leading to the activation of an ATR-dependent ATM signaling pathway.," *Nucleic Acids Res.,* vol. 37, no. 16, pp. 5353-64, 2009.

[154] A. Burger, F. Dai, C. Schultes, A. Reszka, M. Moore, J. Double and S. Neidle, "The G-quadruplex-interactive molecule BRACO-19 inhibits tumor growth, consistent with telomere targeting and interference with telomerase function.," *Cancer Res.,* vol. 65, no. 4, pp. 1489-96, 2005.

[155] M. van Kregten and M. Tijsterman, "The repair of G-quadruplex-induced DNA damage.," *Exp Cell Res,* vol. 329, no. 1, pp. 178-83, 2014.

[156] J. Lopes, A. Piazza, R. Bermejo, B. Kriegsman, A. Colosio, M. Teulade-Fichou, M. Foiani and A. Nicolas, "G-quadruplex-induced instability during leading-strand replication.," *EMBO J,* vol. 30, no. 19, pp. 4033-46, 2011.

[157] B. Lemmens, R. van Schendel and M. Tijsterman, "Mutagenic consequences of a single G-quadruplex demonstrate mitotic inheritance of DNA replication fork barriers.," *Nat Commun,* vol. 6, no. 8909, p. doi: 10.1038/ncomms9909., 2015.

[158] S. Yan and W. Michael, "TopBP1 and DNA polymerase alpha-mediated recruitment of the 9-1-1 complex to stalled replication forks: implications for a replication restart-based mechanism for ATR checkpoint activation.," *Cell Cycle,* vol. 8, no. 18, pp. 2877-84, 2009.

[159] E. Ohashi, Y. Takeishi, S. Ueda and T. Tsurimoto, "Interaction between Rad9-Hus1-Rad1 and TopBP1 activates ATR-ATRIP and promotes TopBP1 recruitment to sites of UV-damage.," *DNA Repair (Amst). ,* vol. 21, pp. 1-11, 2014.

[160] M. Goodman and R. Woodgate, "Translesion DNA polymerases.," *Cold Spring Harb Perspect Biol. ,* vol. 5, no. 10, p. a010363, 2013.

[161] D. Edwards, A. Machwe, Z. Wang and D. Orren, "Intramolecular telomeric G-quadruplexes dramatically inhibit DNA synthesis by replicative and translesion polymerases, revealing their potential to lead to genetic change.," *PLoS One.,* vol. 9, no. 1, p. e80664, 2014.

[162] A. Shibata, D. Moiani, A. Arvai, J. Perry, S. Harding, M. Genois, R. Maity, S. van Rossum-Fikkert, A. Kertokalio, F. Romoli, A. Ismail, E. Ismalaj, E. Petricci, M. Neale, R. Bristow, J. Masson, C. Wyman, P. Jeggo and J. Tainer, "DNA double-strand break repair pathway choice is directed by distinct MRE11 nuclease activities.," *Mol Cell,* vol. 53, no. 1, pp. 7-18, 2014.

[163] S. Ying, F. Hamdy and T. Helleday, "Mre11-dependent degradation of stalled DNA replication forks is prevented by BRCA2 and PARP1.," *Cancer Res,* vol. 72, no. 11, pp. 2814-21, 2012.

[164] H. Bryant, E. Petermann, N. Schultz, A. Jemth, O. Loseva, N. Issaeva, F. Johansson, S. Fernandez, P. McGlynn and T. Helleday, "PARP is activated at stalled forks to mediate Mre11-dependent replication restart and recombination," *EMBO J.,* vol. 28, no. 17, pp. 2601-15, 2009.

[165] S. Ying, Z. Chen, A. Medhurst, J. Neal, Z. Bao, O. Mortusewicz, J. McGouran, X. Song, H. Shen, F. Hamdy, B. Kessler, K. Meek and T. Helleday, "DNA-PKcs and PARP1 Bind to Unresected Stalled DNA Replication Forks Where They Recruit XRCC1 to Mediate Repair.," *Cancer Res.,* vol. 76, no. 5, pp. 1078-88, 2016.

[166] K. Schlacher, N. Christ, N. Siaud, A. Egashira, H. Wu and M. Jasin, "Double-strand break repair-independent role for BRCA2 in blocking stalled replication fork degradation by MRE11.," *Cell,* vol. 145, no. 4, pp. 529-42, 2011.

[167] J. Schwartzentruber, A. Korshunov, X. Liu, D. Jones, E. Pfaff, K. Jacob, D. Sturm, A. Fontebasso, D. Quang, M. Tönjes, V. Hovestadt, S. Albrecht, M. Kool, A. Nantel, C. Konermann, A. Lindroth, N. Jäger, T. Rausch, M. Ryzhova, J. Korbel and e. al., "Driver mutations in histone H3.3 and chromatin remodelling genes in paediatric glioblastoma.," *Nature,* vol. 482, no. 7384, pp. 226-31, 2012.

[168] M. Zeman and K. Cimprich, "Causes and consequences of replication stress.," *Nat Cell Biol. ,* vol. 16, no. 1, pp. 2-9, 2014.

[169] A. Frey, T. Listovsky, G. Guilbaud, P. Sarkies and J. Sale, "Histone H3.3 is required to maintain replication fork progression after UV damage.," *Curr Biol,* vol. 24, no. 18, pp. 2195-201, 2014.

[170] D. Clynes and R. Gibbons, "ATRX and the replication of structured DNA.," *Curr Opin Genet Dev.,* vol. 23, no. 3, pp. 289-94, 2013.

[171] I. Parra and B. Windle, "High resolution visual mapping of stretched DNA by fluorescent hybridization.," *Nat Genet,* vol. 15, no. 1, pp. 17-21, 1993.

[172] F. Martínez, M. Tomás, J. Millán, A. Fernández, F. Palau and F. Prieto, "Genetic localisation of mental retardation with spastic diplegia to the pericentromeric region of the X chromosome:

X inactivation in female carriers.," *J Med Genet.,* vol. 35, no. 4, pp. 284-7, 1998.

[173] L. Woodbine, J. Neal, N. Sasi, M. Shimada, K. Deem, H. Coleman, W. Dobyns, T. Ogi, K. Meek, E. Davies and P. Jeggo, "PRKDC mutations in a SCID patient with profound neurological abnormalities.," *J Clin Invest.,* vol. 123, no. 7, pp. 2969-80, 2013.

[174] Y. Matsumoto, T. Miyamoto, H. Sakamoto, H. Izumi, Y. Nakazawa, T. Ogi, H. Tahara, S. Oku, A. Hiramoto, T. Shiiki, Y. Fujisawa, H. Ohashi, Y. Sakemi and S. Matsuura, "Two unrelated patients with MRE11A mutations and Nijmegen breakage syndrome-like severe microcephaly.," *DNA Repair (Amst).,* vol. 10, no. 3, pp. 314-21, 2011.

[175] C. Weemaes, T. Hustinx, J. Scheres, P. van Munster, J. Bakkeren and R. Taalman, "A new chromosomal instability disorder: the Nijmegen breakage syndrome.," *Acta Paediatr Scand.,* vol. 70, no. 4, pp. 557-64, 1981.

[176] E. Seemanová, E. Passarge, D. Beneskova, J. Houstěk, P. Kasal and M. Sevcíková, "Familial microcephaly with normal intelligence, immunodeficiency, and risk for lymphoreticular malignancies: a new autosomal recessive disorder.," *Am J Med Genet,* vol. 20, no. 4, pp. 639-48, 1985.

[177] G. Barbi, J. Scheres, D. Schindler, R. Taalman, K. Rodens, K. Mehnert, M. Müller and H. Seyschab, "Chromosome instability and X-ray hypersensitivity in a microcephalic and growth-retarded child.," *Am J Med Genet,* vol. 40, no. 1, pp. 44-50, 1991.

[178] R. Waltes, R. Kalb, M. Gatei, A. Kijas, M. Stumm, A. Sobeck, B. Wieland, R. Varon, Y. Lerenthal, M. Lavin, D. Schindler and T. Dörk, "Human RAD50 deficiency in a Nijmegen breakage syndrome-like disorder.," *Am J Hum Genet.,* vol. 84, no. 5, pp. 605-16, 2009.

[179] W. Gibson, R. Hood, S. Zhan, D. Bulman, A. Fejes, R. Moore, A. Mungall, P. Eydoux, R. Babul-Hirji, J. An, M. Marra, F. C. Consortium, D. Chitayat, K. Boycott, D. Weaver and S. Jones, "Mutations in EZH2 cause Weaver syndrome.," *Am J Hum Genet.,* vol. 90, no. 1, pp. 110-8, 2012.

[180] J. Neul, W. Kaufmann, D. Glaze, J. Christodoulou, A. Clarke, N. Bahi-Buisson, H. Leonard, M. Bailey, N. Schanen, M. Zappella, A. Renieri, P. Huppke, A. Percy and R. Consortium, "Rett syndrome: revised diagnostic criteria and nomenclature.," *Ann Neurol.,* vol. 68, no. 6, pp. 944-50, 2010.

[181] A. Musio, A. Selicorni, M. Focarelli, C. Gervasini, D. Milani, S. Russo, P. Vezzoni and L. Larizza, "X-linked Cornelia de Lange syndrome owing to SMC1L1 mutations.," *Nat Genet,* vol. 38, no. 5, pp. 528-30, 2006.

[182] M. Deardorff, M. Kaur, D. Yaeger, A. Rampuria, S. Korolev, J. Pie, C. Gil-Rodríguez, M. Arnedo, B. Loeys, A. Kline, M. Wilson, K. Lillquist, V. Siu, F. Ramos, A. Musio, L. Jackson, D. Dorsett and I. Krantz, "Mutations in cohesin complex members SMC3 and SMC1A cause a mild variant of cornelia de Lange syndrome with predominant mental retardation.," *Am J Hum Genet,* vol. 80, no. 3, pp. 485-94, 2007.

[183] J. Hebert and S. McConnell, "Targeting of cre to the Foxg1 (BF-1) locus mediates loxP recombination in the telencephalon and other developing head structures.," *Dev Biol,* vol. 222, no. 2, pp. 296-306, 2000.

[184] T. Anthony, C. Klein, G. Fishell and N. Heintz, "Radial glia serve as neuronal progenitors in all regions of the central nervous system.," *Neuron,* vol. 41, no. 6, pp. 881-90, 2004.

[185] N. Gaspard, T. Bouschet, R. Hourez, J. Dimidschstein, G. Naeije, J. van den Ameele, I. Espuny-Camacho, A. Herpoel, L. Passante, S. Schiffmann, A. Gaillard and P. Vanderhaeghen, "An intrinsic mechanism of corticogenesis from embryonic stem cells.," *Nature,* vol. 455, no. 7211, pp. 351-7, 2008.

[186] E. Glimore and C. Walsh, "Genetic Causes of Microcephaly and Lessons for Neuronal Development," *Wiley Interdiscip Rev Dev Biol.,* vol. 2, no. 4, pp. 461-78, 2013.

[187] M. Faheem, M. Naseer, M. Rasool, A. Chaudhary, T. Kumosani, A. Ilyas, P. Pushparaj, F. Ahmed, H. Algahtani, M. Al-Qahtani and H. Saleh Jamal, "Molecular genetics of human primary microcephaly: an overview.," *BMC Med Genomics,* vol. 8, no. 1, p. S4, 2015.

[188] M. Curtin, Understanding the role of Parp-1 in the Atrx(null) cortex, URL: http://hdl.handle.net/10393/28512 ed., Master's Thesis: University of Ottawa, 2009.

[189] V. Schreiber, F. Dantzer, J. Ame and G. de Murcia, "Poly(ADP-ribose): novel functions for an old molecule.," *Nat Rev Mol Cell Biol.,* vol. 7, no. 7, pp. 514-28, 2006.

[190] H. Kleine, E. Poreba, K. Lesniewicz, P. Hassa, M. Hottiger, D. Litchfield, B. Shilton and B. Lüscher, "Substrate-assisted catalysis by PARP10 limits its activity to mono-ADP-ribosylation.," *Mol Cell,* vol. 32, no. 1, pp. 57-69, 2008.

[191] A. Ali, G. Timinszky, R. Arribas-Bosacoma, M. Kozlowski, P. Hassa, M. Hassler, A. Ladurner, L. Pearl and A. Oliver, "The zinc-finger domains of PARP1 cooperate to recognize DNA strand breaks.," *Nat Struct Mol Biol,* vol. 19, no. 7, pp. 685-92, 2012.

[192] M. Langelier, J. Planck, S. Roy and J. Pascal, "Structural basis for DNA damage-dependent poly(ADP-ribosyl)ation by human PARP-1.," *Science,* vol. 336, no. 6082, pp. 728-32, 2012.

[193] E. Goodall, Characterizing the enhanced neuronal apoptosis in ATRX knockout mice, Master's

thesis ed., Ottawa: University of Ottawa, 2009.

[194] C. Downes, A. Collins and R. Johnson, "DNA damage in synchronized HeLa cells irradiated with ultraviolet.," *Biophys J,* vol. 25, no. 1, p. 129/50, 1979.

[195] A. Baude, T. Aaes, B. Zhai, N. Al-Nakouzi, H. Oo, M. Daugaard, M. Rohde and M. Jäättelä, "Hepatoma-derived growth factor-related protein 2 promotes DNA repair by homologous recombination.," *Nucleic Acids Res,* vol. 44, no. 5, pp. 2214-26, 2016.

[196] M. Pagano, R. Pepperkok, F. Verde, W. Ansorge and G. Draetta, "Cyclin A is required at two points in the human cell cycle.," *EMBO J,* vol. 11, no. 3, pp. 961-71, 1992.

[197] E. Oricchio, C. Saladino, S. Iacovelli, S. Soddu and E. Cundari, "ATM is activated by default in mitosis, localizes at centrosomes and monitors mitotic spindle integrity.," *Cell Cycle,* vol. 5, no. 1, pp. 88-92, 2006.

[198] C. Beck, I. Robert, B. Reina-San-Martin, V. Schreiber and F. Dantzer, "Poly(ADP-ribose) polymerases in double-strand break repair: focus on PARP1, PARP2 and PARP3.," *Exp Cell Res,* vol. 329, no. 1, pp. 18-25, 2014.

[199] Q. Yan, R. Xu, L. Zhu, X. Cheng, Z. Wang, J. Manis and M. Shipp, "BAL1 and its partner E3 ligase, BBAP, link Poly(ADP-ribose) activation, ubiquitylation, and double-strand DNA repair independent of ATM, MDC1, and RNF8.," *Mol Cell Biol,* vol. 33, no. 4, pp. 845-57, 2013.

[200] S. Rulten, A. Fisher, I. Robert, M. Zuma, M. Rouleau, L. Ju, G. Poirier, B. Reina-San-Martin and K. Caldecott, "PARP-3 and APLF function together to accelerate nonhomologous end-joining.," *Mol Cell,* vol. 41, no. 1, pp. 33-45, 2011.

[201] S. Jungmichel, F. Rosenthal, M. Altmeyer, J. Lukas, M. Hottiger and M. Nielsen, "Proteome-wide identification of poly(ADP-Ribosyl)ation targets in different genotoxic stress responses.," *Mol Cell.,* vol. 52, no. 2, pp. 272-85, 2013.

[202] L. Lan, S. Nakajima, L. Wei, L. Sun, C. Hsieh, R. Sobol, M. Bruchez, B. Van Houten, A. Yasui and A. Levine, "Novel method for site-specific induction of oxidative DNA damage reveals differences in recruitment of repair proteins to heterochromatin and euchromatin.," *Nucleic Acids Res,* vol. 42, no. 4, pp. 2330-45, 2014.

[203] G. Papeo, N. Avanzi, S. Bettoni, A. Leone, M. Paolucci, R. Perego, F. Quartieri, F. Riccardi-Sirtori, S. Thieffine, A. Montagnoli and R. Lupi, "Insights into PARP Inhibitors' Selectivity Using Fluorescence Polarization and Surface Plasmon Resonance Binding Assays.," *J Biomol Screen,* vol. 19, no. 8, pp. 1212-9, 2014.

[204] S. Panier and S. Boulton, "Double-strand break repair: 53BP1 comes into focus.," *Nat Rev Mol*

Cell Biol, vol. 15, no. 1, pp. 7-18, 2014.

[205] H. Farmer, N. McCabe, C. Lord, A. Tutt, D. Johnson, T. Richardson, M. Santarosa, K. Dillon, I. Hickson, C. Knights, N. Martin, S. Jackson, G. Smith and A. Ashworth, "Targeting the DNA repair defect in BRCA mutant cells as a therapeutic strategy.," *Nature,* vol. 434, no. 7035, pp. 917-21, 2005.

[206] F. Chehrehasa, A. Meedeniya, P. Dwyer, G. Abrahamsen and A. Mackay-Sim, "EdU, a new thymidine analogue for labelling proliferating cells in the nervous system.," *J Neurosci Methods.,* vol. 177, no. 1, pp. 122-30, 2009.

[207] H. Kolb, M. Finn and K. Sharpless, "Click Chemistry: Diverse Chemical Function from a Few Good Reactions.," *Angew Chem Int Ed Engl. ,* vol. 40, no. 11, pp. 2004-21, 2001.

[208] R. Scully, N. Puget and K. Vlasakova, "DNA polymerase stalling, sister chromatid recombination and the BRCA genes.," *Oncogene,* vol. 19, no. 53, pp. 6175-83, 2000.

[209] P. Langerak, E. Mejia-Ramirez, O. Limbo and P. Russell, "Release of Ku and MRN from DNA ends by Mre11 nuclease activity and Ctp1 is required for homologous recombination repair of double-strand breaks.," *PLoS Genet,* vol. 7, no. 9, p. e1002271, 2011.

[210] Y. Hashimoto, C. A. Ray, M. Lopes and V. Costanzo, "Rad51 protects nascent DNA from Mre11-dependent degradation and promotes continuous DNA synthesis.," *Nat Struct Mol Biol.,* vol. 17, no. 11, pp. 1305-11, 2010.

[211] J. Lai and W. Herr, "Ethidium bromide provides a simple tool for identifying genuine DNA-independent protein associations.," *Proc Natl Acad Sci U S A,* vol. 89, no. 15, pp. 6958-62, 1992.

[212] P. Drané, K. Ouararhni, A. Depaux, M. Shuaib and A. Hamiche, "The death-associated protein DAXX is a novel histone chaperone involved in the replication-independent deposition of H3.3.," *Genes Dev,* vol. 24, no. 12, pp. 1253-65, 2010.

[213] H. Voon and L. Wong, "New players in heterochromatin silencing: histone variant H3.3 and the ATRX/DAXX chaperone.," *Nucleic Acids Res,* vol. 44, no. 4, pp. 1496-501, 2016.

[214] L. Rapkin, K. Ahmed, S. Dulev, R. Li, H. Kimura, A. Ishov and D. Bazett-Jones, "The histone chaperone DAXX maintains the structural organization of heterochromatin domains.," *Epigenetics Chromatin,* vol. 8, no. 44, pp. 10.1186/s13072-015-0036-2, 2015.

[215] T. Nowakowski, K. Mysiak, T. Pratt and D. Price, "Functional dicer is necessary for appropriate specification of radial glia during early development of mouse telencephalon.," *PLoS One,* vol. 6, no. 8, p. e23013, 2011.

[216] K. Ferguson, J. Vanderluit, J. Hébert, W. McIntosh, E. Tibbo, J. MacLaurin, D. Park, V. Wallace, M. Vooijs, S. McConnell and R. Slack, "Telencephalon-specific Rb knockouts reveal enhanced neurogenesis, survival and abnormal cortical development.," *EMBO J,* vol. 21, no. 13, pp. 3337-46, 2002.

[217] M. Andrusiak, R. Vandenbosch, F. Dick, D. Park and R. Slack, "LXCXE-independent chromatin remodeling by Rb/E2f mediates neuronal quiescence.," *Cell Cycle,* vol. 12, no. 9, pp. 1416-23, 2013.

[218] K. Eagleson, L. Schlueter McFadyen-Ketchum, E. Ahrens, P. Mills, M. Does, J. Nickols and P. Levitt, "Disruption of Foxg1 expression by knock-in of cre recombinase: effects on the development of the mouse telencephalon.," *Neuroscience,* vol. 148, no. 2, pp. 385-99, 2007.

[219] D. Garrick, J. Sharpe, R. Arkell, L. Dobbie, A. Smith, W. Wood, D. Higgs and R. Gibbons, "Loss of Atrx affects trophoblast development and the pattern of X-inactivation in extraembryonic tissues.," *PLoS Genet.,* vol. 2, no. 4, p. e58, 2006.

[220] R. Calado and B. Dumitriu, "Telomere dynamics in mice and humans.," *Semin Hematol,* vol. 50, no. 2, pp. 165-74, 2013.

[221] P. Logan, M. Mitchell and P. Lobie, "DNA methyltransferases and TETs in the regulation of differentiation and invasiveness of extra-villous trophoblasts.," *Front Genet.,* vol. 4, no. 265, p. 10.3389, 2013.

[222] R. Gibbons, T. McDowell, S. Raman, D. O'Rourke, D. Garrick, H. Ayyub and D. Higgs, "Mutations in ATRX, encoding a SWI/SNF-like protein, cause diverse changes in the pattern of DNA methylation.," *Nat Genet,* vol. 24, no. 4, pp. 368-71, 2000.

[223] X. Luo and W. Kraus, "On PAR with PARP: cellular stress signaling through poly(ADP-ribose) and PARP-1.," *Genes Dev,* vol. 26, no. 5, pp. 417-32, 2012.

[224] P. Jagtap and C. Szabó, "Poly(ADP-ribose) polymerase and the therapeutic effects of its inhibitors.," *Nat Rev Drug Discov.,* vol. 4, no. 5, pp. 421-40, 2005.

[225] T. Neira-Peña, E. Rojas-Mancilla, V. Munoz-Vio, R. Perez, M. Gutierrez-Hernandez, D. Bustamante, P. Morales, M. Hermoso, P. Gebicke-Haerter and M. Herrera-Marschitz, "Perinatal asphyxia leads to PARP-1 overactivity, p65 translocation, IL-1β and TNF-α overexpression, and apoptotic-like cell death in mesencephalon of neonatal rats: prevention by systemic neonatal nicotinamide administration.," *Neurotox Res,* vol. 27, no. 4, pp. 453-65, 2015.

[226] C. Brochier, J. Jones, D. Willis and B. Langley, "Poly(ADP-ribose) polymerase 1 is a novel target to promote axonal regeneration.," *Proc Natl Acad Sci U S A,* vol. 112, no. 49, pp. 15220-5,

2015.

[227] W. Zong, D. Ditsworth, D. Bauer, Z. Wang and C. Thompson, "Alkylating DNA damage stimulates a regulated form of necrotic cell death.," *Genes Dev,* vol. 18, no. 11, pp. 1272-82, 2004.

[228] D. Buonvicino, L. Formentini, G. Cipriani and A. Chiarugi, "Glucose deprivation converts poly(ADP-ribose) polymerase-1 hyperactivation into a transient energy-producing process.," *J Biol Chem.,* vol. 288, no. 51, pp. 36530-7, 2013.

[229] J. Ménisser-de Murcia, M. Mark, O. Wendling, A. Wynshaw-Boris and G. de Murcia, "Early embryonic lethality in PARP-1 Atm double-mutant mice suggests a functional synergy in cell proliferation during development.," *Mol Cell Biol,* vol. 21, no. 5, pp. 1828-32, 2001.

[230] M. Henrie, A. Kurimasa, S. Burma, J. Ménissier-de Murcia, G. de Murcia, G. Li and D. Chen, "Lethality in PARP-1/Ku80 double mutant mice reveals physiological synergy during early embryogenesis.," *DNA Repair (Amst),* vol. 2, no. 2, pp. 151-8, 2003.

[231] Y. Ichikawa, N. Morohashi, Y. Nishimura, H. Kurumizaka and M. Shimizu, "Telomeric repeats act as nucleosome-disfavouring sequences in vivo," *Nucleic Acids Res,* vol. 42, no. 3, pp. 1541-52, 2014.

[232] Y. Wang, R. Gellibolian, M. Shimizu, R. Wells and J. Griffith, "Long CCG triplet repeat blocks exclude nucleosomes: a possible mechanism for the nature of fragile sites in chromosomes.," *J Mol Biol,* vol. 263, no. 4, pp. 511-6, 1996.

[233] J. Lormand, N. Buncher, C. Murphy, P. Kaur, M. Lee, P. Burgers, H. Wang, T. Kunkel and P. Opresko, "DNA polymerase δ stalls on telomeric lagging strand templates independently from G-quadruplex formation.," *Nucleic Acids Res,* vol. 41, no. 22, pp. 10323-33, 2013.

[234] J. Yeeles, J. Poli, K. Marians and P. Pasero, "Rescuing stalled or damaged replication forks.," *Cold Spring Harb Perspect Biol,* vol. 5, no. 5, p. a012815, 2013.

[235] A. Mazin, O. Mazina, D. Bugreev and M. Rossi, "Rad54, the motor of homologous recombination.," *DNA Repair (Amst),* vol. 9, no. 3, pp. 286-302, 2010.

[236] R. Maher, A. Branagan and S. Morrical, "Coordination of DNA replication and recombination activities in the maintenance of genome stability.," *J Cell Biochem,* vol. 112, no. 10, pp. 2672-82, 2011.

[237] J. Spies, A. Waizenegger, O. Barton, M. Sürder, W. Wright, W. Heyer and M. Löbrich, "Nek1 Regulates Rad54 to Orchestrate Homologous Recombination and Replication Fork Stability.," *Mol Cell,* vol. 62, no. 6, pp. 903-17, 2016.

[238] R. Ceccaldi, B. Rondinelli and A. D'Andrea, "Repair Pathway Choices and Consequences at the Double-Strand Break.," *Trends Cell Biol,* vol. 26, no. 1, pp. 52-64, 2016.

[239] Y. Ohno, Y. Ogiyama, Y. Kubota, T. Kubo and K. Ishii, "Acentric chromosome ends are prone to fusion with functional chromosome ends through a homology-directed rearrangement.," *Nucleic Acids Res,* vol. 44, no. 1, pp. 232-44, 2016.

[240] A. Kalousi and E. Soutoglou, "Nuclear compartmentalization of DNA repair.," *Curr Opin Genet Dev,* vol. 37, pp. 148-57, 2016.

[241] M. Parks, C. Lawrence and B. Raphael, "Detecting non-allelic homologous recombination from high-throughput sequencing data.," *Genome Biol,* vol. 16, no. 72, pp. doi: 10.1186/s13059-015-0633-1., 2015.

[242] A. Kakarougkas, A. Ismail, K. Klement, A. Goodarzi, S. Conrad, R. Freire, A. Shibata, M. Lobrich and P. Jeggo, "Opposing roles for 53BP1 during homologous recombination.," *Nucleic Acids Res,* vol. 41, no. 21, pp. 9719-31, 2013.

[243] A. Beucher, J. Birraux, L. Tchouandong, O. Barton, A. Shibata, S. Conrad, A. Goodarzi, A. Krempler, P. Jeggo and M. Löbrich, "ATM and Artemis promote homologous recombination of radiation-induced DNA double-strand breaks in G2.," *EMBO J,* vol. 28, no. 21, pp. 3413-27, 2009.

[244] C. Koschmann, A. Calinescu, F. Nunez, A. Mackay, J. Fazal-Salom, D. Thomas, F. Mendez, N. Kamran, M. Dzaman, L. Mulpuri, J. Krasinkiewicz, R. Doherty, R. Lemons, J. Brosnan-Cashman, Y. Li, S. Roh, L. Zhao and C. M. ..., "ATRX loss promotes tumor growth and impairs nonhomologous end joining DNA repair in glioma.," *Sci Transl Med,* vol. 8, no. 328, p. 328ra28, 2016.

[245] N. Bérubé, J. Healy, C. Medina, S. Wu, T. Hodgson, M. Jagla and D. Picketts, "Patient mutations alter ATRX targeting to PML nuclear bodies.," *Eur J Hum Genet,* vol. 16, no. 2, pp. 192-201, 2008.

[246] B. Sirbu, F. Couch, J. Feigerle, S. Bhaskara, S. Hiebert and D. Cortez, "Analysis of protein dynamics at active, stalled, and collapsed replication forks.," *Genes Dev,* vol. 25, no. 12, pp. 1320-7, 2011.

[247] D. Rasio, Y. Murakumo, D. Robbins, T. Roth, A. Silver, M. Negrini, C. Schmidt, J. Burczak, R. Fishel and C. Croce, "Characterization of the human homologue of RAD54: a gene located on chromosome 1p32 at a region of high loss of heterozygosity in breast tumors.," *Cancer Res.,* vol. 57, no. 12, pp. 2378-83, 1997.

[248] A. Olovnikov, "A theory of marginotomy. The incomplete copying of template margin in enzymic synthesis of polynucleotides and biological significance of the phenomenon.," *J Theor Biol.,* vol. 41, no. 1, pp. 181-90, 1973.

[249] D. Conomos, H. Pickett and R. Reddel, "Alternative lengthening of telomeres: remodeling the telomere architecture.," *Front Oncol. ,* vol. 3, no. 27, 2013.

[250] T. Bryan, L. Marusic, S. Bacchetti, M. Namba and R. Reddel, "The telomere lengthening mechanism in telomerase-negative immortal human cells does not involve the telomerase RNA subunit.," *Hum Mol Genet.,* vol. 6, no. 6, pp. 921-6, 1997.

[251] C. Heaphy, R. Wilde, Y. Jiao, A. Klein, B. Edil, C. Shi, C. Bettegowda, F. Rodriguez, C. Eberhart, S. Hebbar, G. Offerhaus, R. McLendon, B. Rasheed, Y. He, H. Yan, D. Bigner, S. Oba-Shinjo, S. Marie, G. Riggins, K. Kinzler, B. Vogelstein and e. al., "Altered telomeres in tumors with ATRX and DAXX mutations.," *Science,* vol. 333, no. 6041, p. 425, 2011.

[252] A. Farooqi, R. Dagg, L. Choi, J. Shay, C. Reynolds and L. Lau, "Alternative lengthening of telomeres in neuroblastoma cell lines is associated with a lack of MYCN genomic amplification and with p53 pathway aberrations.," *J Neurooncol,* vol. 119, no. 1, pp. 17-26, 2014.

[253] I. Marinoni, A. Kurrer, E. Vassella, M. Dettmer, T. Rudolph, V. Banz, F. Hunger, S. Pasquinelli, E. Speel and A. Perren, "Loss of DAXX and ATRX are associated with chromosome instability and reduced survival of patients with pancreatic neuroendocrine tumors.," *Gastroenterology.,* vol. 146, no. 2, pp. 453-60, 2014.

[254] J. Liau, J. Tsai, Y. Jeng, J. Lee, H. Hsu and C. Yang, "Leiomyosarcoma With Alternative Lengthening of Telomeres Is Associated With Aggressive Histologic Features, Loss of ATRX Expression, and Poor Clinical Outcome.," *Am J Surg Pathol.,* 2014.

[255] C. Lovejoy, W. Li, S. Reisenweber, S. Thongthip, J. Bruno, T. de Lange, S. De, J. Petrini, P. Sung, M. Jasin, J. Rosenbluh, Y. Zwang, B. Weir, C. Hatton, E. Ivanova, L. Macconaill, M. Hanna, W. Hahn, N. Lue, R. Reddel and .. A. S. C. Consortium, "Loss of ATRX, genome instability, and an altered DNA damage response are hallmarks of the alternative lengthening of telomeres pathway.," *PLoS Genet.,* vol. 8, no. 7, p. e1002772, 2012.

[256] C. Koelsche, M. Renner, P. Johann, I. Leiss, F. Sahm, S. Schimmack, E. Wardelmann, E. Renker, P. Schirmacher, A. Korshunov, A. von Deimling and G. Mechtersheimer, "Differential nuclear ATRX expression in sarcomas.," *Histopathology.,* vol. 68, no. 5, pp. 738-45, 2016.

[257] M. Abedalthagafi, J. Phillips, G. Kim, S. Mueller, D. Haas-Kogen, R. Marshall, S. Croul, M. Santi, J. Cheng, S. Zhou, L. Sullivan, M. Martinez-Lage, A. Judkins and A. Perry, "The alternative lengthening of telomere phenotype is significantly associated with loss of ATRX expression in high-grade pediatric and adult astrocytomas: a multi-institutional study of 214 astrocytomas.,"

Mod Pathol, vol. 26, no. 1, pp. 1425-32, 2013.

[258] K. Masui, P. Mischel and G. Reifenberger, "Molecular classification of gliomas.," *Handb Clin Neurol. ,* vol. 134, pp. 97-120, 2016.

[259] K. Kannan, A. Inagaki, J. Silber, D. Gorovets, J. Zhang, E. Kastenhuber, A. Heguy, J. Petrini, T. Chan and J. Huse, "Whole-exome sequencing identifies ATRX mutation as a key molecular determinant in lower-grade glioma.," *Oncotarget.,* vol. 3, no. 10, pp. 1194-203, 2012.

[260] C. Napier, L. Huschtscha, A. Harvey, K. Bower, J. Noble, E. Hendrickson and R. Reddel, "ATRX represses alternative lengthening of telomeres.," *Oncotarget.,* vol. 6, no. 18, pp. 16543-58, 2015.

[261] J. Lee, J. Ledermann and E. Kohn, "PARP Inhibitors for BRCA1/2 mutation-associated and BRCA-like malignancies.," *Ann Oncol,* vol. 25, no. 1, pp. 32-40, 2014.

[262] C. Lord, A. Tutt and A. Ashworth, "Synthetic lethality and cancer therapy: lessons learned from the development of PARP inhibitors.," *Annu Rev Med,* vol. 66, pp. 455-70, 2015.

[263] T. Xiong, H. Wei, X. Chen and H. Xiao, "PJ34, a poly(ADP-ribose) polymerase (PARP) inhibitor, reverses melphalan-resistance and inhibits repair of DNA double-strand breaks by targeting the FA/BRCA pathway in multidrug resistant multiple myeloma cell line RPMI8226/R.," *Int J Oncol,* vol. 46, no. 1, pp. 223-32, 2015.

[264] A. Sistigu, G. Manic, F. Obrist and I. Vitale, "Trial watch - inhibiting PARP enzymes for anticancer therapy.," *Mol Cell Oncol,* vol. 3, no. 2, p. e1053594, 2015.

[265] J. Ledermann, "PARP inhibitors in ovarian cancer.," *Ann Oncol,* vol. 1, pp. 40-44, 2016.

[266] D. Lim and J. Ngeow, "Evaluation of the methods to identify patients who may benefit from PARP inhibitor use.," *Endocr Relat Cancer,* pp. 16-0116, 2016.

[267] N. Berube, M. Mandelsdorf, M. Jagla, J. Vanderluit, D. Garrick, R. Gibbons, D. Higgs, R. Slack and D. Picketts, "The chromatin-remodeling protein ATRX is critical for neuronal survival during corticogenesis.," *J Clin Invest,* vol. 115, no. 2, pp. 258-67, 2005.

[268] R. Gibbons, D. Picketts, L. Villard and D. Higgs, "Mutations in a putative global transcriptional regulator cause X-linked mental retardation with alpha-thalassemia (ATR-X syndrome).," *Cell,* vol. 80, no. 6, pp. 837-45, 1995.

[269] D. Clynes, C. Jelinska, B. Xella, H. Ayyub, S. Taylor, M. Mitson, C. Bachrati, D. Higgs and R. Gibbons, "ATRX dysfunction induces replication defects in primary mouse cells.," *PLoS One,* vol. 9, no. 3, p. e92912, 2014.

[270] M. Huh, P. O. T. D. Ouazia, B. McKay, G. Parise, R. Parks, M. Rudnicki and D. Picketts, "Compromised genomic integrity impedes muscle growth after Atrx inactivation.," *J Clin Invest.,* vol. 122, no. 12, pp. 4412-23, 2012.

[271] J. Smith, L. Tho, N. Xu and D. Gillespie, "The ATM-Chk2 and ATR-Chk1 pathways in DNA damage signaling and cancer.," *Adv Cancer Res.,* vol. 108, pp. 73-112, 2010.

[272] R. Gibbons, T. Wada, C. Fisher, N. Malik, M. Mitson, D. Steensma, A. Fryer, D. Goudie, I. Krantz and J. Traeger-Synodinos, "Mutations in the chromatin-associated protein ATRX.," *Hum Mutat,* vol. 29, no. 6, pp. 796-802, 2008.

[273] B. Lamarche, N. Orazio and M. Weitzman, "The MRN complex in double-strand break repair and telomere maintenance.," *FEBS Lett,* vol. 582, no. 17, pp. 3682-95, 2010.

[274] M. Lieber, "The mechanism of double-strand DNA break repair by the nonhomologous DNA end-joining pathway.," *Annu Rev Biochem.,* vol. 79, pp. 181-211, 2010.

[275] R. Roy, J. Chun and S. Powell, "BRCA1 and BRCA2: different roles in a common pathway of genome protection.," *Nat Rev Cancer,* vol. 12, no. 1, pp. 68-78, 2011.

[276] P. McKinnon, "Maintaining genome stability in the nervous system.," *Nat Neurosci,* vol. 16, no. 11, pp. 1523-9, 2013.

[277] M. van Kregten and M. Tijsterman, "The repair of G-quadruplex-induced DNA damage.," *Exp Cell Res.,* vol. 329, no. 1, pp. 178-83, 2014.

[278] J. Hebert and S. McConnell, "Targeting of cre to the Foxg1 (BF-1) locus mediates loxP recombination in the telencephalon and other developing head structures.," *Dev Biol,* vol. 222, no. 2, pp. 296-306, 2000.

[279] M. Curtin, Understanding the role of Parp-1 in the Atrx(null) cortex, URL: http://hdl.handle.net/10393/28512 ed., Master's Thesis: University of Ottawa, 2009.

[280] J. Hebert and S. McConnell, "The chromatin-remodeling protein ATRX is critical for neuronal survival during corticogenesis.," *Dev Biol,* vol. 222, no. 2, pp. 296-306, 2000.

6. Contributions of Collaborators

The thesis was written by the author with editing and input from Dr. David Picketts and Dr. Michael Huh.

All experiments were performed by the author with the following exceptions:

Mouse breeding, neuronal cryosectioning, and neuronal immunofluorescent staining was performed by Keqin Yan (see **Figures 9 and 10**).

Neuronal immunofluorescent image quantification was performed by Dr. Michael Huh and Keqin Yan (see **Figures 9 and 10**).

Western blot analysis of PJ34 treated ATRX KD HeLa cell protein lysates was performed by Dr. Michael Huh (see **Figure 13B**).

TUNEL staining on PJ34 treated ATRX KD HeLa cells was performed and analyzed by Keqin Yan and Dr. Michael Huh (see **Figure 14B**).

The collective work of this thesis was a contribution to a published paper entitled “Stalled replication forks within heterochromatin require ATRX for protection” (see Appendix).

7. Appendix

OPEN

Citation: Cell Death and Disease (2016) 7, e2220; doi:10.1038/cddis.2016.121

www.nature.com/cddis

Stalled replication forks within heterochromatin require ATRX for protection

Michael S. Huh[1,#], Danton Ivanochko[1,2,#], Emile L. Hashem[1,3], Maureen Curtin[1,2], Marilyne Delorme[1,2], Emma Goodall[1,2], Keqin Yan[1], and David J. Picketts[1-3,*]

[1] Regenerative Medicine Program, Ottawa Hospital Research Institute, Ottawa, Ontario, K1H 8L6, Canada;

[2] Department of Biochemistry, Microbiology, and Immunology, Faculty of Medicine, University of Ottawa, Ontario, K1H 8M5, Canada

[3] Department of Cellular and Molecular Medicine, Faculty of Medicine, University of Ottawa, Ontario, K1H 8M5, Canada

[#] These authors made equal contributions to the manuscript.

[*] To whom correspondence should be addressed: Regenerative Medicine Program, Ottawa Hospital Research Institute, 501 Smyth Road, Ottawa, Ontario, K1H 8L6, Canada;
E-Mail: dpicketts@ohri.ca; Tel.: +1-613-737-8989; Fax: +1-613-737-8803.

Summary

Expansive growth of neural progenitor cells (NPCs) is a prerequisite to the temporal waves of neuronal differentiation that generate the six-layered neocortex, while also placing a heavy burden on proteins that regulate chromatin packaging and genome integrity. This problem is further reflected by the growing number of developmental disorders caused by mutations in chromatin regulators. ATRX gene mutations cause a severe intellectual disability disorder (ATR-X syndrome; OMIM#301040) characterized by microcephaly, urogenital abnormalities and alpha-thalassemia. While the ATRX protein is required for the maintenance of repetitive DNA within heterochromatin, how this translates to disease pathogenesis remains poorly understood and was a focus of this study. We demonstrate that *Atrx*^{FoxG1Cre} forebrain-specific conditional knockout mice display Parp1 hyperactivation during neurogenesis and generate fewer late-born Cux1 and Brn2 positive neurons that accounts for the reduced cortical size. Moreover, DNA damage, induced Parp1 and Atm activation is elevated in progenitor cells and contributes to their increased level of cell death. ATRX-null HeLa cells are similarly sensitive to hydroxyurea-induced replication stress, accumulate DNA damage, and proliferate poorly. Impaired BRCA1-RAD51 co-localization and PARP1 hyperactivation indicated that that stalled replication forks are not efficiently protected. DNA fiber assays confirmed that MRE11 degradation of stalled replication forks was rampant in the absence of ATRX or DAXX. Indeed, fork degradation in ATRX-null cells could be attenuated by treatment with the MRE11 inhibitor mirin, or exacerbated by inhibiting PARP1 activity. Taken together, these results suggest that ATRX is required to limit replication stress during cellular proliferation, while upregulation of PARP1 activity functions as a compensatory mechanism to protect stalled forks, limiting genomic damage and facilitating late-born neuron production.

Introduction

Mutations in genes encoding epigenetic regulators are the cause of many neurodevelopmental disorders thereby highlighting the importance of chromatin remodelling to progenitor cell growth, competency, cell fate and differentiation capacity[1]. In this regard, mutations in the human *ATRX* gene cause Alpha-Thalassemia Mental Retardation X-linked (ATR-X; OMIM# 301040) syndrome, a severe intellectual disability disorder commonly associated with urogenital abnormalities, facial dysmorphism, and alpha-thalassemia[2,3].

The *ATRX* gene encodes a 280 kDa protein with two chromatin-interaction domains, a C-terminal SNF2 helicase-like domain that provides DNA dependent ATPase activity; and an N-terminal ADD (ATRX-DNMT3-DNMT3L) domain that serves as a dual histone modification recognition module (H3K9me3/H3K4me0; H3K9me3/H3S10p) to target ATRX to heterochromatin[4-6]. Moreover, ATRX complexes with DAXX to form a histone chaperone complex that loads histone H3.3 onto telomeres, imprinted genes, and endogenous retroviral elements, to establish and maintain a heterochromatin environment[7-11]. Nonetheless, it remains unclear how these biochemical functions contribute to brain development.

Forebrain-specific inactivation of *Atrx* in mice results in enhanced apoptosis and cerebral hypocellularity[12], a phenotypic feature commonly observed in ATR-X patients[13]. Further characterization of proliferating cells lacking *Atrx* demonstrate that S-phase progression is delayed and accompanied with an activated DNA damage response, fragile telomeres, and mitotic catastrophe that enhances cell death in rapidly expanding progenitors of the testis, skeletal muscle, and CNS[12,14-16]. Aberrant replication of heterochromatin was suggested by ChIP-Seq analysis as Atrx binding sites are enriched at simple repeats including telomeres and other guanine-rich sequences with a propensity to form G4-quadruplexes[17]. Moreover, it was proposed that disease pathogenesis could arise from an inability to prevent G4-quadruplex formation, which would impede replication and

transcription[18,19]. Initial support for this model came from studies showing that Atrx interacts with the Mre11-Rad50-Nbs1 (MRN) complex and that Atrx deficient cells have an increase in stalled replication forks[15,20]. Mechanisms that protect stalled replication forks are especially critical during mid-late S-phase, due to the abundance of natural barriers present in heterochromatin[21].

Here, we examined whether Atrx functions to protect stalled replication forks from collapse and subsequent DNA damage. Indeed, we observed that *Atrx*-deficient cells acquire DNA damage in S-phase, which persists and accumulates in a cell-cycle progressive manner. The replication stress is defined by reduced co-localization of BRCA1 with RAD51, indicating aberrant replication fork protection. The degradation of replication forks is mediated by Mre11, which leads to an increase in double strand DNA breaks, fork collapse, genomic instability and cell death that reduces the progenitor cell pool. As a consequence of fork degradation, neural progenitors activate Parp-1 to promote fork protection and cell survival thereby limiting upper layer neuron loss. Indeed, PARP-1 inhibition further perturbed cell growth. Moreover, acute knockdown of Daxx resulted in a similar degradation of nascent DNA strands suggesting that histone H3.3 loading facilitates replication fork protection.

Results

Increased DNA damage in neural progenitors compromises late-born neuron production

Previous work in our lab demonstrated that *Atrx*-null primary myoblasts were incapable of prolonged expansion due to S-phase defects and genomic instability that severely compromised muscle regeneration[16]. If forebrain progenitor expansion was similarly affected, we reasoned that early-born neuron production would not be compromised but later-born neuron production would be decreased resulting in the reduced cortical mass we observed in $Atrx^{FoxG1Cre}$ forebrain-specific conditional knockout (*Atrx* cKO) mice[12]. To assess neuron production in *Atrx* cKO mice, we determined the proportion of cells comprising the different cortical layers using layer-specific markers. The earliest born neurons comprise the subplate and the deep layers (VI and V) of the cortex as the forebrain is generated in an inside-out manner. We observed a significant proportional increase in Nurr1+ subplate neurons but no differences in the layer VI (Tbr1+), layer V (Ctip2+), or layer IV (Foxp1+) cells in the *Atrx* cKO brains compared to WT littermates (Figure 1A; Suppl Fig 1). While this suggested that a sufficient progenitor pool existed to generate the early-born neurons, we observed a significant reduction in the latest born Cux1+ neurons (layer II/III), while Brn2+ and Satb2+ neurons showed reduced levels that did not reach statistical significance (Figure 1B). Moreover, the cerebral cortex of *Atrx* cKO mice contained significantly fewer neurons than their WT littermates at E18.5 (Figure 1C), indicating that progenitor cell expansion was compromised.

To determine whether genome instability might be the cause of reduced neuron production, we examined the DNA damage marker γH2AX by immunofluorescent (IF) staining of E13.5 cortical sections. We observed a significant increase in γH2AX+ cells that was predominantly located in the proliferative ventricular (VZ) and intermediate (IZ) zones (Figure 1D). Furthermore, we observed an accumulation of genomic damage by E15.5 as

assessed by the co-localization of γH2AX signalling with markers for radial glial (Pax6+) and intermediate (Tbr2+) progenitor cells (Suppl Figure 2). Since the genomic instability in *Atrx* cKO myoblasts was caused by DNA replication stress, we examined Parp-1 activity, a known effector of this pathway. Parp-1 activity was assessed using antibodies specific to Parp-1 and polyADP-ribose (PAR), the moiety added to substrates when the polymerase is active. IF staining of E13.5 Atrx cKO neocortices revealed increased PAR staining primarily within the proliferative zone (Figure 2A,B). Immunoblots from cortical extracts demonstrated this was not due to changes in Parp-1 expression but increased activity (Figure 2C). Indeed, a high level of PARylation was observed at E12.5 and E13.5 in all embryos but it persisted only in the *Atrx* cKO embryos at E14.5 and E15.5 (Figure 2C). As such, we used the E13.5 cortical extracts to assess the activation of the DNA damage response via phosphorylation of ataxia telangiectasia mutated (pATM) and H2AX (□H2AX). Both mutant and WT samples showed active PARylation, but only *Atrx* cKO extracts showed increased pATM and γH2AX to indicate an activated DNA damage response (Figure 2C). Interestingly, the Parp-1 immunoblots show a shift in size only in the mutant lanes that probably reflects significant auto-PARylation of the Parp-1 protein (Figure 2C & Suppl. Figure 4). As an indication that DNA damage was leading to cell death, we harvested embryonic cortical extracts from *Atrx* cKO and WT littermates at E12.5 and E17.5 for caspase activity assays. We observed a significant increase in the activation of the executioner caspase, caspase 3 that was mediated by an intrinsic response, since we observed an increase in caspase 9 activity but not caspase 8 (Suppl Figure 3).

Collectively, these data suggest that genomic instability within the neural precursor population contributes to the observed neuronal cell loss. As depicted in Figure 2D, we postulate that genomic damage accumulates with each successive pass through S-phase in the *Atrx*-null progenitor cells, and with 7 to 8 cell cycles within the span of 3 days there is

diminished viability thereby reducing the pool of late-stage progenitors that generate the upper layer neurons.

Delayed S-phase in ATRX knockdown cells leads to increased activation of p53-ATM checkpoint in the subsequent G1

To further investigate the mechanisms by which ATRX regulates genomic stability, we generated both acute and stable knockdown (KD) HeLa cells using siATRX or short hairpin expressing plasmids (psiRNA ATRX) with their respective controls (siScram and psiRNA LacZ). Cell cycle progression analysis of BrdU labeled cells revealed that psiRNA ATRX cells were delayed through S-phase and G2-M, similar to primary myoblasts (Suppl Figure 5;[16]). Since extended passaging of our psiRNA ATRX stable clones resulted in the selective suppression of the shRNA *ATRX* transgene the remainder of our experiments used the acute KD model. Following transfection, protein levels of ATRX were nearly undetectable by 48 hours and remained absent until 120 hours, while we also observed an increase in γH2AX signalling over this timeline (Suppl Figure 6). As such, this model is able to replicate our *in vivo* results and can be used to explore the role of ATRX during replication stress.

Previous work has demonstrated that Atrx-null cells are delayed through S-phase and have an increased incidence of stalled replication forks[15,16,20]. Since stalled replication forks often collapse and form DNA double stranded breaks[22], we reasoned that the cell loss observed in ATRX KD cells may be due to the progressive accumulation of DSBs during progenitor proliferation. For this study, we examined the activation status of ATM with respect to cell cycle stage (S/G2 or G1) at 72 and 96 hours post transfection. In this regard, cells were co-stained for pATM and Cyclin A (Figure 3A). To quantify pATM signaling pertaining to DNA damage, cells with punctate staining were scored while cytoplasmic pATM+ cells were excluded, as these represent cells undergoing mitosis[23,24]. Similarly, cells transiting S/G2 phases of the cell cycle were distinguished by Cyclin A staining[25,26], and this

was confirmed in our hands (Suppl Figure 7). At both the 72 and 96 hour time points, we observed a significant increase in the proportion of ATRX KD cells (45.8% and 48.5%, respectively) with focal pATM nuclear staining compared to siScram (39.3% and 36.1%, respectively) control cells (Figure 3B). When total pATM cell counts were dissected into cells in S/G2 (Cyclin A+) or G1 (Cyclin A-) phase of the cell cycle we observed a >50% increase in pATM staining in S/G2 at both 72 and 96 hours (Figure 3C). Interestingly, we observed a time-dependent increase in pATM staining in the ATRX KD cells within the G1 subpopulations. The ATRX KD and control cells showed no difference at 72 hours, but at 96 hours post transfection focal pATM staining significantly increased (compare 38.8% vs. 29.8%) in the ATRX KD cells (Figure 3D). These findings illustrate the persistence and accumulation of a replication dependent DDR response in the subsequent G1 of ATRX KD cells. Moreover, it further supports the model that progenitors accumulate more DSBs, ultimately resulting in genomic instability and activation of cell death pathways.

Impaired RAD51 co-localization to BRCA1 foci in ATRX KD cells

Heterochromatin contains an abundance of simple repeats that are prone to instability during replication, forming unusual DNA structures (eg. Cruciform, Z-DNA, and G-quadruplexes) that can cause replication fork stalling[21,27]. ATRX is a heterochromatin associated protein that preferentially binds to G-rich tandemly repeated DNA sequences that form G-quadruplexes[17,28]. Since such structures require homology directed recombination (HR) repair to remove them[29], we hypothesized that the absence of ATRX during replication may compromise the function of the HR machinery at replicating heterochromatin. In this regard, both ATRX and BRCA1 co-localized to replicating heterochromatin domains marked by either heterochromatin protein 1 alpha (HP1α) or mid-late S-phase BrdU labeled foci (Suppl Figure 8A, B). To assess whether there was active HR repair after ATRX KD we co-labeled cells with BRCA1 and Rad51, functional beacons for HR machinery recruitment at sites of stalled replication forks[22,30-32]. Double

immunoflourescent detection of BRCA1 and RAD51 revealed co-localized nuclear focal signals (Figure 3E). Quantification of BRCA1 foci revealed a greater number of BRCA1 foci present in ATRX KD cells versus controls (compare 11.5 foci/nucleus versus 7.4 foci/nucleus respectively; Figure 3F). Despite this overall increase in the frequency of BRCA1 foci, the proportion of BRCA1 foci with co-localized RAD51 signals were dramatically reduced in ATRX KD cells by 31% relative to controls (Figure 3H). Taken together, this data suggests that insufficient loading of RAD51 at BRCA1 foci may compromise HR-mediated fork restart or stability in the absence of ATRX.

PARP1 activation functions as a compensatory protective response to stalled replication forks

We next questioned whether the increased PAR activity we observed in the *Atrx* cKO forebrain indicated a compensatory mechanism to protect stalled replication forks upon RAD51 dysregulation. Poly(ADP-Ribose) polymerases (PARPs) are multi-functional enzymes that affect DNA repair, replication fork protection and restart[24,33-35]. Moreover, PARP1 hyperactivation in cells with compromised HR pathways has been attributed to a protective response induced by stalled and collapsed replication forks[36,37]. We first confirmed that increased PAR signalling was also detected in ATRX KD cells while total PARP1 levels remained unchanged (Figure 4A, compare lanes 3 and 1). In addition, we used siPARP1 to attribute increased PARylation specifically to PARP1. Indeed, PARP1 accounts for approximately 90% of PARylation[38], and we observed a dramatic decrease in PAR signalling when cells were treated with both siATRX and siPARP1 (Suppl. Figure 10). As other studies have shown that HR-deficient cells are commonly hypersensitive to PARP inhibition [39], we used the PARP inhibitor PJ34 to assess whether the ATRX KD cells were similarly sensitive. PARP inhibition by PJ34 potently suppressed PAR signalling in ATRX KD cells, with a concomitant increase in 53BP1 protein levels compared to siScram controls (Figure 4A, lane 4 and 3). Quantification of 53BP1 positive nuclei revealed an 83% increase

in frequency within PJ34 treated ATRX KD cells relative to PJ34 treated controls (Figures 4B & Suppl. Figure 9A). Moreover, PJ34 treated ATRX KD cells showed an increased level of TUNEL+ nuclei and a severe attenuation of their growth rate over a 5-day time course measured with a WST-1 cell viability assay (Figure 4C-E). Together these experiments suggest that increased PARP1 activity observed in the absence of ATRX represents a protective response to maintain the integrity of stalled replication forks.

The ATRX-DAXX complex facilitates replication fork processivity and protection

ATRX depleted ES cells exhibit a greater sensitivity to hydroxyurea-induced replication fork stalling and delayed replication restart[15,20]. These studies also identified a physical interaction between ATRX and the MRN complex[15,20]. However, the mechanism causing the increased fork stalling was not determined. Based on reduced Rad51 co-localization with BRCA1 and active PARP1, we reasoned that replication fork protection could be compromised. In this regard, HR proteins such as BRCA1/2, RAD51, and MRE11 are functionally critical for the protection of stalled replication forks, independent of their role in double stranded DNA-repair[40]. RAD51 nucleofilament formation at stalled replication forks prevents MRE11-dependent degradation of newly synthesized DNA to allow for the resumption of DNA synthesis[41]. Indeed, artificially blocking RAD51 nucleofilament formation by overexpressing the RAD51 binding peptide BRC4, potently induced fork destabilization upon hydroxyurea (HU) exposure[30]. To assess whether MRE11 exonuclease activity was overly active, we performed DNA fiber studies following HU-induced replication fork stalling, with or without ATRX present. Previous work has implicated BRCA1 in the protection of stalled replication forks[30]. Indeed, we confirmed that BrdU labelled nascent replication tracts of BRCA1-deficent cells (siBRCA1) were dramatically shorter following HU treatment compared to controls (Suppl. Figure 11). Quite strikingly, nascent replication tracts in ATRX KD cells were equally as short as the tracts observed in BRCA1 KD cells (Suppl. Figure 11). Shorter BrdU labelled nascent DNA tracts may be the result of decreased replisome

processivity rates and/or the instability to protect nascent strands from degradation at sites of stalled forks. In order to delineate the contribution of these processivity mechanisms, DNA track lengths were compared between the ATRX KD cells and siScrambled control cells without HU-induced fork stalling. While we observed that ATRX KD cells produced significantly shorter tracks than siScram control cells, track length reduction was significantly exacerbated upon HU treatment indicating that fork protection is also compromised (Figure 5A). Moreover, chemical inhibition of MRE11 with the small molecule mirin has been demonstrated to protect stalled replication forks from exonuclease resectioning[35,42]. Indeed, mirin treatment of ATRX KD cells produced mean replication tract lengths that were comparable to that of controls (Figure 5B) suggesting that ATRX mediates MRE11-dependent degradation at stalled replication forks. Accordingly, ATRX may directly suppress MRE11-dependent degradation at stalled forks as it co-immunoprecipitates with both MRE11 and NBS1 in wildtype asynchronous cells (Suppl. Figure 12A). Regardless, H3.3 has been shown to facilitate replication fork processivity during replication stress and the ATRX-DAXX complex serves as a chaperone for loading this histone variant[43,44]. To determine if replication fork protection may be mediated by ATRX-DAXX loading of histone H3.3, we performed a DNA fiber assay after depleting Daxx protein expression using a targeted siRNA (siDAXX). DAXX depletion did not affect ATRX protein levels (Suppl. Figure 12C) but did have a significant effect on DNA tract length (Figure 5C & D). Pertaining to processivity, tracts from siDAXX treated cells without HU were shorter than those from siScrambled control cells, however as with the ATRX KD, HU-induced fork stalling resulted in significantly shorter labeled tracts. These findings are consistent with a role for both ATRX and DAXX in the regulation of both replication fork processivity and protection upon fork stalling.

Discussion

Neuronal progenitor cells of the ventricular/subventricular zones sequentially exit the cell cycle to populate the distinct neuronal layers of the forebrain. Inherently, the most proliferative NPCs that become the upper neuronal layers have the greatest potential to incur replication-induced DNA damage and subsequent genomic instability. In this regard, we demonstrated that Atrx deletion *in vivo* in neural progenitor cells specifically compromised the genesis of cells targeted for the upper neocortical layers (Figure 1B, 2E). At the molecular level, we demonstrate that ATRX is required to diminish DNA replication stress, by protecting stalled replication forks, thereby preventing genomic damage and cell loss. Collectively, we propose a model in which ATRX is critical for heterochromatin maintenance throughout the cell cycle (Figure 6).

ATRX and DAXX function to maintain heterochromatin stability

Simple repeats are poor substrates for nucleosome recycling during DNA replication and represent regions of latent epigenomic instability[45-48]. Heterochromatin environments are essential for the preservation of structural elements, such as centromeres and telomeres, as well as for the repression of malicious DNA sequences encoding endogenous retroviral elements. The ATRX-DAXX histone chaperone deposits H3.3 at globally diffuse heterochromatic loci including telomeres, centromeres, differentially methylated regions (DMRs), CpG islands and endogenous retroviral elements in a replication-independent manner[9,11,44,49]. Accordingly, the loss of ATRX leads to the dysregulation of these loci[9,16,49] and therefore, we propose a replication-independent mechanism for ATRX and DAXX to establish and maintain heterochromatin (Figure 6A). While ATRX can recognize both HP1 and H3K9me3[4,50,51], its H3.3-chaperone function appears to be upstream of SUV39H-mediated H3K9 trimethylation[9,49]. Additionally, ATRX's ability to bind to G4-structured DNA *in vitro*, as well as its high binding enrichment at G4-motif containing DNA sequences *in vivo*[17] elicits the possibility that ATRX may recruit DAXX and H3.3 to G4 structured DNA for

localized heterochromatinization (Figure 6A). Regardless, further experimentation is required to validate a role for ATRX in re-establishing heterochromatin, similar to studies identifying a role for Asf1 in histone recycling[52]. Importantly, G4 structured DNA can cause replication fork stalling, necessitating its suppression prior to S-phase[21], while other studies have demonstrated fluid replication though G4 motif DNA is required for the preservation of distinct epigenomic loci[46,47].

ATRX actively protects stalled replication forks

Here we progress our model into S-phase and propose a mechanism wherein ATRX actively protects stalled replication forks within heterochromatin (Figure 6B). ATRX deficient cells are burdened by increased replication fork stalling events[15,20], which are subsequently degraded by MRE11 (Figure 5A, B) in a manner akin to BRCA1/2 deficient cells (Supplemental Figure 11)[30,53]. Adapting a previous model for ATRX regarding telomere maintenance[54], we propose that ATRX physically sequesters MRE11 to inhibit its exonuclease activity, thereby preventing fork degradation. BRCA1 co-localization with RAD51 marks the protection of stalled replication forks[29], and we observed an increase in BRCA1 foci formation without a concomitant increase in RAD51 co-localization in ATRX deficient cells. Unfettered MRE11 activity with an increased number of stalled replication forks may deplete RAD51 pools, and this may further attenuate stalled fork protection. In fact, a similar model has been proposed wherein ATR inhibition promoted precocious restart of stalled replication forks, thereby depleting RPA protein levels and ultimately leading to fork collapse[55]. Alternatively, dysregulated heterochromatin proximal to G4-structrured DNA may cause ineffective mobilization of homologous recombination factors such as RAD51 in ATRX deficient cells.

Furthermore, we propose that the upregulation of PARP1 activity (Figure 2C, 4A) can be attributed to a compensatory mechanism that engages to protect stalled replication forks from MRE11-dependent degradation by PARP1-mediated replication fork reversal[35,56]

(Figure 6B). In this way, the excessive processing of replicating heterochromatin in ATRX-null cells likely contributes to delayed S-phase progression (Suppl Fig 5B;[15,16]). Therefore, unresolved replication intermediates become dsDNA breaks (DSB) in the subsequent G2-phase[57], which may explain the increased DNA damage observed throughout the cell cycle (Figure 3 B-D, 6C).

Heterochromatin instability drives ATRX-associated disease

Collectively, our data and others' suggests that enhanced cell death and reduced tissue size occurs from an inability to faithfully replicate heterochromatin under periods of rampant proliferation. The replication intermediates lead to dsDNA breaks, genomic instability and mitotic catastrophe that reduces cell number (Figure 6C). Paradoxically, ATRX loss in cancer is beneficial to cell survival through the promotion of the alternative lengthening of telomeres (ALT) phenotype. In this regard, ATRX loss is believed to be a late event, presumably after sufficient growth control checkpoints are eliminated. The instability of telomeric heterochromatin in the absence of ATRX facilitates telomere sister chromatid exchange which maintains telomere length in ALT. Conversely, reintroduction of ATRX into ATRX-null ALT cancer cells restores H3.3 deposition at telomeres thereby inhibiting sister telomere exchange (SCE) and causing growth suppression[54]. Thus, our finding that small molecule inhibition of PARP1 activity attenuated growth of ATRX deficient cells offers a potentially therapeutic avenue towards treatment of ALT positive cancers, analogous to PARP inhibitor treatment to eliminate BRCA1/2 deficient cancer cells[58-60].

Materials and Methods

Animal husbandry

Atrx conditional knockouts were generated by crossing ATRX floxed females (*ATRX* $^{fl/fl}$) to ATRX$^{+/Y}$:*FoxG1-Cre*$^{+/-}$ males on a C57BL/6 background as described previously[12]. *ATRX*$^{fl/y}$*:FoxG1-Cre*$^{+/-}$ and *ATRX*$^{fl/y}$ (control) male littermates were harvested for analysis. Animal experiments were approved by the University of Ottawa's Animal Care ethics committee as per the guidelines set out by the Canadian Council on Animal Care.

Generation of ATRX shRNA cell lines

The expression vector psiRNA-hH1neo (InvivoGen, Sand Diego, CA) was digested with Bbs1 and purified for cloning the ATRX shRNA oligonucleotide. The ATRX sense (5'-ACCTAACACTCATCAGAAGAATCTGACCACCTCAGATTCTTCTGATGAGTGTTT-3') and antisense (5'-CAAAAAACACTCATCAGAAGAATCTGAGGTGGTCAGATTCTTCTGATGAGTGTT-3') oligonucleotides were designed with Bbs1 overhangs. The oligonucleotides (25□M) were annealed in 150 mM NaCl by heating to 80^{o}C for 2 min followed by slow cooling to 37^{o}C. Annealed oligonucleotides were then ligated and cloned into the psiRNA-hH1neo plasmid. Recombinants were identified by an AseI digestion, purified using a Qiagen Maxiprep kit (Qiagen), and sent for sequencing (StemCore, OHRI). To generate stable cell lines, HeLa cells (5x10^{7}) were transfected with psiRNA expressing vectors by Lipofectamine (Life Technologies) as per the manufacturer's instructions. Clones were selected in DMEM supplemented with 800 µg/mL G418 (Life Technologies) after two weeks in culture. Individual clones were isolated and knockdown of ATRX protein expression was determined by western blot.

Cell culture

HeLa cells were cultured at 37º C in DMEM with 10% FBS and 1% penicillin-streptomycin. Transient knockdown of ATRX and BRCA1 were performed on 50% confluent

cells using 0.72% (v/v) INTERFERin (Polyplus) in Opti-MEM® I Reduced Serum Medium (Thermo Fisher Scientific Inc.) as per the manufacturer's instructions, with 100nM of either siATRX Smart Pool or a Scrambled control (G.E. Healthcare, Amersham). siBRCA1 was a kind gift from Dr. Christine Pratt (University of Ottawa). PARP1 was inhibited with 5 μM PARP Inhibitor VIII (PJ34; Santa Cruz Biotechnology Inc., sc-204161A).

For stable shRNA expressing clone growth curves, WT HeLa cells, psiRNA LacZ, and psiRNA ATRX stable clones were G1 synchronized by 72 hr serum withdrawal. Growth media was reintroduced at time 0 and cells were enumerated at the indicated time points.

Protein extraction and immunoblot analysis

Cortical lysates were extracted by homogenization using the Tissue Tearor™ (Biospec Products, Inc.) in RIPA buffer (1 X PBS, 1% NP-40, 0.1% SDS, 0.5% sodium deoxycholate, protease inhibitor Complete Mini EDTA-free in ddH_2O). Cell culture lysates were extracted in RIPA buffer by gentle agitation. Protein samples were cleared by centrifugation at 4°C and supernatants were quantified using the Bio-Rad Protein Assay reagent (Bio-Rad). Protein samples were resolved on pre-cast 3-8% Tris-Acetate or 4-12% Tris-Bis gels (NuPage; Life Technologies) and transferred onto PVDF membrane (Immobilon-P; Millipore). Membranes were probed with the indicated primary antibodies (see Table S1) and HRP-conjugated secondary antibodies. Immunoblots were incubated with enhanced chemiluminescent substrate and signals were exposed to film. Densitometric gel analysis was performed using ImageJ (version 1.46r) software by integrating pixel density plots with background subtraction.

Immunofluorescent microscopy for cell culture

Cells were grown on coverslips or cytospun (Cytospin™ 4 Cytocentrifuge; Thermo Fisher Scientific Inc) onto slides and fixed in 2% PFA and permeabilized with 0.1% triton-x. Primary antibodies (see Table S1) were diluted in blocking buffer (20% horse serum, 0.1%

fetal bovine serum, 0.03% sodium azide, in PBS) and incubated overnight at 4°C in a humidifying chamber. Secondary antibodies (Alexas 488 & 594; Life Technologies) were applied and nuclei were counterstained with DAPI. Images were taken with an Axio Imager M1 microscope (Zeiss) and analyzed using ImageJ software. Positively stained cells were scored as indicated, relative to DAPI stained nuclei.

Immunofluorescent microscopy for brain sections

Embryos were harvested at the indicated gestational time points. Heads from embryos were fixed in 4% PFA overnight at 4°C. The heads were washed in PBS, cryoprotected in a 30% sucrose/PBS solution overnight at 4°C, embedded in a 1:1 solution of 30% sucrose and O.C.T. Compound (Tissue-Tek®) and flash frozen on liquid nitrogen. Embedded tissue were serially sectioned at 10 μm (Leica 1850 cryostat) and mounted onto Superfrost Plus coated slides (Fisher Scientific) and dried at room temperature for 2 hours. Slides were fixed with 70% ethanol for 5 minutes at 4^{o}C (IHC) or 2% PFA 10 minutes at room temperature and then rehydrated in 1 X PBS for 5 minutes prior to staining. When probing for PAR, slides were incubated in 2N HC1 for 20 minutes at 37°C. Sections were permeabilized (0.1% tween-20, 0.1M Tris-HCl pH 8.8) and incubated in blocking buffer (20% goat serum, 0.3% Triton-X in PBS). Primary antibodies (see Table S1) were diluted in blocking buffer and applied onto sections. Sections were washed in PBS, incubated in secondary antibody solution, and counterstained with DAPI. Images were taken with an Axio Imager M1 microscope (Zeiss). Marker positive cell counts were performed on multiple (n>3) 200□M brain sections from the dorsal cortex and plotted as a percentage of the total number of DAPI-positive cells.

Cell cycle progression analysis

HeLa psiRNA-LacZ and psiRNA-ATRX cells were pulsed with 30 μM BrdU containing media in triplicate for each time point (0, 6, 12, 16, 20, 24 and 28hrs). 10^6 cells were fixed with 1 mL of 70% ethanol solution at -20°C, overnight, resuspended in 0.1N HCL

+ 0.7% Triton-X on ice for 15 min and washed with PBS. Cells were stained in 1:100 dilution the primary antibody anti-BrdU (BD Biosciences) diluted in HBT (PBS, 0.05% FBS, 0.005% Tween 20), washed with HBT and stained with FITC conjugated secondary antibody anti-mouse diluted 1:20 in HBT for 30 min in the dark and precipitated for 7 min at 1,500 rpm. Cells were resuspended in PI (propidium idodine) solution with RNAse A (50 µg/ml PI, 40µg/ml RNase A) at 2000 cells/µL and analyzed by flowcytometry using a Beckman Coulter FACS station. Cell cycle distribution of the cell population was analyzed with the FCS Express 2 software (DeNovo Software, Thornhill, ON) and the cell cycle profile of each time point was analyzed with the ModFit software (Verity Software House, Topsham, ME).

Caspase assays

Cortical lysate protein was added to freshly prepared caspase activity buffer (25mM HEPES, 10% sucrose, 1 mM EDTA, 0.1% CHAPS, 10 mM DTT in ddH20) for a total volume of 199 µL/well. The reaction was initiated by the addition of 1 µL of 10 mM fluorescent substrate (Caspase 3 substrate, Ac-DEVD-AMC (BioMol P411),Caspase 8 substrate, Ac-IETD-AMC (BioMol P432) 49 Caspase 9 substrate, Ac-LEHD.AMC (BioMol P444)) to each well. A ThermoLabsystems Fluoroskan Ascent FL fluorometer using an excitation filter set to 380 nm and an emission filter set to 460 nm was used to read the absorbance of each well every 5 minutes over a 2 hour period.

DNA fiber assay

Nascent DNA of HeLa cells treated with siATRX, siBRCA1 or siScrambled was labeled with a 50 µM BrdU pulse and replication forks we stalled with 4mM hydroxyurea. Where indicated, cells were treated with the MRE11 inhibitor mirin at a concentration of 50 µM. 10^6 cells/2 µL were spotted onto glass slides and lysed with 7 µl of fiber lysis solution (50 mM EDTA, 0.5% SDS and 200 mM Tris-HCl) for 5 min at RT. Slides were tilted 15° to horizontal to spread DNA across the length of the slide, then air dried and fixed in methanol/acetic acid (3:1). Slides were immersed in 2.5 N HCl for 80 minutes, washed in

PBS, blocked in 5% BSA and stained with 1:500 Mouse anti-BrdU primary antibody (BD Biosciences) followed by 1:4000 Donkey anti-Mouse IgG (H+L) with Alexa Fluor® 488 conjugate secondary antibody (Thermo Fisher Scientific Inc.). Indicated numbers of labeled DNA fibers from three independent experiments per condition were imaged (Zeiss Axio Imager M1 microscope) and analyzed using ImageJ software.

WST- assay

WST-1 proliferation assay was performed as per manufacturer's instructions (Abcam, ab65473). HeLa cells were seeded at 1000 cells/well on a 96 well plate and absorbance measured at 450nm.

TUNEL assay

Cells were fixed with 2% PFA and were permeabilized in 0.1% Triton-X/0.1% sodium citrate for 2 minutes on ice. The TUNEL labeling (terminal uridine deoxynucleotidyl transferase dUTP nick end labeling) was performed using the In Situ Cell Death Detection Kit (Roche Applied Science) according to the manufacturer's instructions.

Statistical analysis

Statistical analysis was performed using Microsoft Excel statistical analysis package with means and standard error calculated. Significance was determined by two-tailed t tests of unequal variance (95% and 99% confidence intervals). Additionally, p-values for fiber assays were determined by Mann-Whitney test. All significant p-values were marked with asterisks, as follows: (*) $p < 0.05$, (**) $p < 0.01$, (***) $p < 0.001$.

Conflict of Interest

The authors declare no conflict of interest.

Acknowledgements

The authors would like to thank Jeff Hamill and Dr. Bruce McKay for assistance with FACS analysis. This work was supported by operating grants to DJP from the Canadian Institutes of Health Research (MOP-133586) and from the Cancer Research Society, University of Ottawa, and Ottawa Hospital Research Institute partnership program. DI was supported by a CIHR CGS-M award.

References

1 Kleefstra, T., Schenck, A., Kramer, J. M. & van Bokhoven, H. The genetics of cognitive epigenetics. *Neuropharmacology* **80**, 83-94, doi:10.1016/j.neuropharm.2013.12.025 (2014).

2 Gibbons, R. J. & Higgs, D. R. Molecular-clinical spectrum of the ATR-X syndrome. *Am J Med Genet* **97**, 204-212. (2000).

3 Gibbons, R. J., Picketts, D. J., Villard, L. & Higgs, D. R. Mutations in a putative global transcriptional regulator cause X-linked mental retardation with alpha-thalassemia (ATR-X syndrome). *Cell* **80**, 837-845 (1995).

4 Iwase, S. *et al.* ATRX ADD domain links an atypical histone methylation recognition mechanism to human mental-retardation syndrome. *Nature structural & molecular biology* **18**, 769-776, doi:10.1038/nsmb.2062 (2011).

5 Noh, K. M. *et al.* ATRX tolerates activity-dependent histone H3 methyl/phos switching to maintain repetitive element silencing in neurons. *Proc Natl Acad Sci U S A*, doi:10.1073/pnas.1411258112 (2014).

6 Picketts, D. J. *et al.* ATRX encodes a novel member of the SNF2 family of proteins: mutations point to a common mechanism underlying the ATR-X syndrome. *Hum Mol Genet* **5**, 1899-1907 (1996).

7 Lewis, P. W., Elsaesser, S. J., Noh, K. M., Stadler, S. C. & Allis, C. D. Daxx is an H3.3-specific histone chaperone and cooperates with ATRX in replication-independent chromatin assembly at telomeres. *Proc Natl Acad Sci U S A* **107**, 14075-14080, doi:10.1073/pnas.1008850107 (2010).

8 Tang, J. *et al.* A novel transcription regulatory complex containing Daxx and the ATR-X syndrome protein. *J Biol Chem* **279**, 20369-20377 (2004).

9 Voon, H. P. *et al.* ATRX Plays a Key Role in Maintaining Silencing at Interstitial Heterochromatic Loci and Imprinted Genes. *Cell reports* **11**, 405-418, doi:10.1016/j.celrep.2015.03.036 (2015).

10 Wong, L. H. *et al.* ATRX interacts with H3.3 in maintaining telomere structural integrity in pluripotent embryonic stem cells. *Genome Res* **20**, 351-360, doi:10.1101/gr.101477.109 (2010).

11 Elsasser, S. J., Noh, K. M., Diaz, N., Allis, C. D. & Banaszynski, L. A. Histone H3.3 is required for endogenous retroviral element silencing in embryonic stem cells. *Nature* **522**, 240-244, doi:10.1038/nature14345 (2015).

12 Berube, N. G. *et al.* The chromatin-remodeling protein ATRX is critical for neuronal survival during corticogenesis. *J Clin Invest* **115**, 258-267 (2005).

13 Gibbons, R. Alpha thalassaemia-mental retardation, X linked. *Orphanet J Rare Dis* **1**, 15 (2006).

14 Bagheri-Fam, S. *et al.* Defective survival of proliferating Sertoli cells and androgen receptor function in a mouse model of the ATR-X syndrome. *Hum Mol Genet* **20**, 2213-2224, doi:10.1093/hmg/ddr109 (2011).

15 Clynes, D. *et al.* ATRX dysfunction induces replication defects in primary mouse cells. *PloS one* **9**, e92915, doi:10.1371/journal.pone.0092915 (2014).

16 Huh, M. S. *et al.* Compromised genomic integrity impedes muscle growth after Atrx inactivation. *J Clin Invest* **122**, 4412-4423, doi:10.1172/JCI63765 (2012).

17 Law, M. J. *et al.* ATR-X syndrome protein targets tandem repeats and influences allele-specific expression in a size-dependent manner. *Cell* **143**, 367-378, doi:10.1016/j.cell.2010.09.023 (2010).

18 Clynes, D. & Gibbons, R. J. ATRX and the replication of structured DNA. *Curr Opin Genet Dev* **23**, 289-294, doi:10.1016/j.gde.2013.01.005 (2013).

19 Clynes, D., Higgs, D. R. & Gibbons, R. J. The chromatin remodeller ATRX: a repeat offender in human disease. *Trends Biochem Sci* **38**, 461-466, doi:10.1016/j.tibs.2013.06.011 (2013).
20 Leung, J. W. *et al.* Alpha thalassemia/mental retardation syndrome X-linked gene product ATRX is required for proper replication restart and cellular resistance to replication stress. *J Biol Chem* **288**, 6342-6350, doi:10.1074/jbc.M112.411603 (2013).
21 Mirkin, E. V. & Mirkin, S. M. Replication fork stalling at natural impediments. *Microbiol Mol Biol Rev* **71**, 13-35, doi:10.1128/MMBR.00030-06 (2007).
22 Petermann, E., Orta, M. L., Issaeva, N., Schultz, N. & Helleday, T. Hydroxyurea-stalled replication forks become progressively inactivated and require two different RAD51-mediated pathways for restart and repair. *Mol Cell* **37**, 492-502, doi:10.1016/j.molcel.2010.01.021 (2010).
23 Palazzo, L., Della Monica, R., Visconti, R., Costanzo, V. & Grieco, D. ATM controls proper mitotic spindle structure. *Cell Cycle* **13**, 1091-1100, doi:10.4161/cc.27945 (2014).
24 Yang, Y. G., Cortes, U., Patnaik, S., Jasin, M. & Wang, Z. Q. Ablation of PARP-1 does not interfere with the repair of DNA double-strand breaks, but compromises the reactivation of stalled replication forks. *Oncogene* **23**, 3872-3882, doi:10.1038/sj.onc.1207491 (2004).
25 Hunt, T., Luca, F. C. & Ruderman, J. V. The requirements for protein synthesis and degradation, and the control of destruction of cyclins A and B in the meiotic and mitotic cell cycles of the clam embryo. *J Cell Biol* **116**, 707-724 (1992).
26 Pines, J. & Hunter, T. Human cyclins A and B1 are differentially located in the cell and undergo cell cycle-dependent nuclear transport. *J Cell Biol* **115**, 1-17 (1991).
27 Peng, J. C. & Karpen, G. H. Epigenetic regulation of heterochromatic DNA stability. *Curr Opin Genet Dev* **18**, 204-211, doi:10.1016/j.gde.2008.01.021 (2008).
28 McDowell, T. L. *et al.* Localization of a putative transcriptional regulator (ATRX) at pericentromeric heterochromatin and the short arms of acrocentric chromosomes. *Proc Natl Acad Sci U S A* **96**, 13983-13988 (1999).
29 Feng, Z. & Zhang, J. A dual role of BRCA1 in two distinct homologous recombination mediated repair in response to replication arrest. *Nucleic Acids Res* **40**, 726-738, doi:10.1093/nar/gkr748 (2012).
30 Schlacher, K., Wu, H. & Jasin, M. A distinct replication fork protection pathway connects Fanconi anemia tumor suppressors to RAD51-BRCA1/2. *Cancer Cell* **22**, 106-116, doi:10.1016/j.ccr.2012.05.015 (2012).
31 Scully, R. *et al.* Dynamic changes of BRCA1 subnuclear location and phosphorylation state are initiated by DNA damage. *Cell* **90**, 425-435 (1997).
32 Scully, R. *et al.* Association of BRCA1 with Rad51 in mitotic and meiotic cells. *Cell* **88**, 265-275 (1997).
33 Bryant, H. E. *et al.* PARP is activated at stalled forks to mediate Mre11-dependent replication restart and recombination. *EMBO J* **28**, 2601-2615, doi:10.1038/emboj.2009.206 (2009).
34 Hassler, M. & Ladurner, A. G. Towards a structural understanding of PARP1 activation and related signalling ADP-ribosyl-transferases. *Curr Opin Struct Biol* **22**, 721-729, doi:10.1016/j.sbi.2012.08.005 (2012).
35 Ying, S., Hamdy, F. C. & Helleday, T. Mre11-dependent degradation of stalled DNA replication forks is prevented by BRCA2 and PARP1. *Cancer Res* **72**, 2814-2821, doi:10.1158/0008-5472.CAN-11-3417 (2012).

36 De Lorenzo, S. B., Patel, A. G., Hurley, R. M. & Kaufmann, S. H. The Elephant and the Blind Men: Making Sense of PARP Inhibitors in Homologous Recombination Deficient Tumor Cells. *Front Oncol* **3**, 228, doi:10.3389/fonc.2013.00228 (2013).
37 Gottipati, P. *et al.* Poly(ADP-ribose) polymerase is hyperactivated in homologous recombination-defective cells. *Cancer Res* **70**, 5389-5398, doi:10.1158/0008-5472.CAN-09-4716 (2010).
38 Ame, J. C., Spenlehauer, C. & de Murcia, G. The PARP superfamily. *Bioessays* **26**, 882-893, doi:10.1002/bies.20085 (2004).
39 Steffen, J. D., Brody, J. R., Armen, R. S. & Pascal, J. M. Structural Implications for Selective Targeting of PARPs. *Front Oncol* **3**, 301, doi:10.3389/fonc.2013.00301 (2013).
40 Petermann, E. & Helleday, T. Pathways of mammalian replication fork restart. *Nat Rev Mol Cell Biol* **11**, 683-687, doi:10.1038/nrm2974 (2010).
41 Hashimoto, Y., Ray Chaudhuri, A., Lopes, M. & Costanzo, V. Rad51 protects nascent DNA from Mre11-dependent degradation and promotes continuous DNA synthesis. *Nature structural & molecular biology* **17**, 1305-1311, doi:10.1038/nsmb.1927 (2010).
42 Dupre, A. *et al.* A forward chemical genetic screen reveals an inhibitor of the Mre11-Rad50-Nbs1 complex. *Nat Chem Biol* **4**, 119-125, doi:10.1038/nchembio.63 (2008).
43 Frey, A., Listovsky, T., Guilbaud, G., Sarkies, P. & Sale, J. E. Histone H3.3 is required to maintain replication fork progression after UV damage. *Curr Biol* **24**, 2195-2201, doi:10.1016/j.cub.2014.07.077 (2014).
44 Goldberg, A. D. *et al.* Distinct factors control histone variant H3.3 localization at specific genomic regions. *Cell* **140**, 678-691, doi:10.1016/j.cell.2010.01.003 (2010).
45 Sarkies, P. *et al.* FANCJ coordinates two pathways that maintain epigenetic stability at G-quadruplex DNA. *Nucleic Acids Res* **40**, 1485-1498, doi:10.1093/nar/gkr868 (2012).
46 Sarkies, P., Reams, C., Simpson, L. J. & Sale, J. E. Epigenetic instability due to defective replication of structured DNA. *Mol Cell* **40**, 703-713, doi:10.1016/j.molcel.2010.11.009 (2010).
47 Schiavone, D. *et al.* Determinants of G quadruplex-induced epigenetic instability in REV1-deficient cells. *EMBO J* **33**, 2507-2520, doi:10.15252/embj.201488398 (2014).
48 Schneiderman, J. I., Sakai, A., Goldstein, S. & Ahmad, K. The XNP remodeler targets dynamic chromatin in Drosophila. *Proc Natl Acad Sci U S A* **106**, 14472-14477, doi:10.1073/pnas.0905816106 (2009).
49 He, Q. *et al.* The Daxx/Atrx Complex Protects Tandem Repetitive Elements during DNA Hypomethylation by Promoting H3K9 Trimethylation. *Cell stem cell* **17**, 273-286, doi:10.1016/j.stem.2015.07.022 (2015).
50 Berube, N. G., Smeenk, C. A. & Picketts, D. J. Cell cycle-dependent phosphorylation of the ATRX protein correlates with changes in nuclear matrix and chromatin association. *Hum Mol Genet* **9**, 539-547 (2000).
51 Eustermann, S. *et al.* Combinatorial readout of histone H3 modifications specifies localization of ATRX to heterochromatin. *Nature structural & molecular biology* **18**, 777-782, doi:10.1038/nsmb.2070 (2011).
52 Jasencakova, Z. *et al.* Replication stress interferes with histone recycling and predeposition marking of new histones. *Mol Cell* **37**, 736-743, doi:10.1016/j.molcel.2010.01.033 (2010).
53 Schlacher, K. *et al.* Double-strand break repair-independent role for BRCA2 in blocking stalled replication fork degradation by MRE11. *Cell* **145**, 529-542, doi:10.1016/j.cell.2011.03.041 (2011).

54 Clynes, D. *et al.* Suppression of the alternative lengthening of telomere pathway by the chromatin remodelling factor ATRX. *Nature communications* **6**, 7538, doi:10.1038/ncomms8538 (2015).
55 Toledo, L. I. *et al.* ATR prohibits replication catastrophe by preventing global exhaustion of RPA. *Cell* **155**, 1088-1103, doi:10.1016/j.cell.2013.10.043 (2013).
56 Ray Chaudhuri, A. *et al.* Topoisomerase I poisoning results in PARP-mediated replication fork reversal. *Nature structural & molecular biology* **19**, 417-423, doi:10.1038/nsmb.2258 (2012).
57 Bruhn, C., Zhou, Z. W., Ai, H. & Wang, Z. Q. The essential function of the MRN complex in the resolution of endogenous replication intermediates. *Cell reports* **6**, 182-195, doi:10.1016/j.celrep.2013.12.018 (2014).
58 Lee, J. M., Ledermann, J. A. & Kohn, E. C. PARP Inhibitors for BRCA1/2 mutation-associated and BRCA-like malignancies. *Ann Oncol* **25**, 32-40, doi:10.1093/annonc/mdt384 (2014).
59 Lord, C. J., Tutt, A. N. & Ashworth, A. Synthetic lethality and cancer therapy: lessons learned from the development of PARP inhibitors. *Annu Rev Med* **66**, 455-470, doi:10.1146/annurev-med-050913-022545 (2015).
60 Xiong, T., Wei, H., Chen, X. & Xiao, H. PJ34, a poly(ADP-ribose) polymerase (PARP) inhibitor, reverses melphalan-resistance and inhibits repair of DNA double-strand breaks by targeting the FA/BRCA pathway in multidrug resistant multiple myeloma cell line RPMI8226/R. *Int J Oncol* **46**, 223-232, doi:10.3892/ijo.2014.2726 (2015).

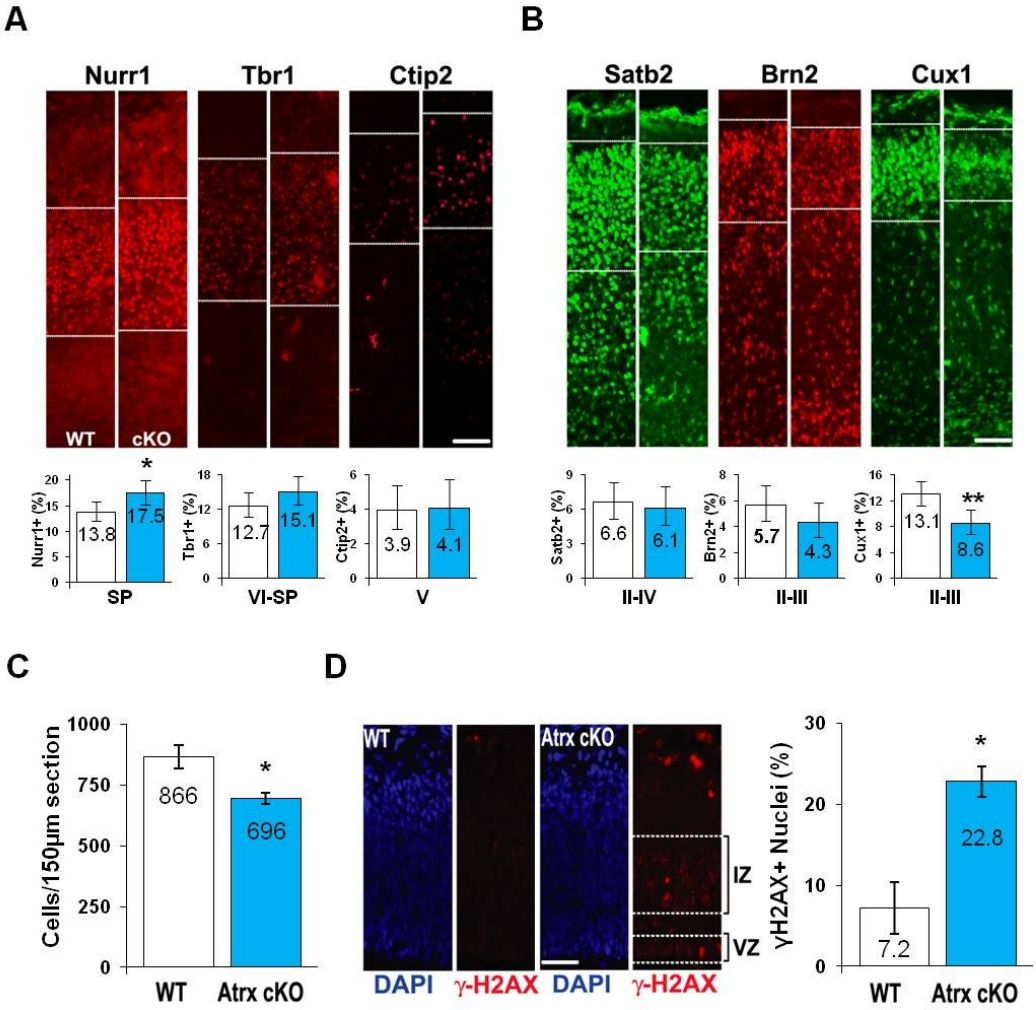

Figure 1. Atrx facilitates the production of late-born cortical neurons by preventing genomic instability in neural precursor cells. Representative micrographs and quantification of neurons located in the deep (A) or upper (B) neocortical layers from E18.5 *Atrx* cKO and wildtype coronal brain sections. Sections were probed with antibodies that specifically labelled the subplate (SP; Nurr1), layer VI-SP (Tbr1), and layer V (Ctip2), layers II-IV (Satb2), and layers II/III (Brn2 & Cux1). Labelled neurons within bounded areas were quantified as a percent of total nuclei within the neocortex. Values represent percent total ± 95% CI. * denotes p< 0.05 by z-score, while ** denotes p < 0.01 by z-score. 200X magnification. Scale bar, 100 µm. (C) Average cell density counts from E18.5 WT and *Atrx* cKO cortical sections following DAPI staining. (D) Representative immunofluorescent micrographs of E13.5 *Atrx* cKO and WT embryos coronal brain sections stained for γ-H2AX (red) or counterstained with DAPI (blue) to label all nuclei. Neural progenitor cells (NPC) reside in the ventricular and intermediate zones (VZ and IZ), as indicated by dotted lines. 200X magnification. Scale bar, 100 µm. Values represent proportional mean ± SEM. *, p < 0.05 by student t-test.

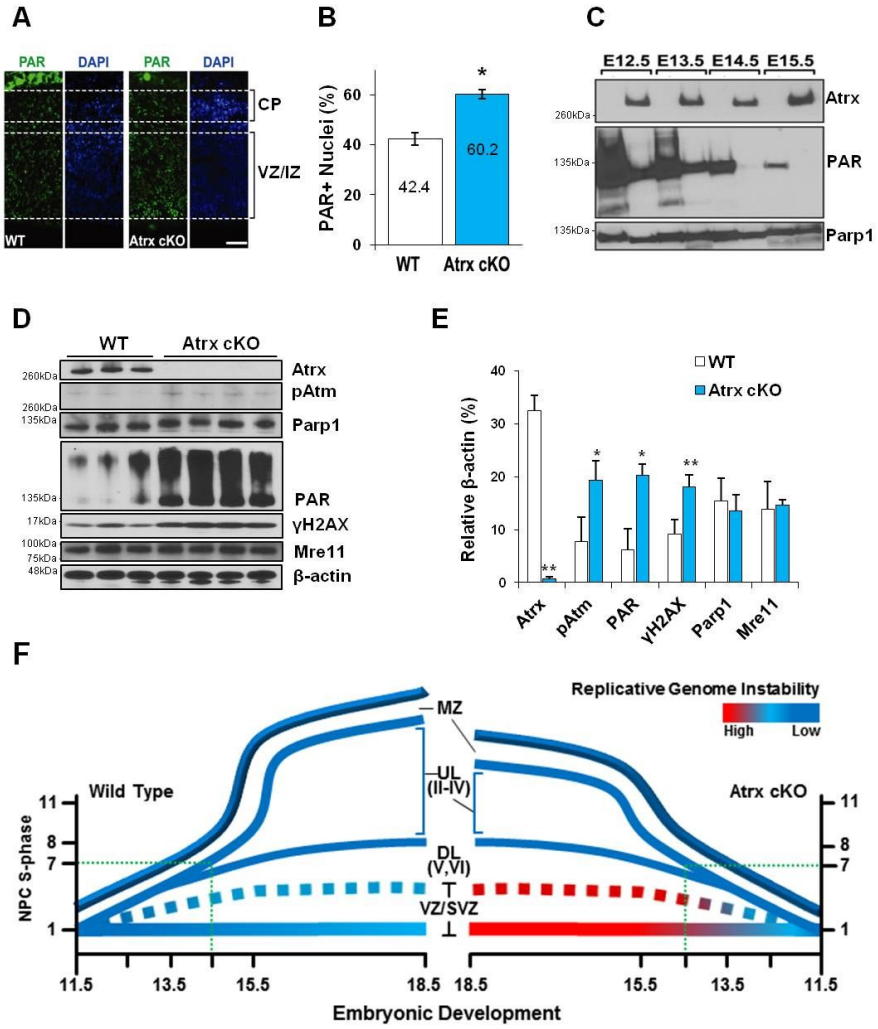

Figure 2. Enhanced activation of DNA damage response pathways in Atrx cKO neuroprogenitors. (A) Representative immunofluorescent micrographs of E13.5 coronal cortical sections from Atrx cKO and WT embryos stained with poly(ADP-ribose) antibodies (PAR; green) and counterstained with DAPI (blue). The cortical plate (CP) and NPC proliferative zones (VZ/IZ) are marked by dotted lines. 200X magnification. Scale bar, 100 μm. (B) Quantification of PAR positive nuclei shown in panel A. Values represent the mean ± SEM; n=3; *, $p < 0.05$ by student t-test. (C) Protein extracts from Atrx cKO and WT cortices were harvested daily from E12.5 until E15.5 and immunoblotted for Parp activity (PAR), Parp1 or Atrx. (D) Immunoblot analysis for DNA damage signalling in E13.5 cortical extracts from WT (n=3) and Atrx cKO (n=4) embryos. (E) Densitometry quantification of blot shown in panel D. Values are the mean ± SEM. *, $p<0.05$; **, $p<0.01$, by student t-test. (F) Developmental model of replicative stress induced loss of late-born neurons in the *Atrx* cKO mice. The X-axis shows the developmental time and the Y-axis shows the number of cycles the NPCs have undergone. Blue lines depict the generation of deep (DL) and upper layer (UL) neurons. Dotted green lines indicate the timing of progenitor cell loss. At this point, progenitors from *Atrx* cKO mice within the VZ/SVZ (red line) have high levels of genomic damage that compromise their survival resulting in a smaller cortex by E18.5.

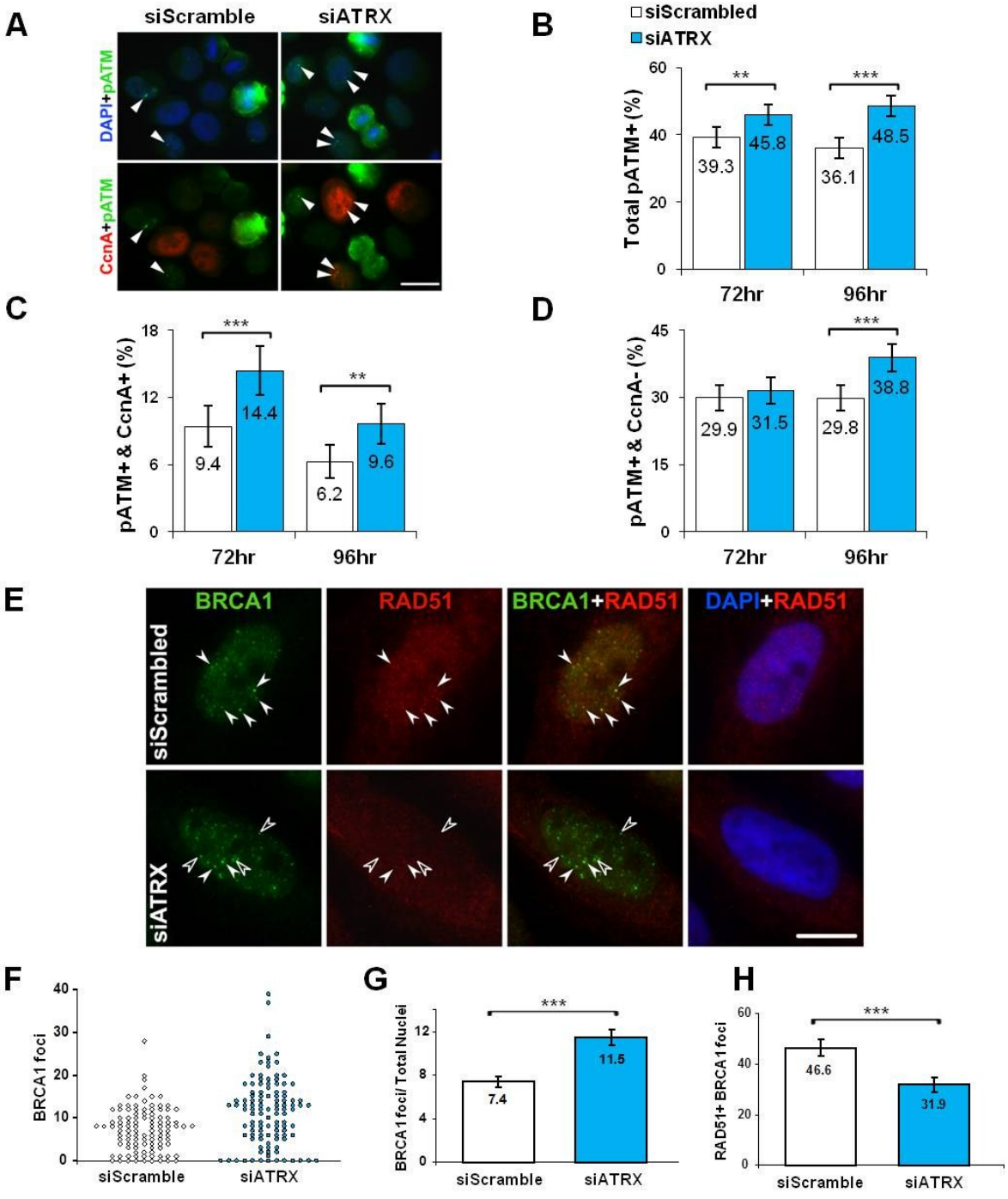
A
siScramble
siATRX
DAPI+pATM
CcnA+pATM
B
siScrambled
siATRX
Total pATM+ (%)
39.3
45.8
36.1
48.5
72hr
96hr
C
pATM+ & CcnA+ (%)
9.4
14.4
6.2
9.6
72hr
96hr
D
pATM+ & CcnA- (%)
29.9
31.5
29.8
38.8
72hr
96hr
E
BRCA1
RAD51
BRCA1+RAD51
DAPI+RAD51
siScrambled
siATRX
F
BRCA1 foci
siScramble
siATRX
G
BRCA1 foci/ Total Nuclei
7.4
11.5
siScramble
siATRX
H
RAD51+ BRCA1 foci
46.6
31.9
siScramble
siATRX

Figure 3. ATRX knockdown cells have increased activation of p53-ATM checkpoint upon mitotic progression and impaired RAD51 co-localization to BRCA1 foci. (A) Representative micrographs of phosphorylated $ATM^{Ser1981}$ (pATM; green) and Cyclin A (CcnA; red) double immunofluorescent staining of siScrambled and siATRX transfected HeLa cells at 96 hours post transfection. Arrowheads point to cells with DNA damage foci. (B) Percentage of total interphase nuclei containing pATM foci in siATRX versus siScrambled transfected HeLa cells at 72 and 96 hrs post transfection. siATRX: 72 hr, n = 1001; 96 hr, n = 1007. siScrambled: 72 hr, n = 999; 96 hr, n = 1009. (C) Percentage of S-G2 (CcnA+) nuclei containing pATM foci at 72 and 96 hrs post transfection. siATRX: 72 hr, n = 365; 96 hr, n = 366. siScrambled: 72 hr, n = 342; 96 hr, n = 308. (D) Percentage of G1 (CcnA-) nuclei containing pATM foci at 72 and 96 hours post transfection. siATRX: 72 hr, n = 636; 96 hr, n = 641. siScrambled: 72 hr, n = 657; 96 hr, n = 701. (E) Representative micrographs of BRCA1 and RAD51 double immunostaining in siScrambled control and siATRX knockdown HeLa nuclei 72 hours post transfection. Solid arrowheads point to foci that are $BRCA1^{+}$ and $RAD51^{+}$ and open arrowheads point to foci that are only $BRCA1^{+}$. (F) Scatterplot distribution profile of BRCA1 foci from the experiment described in (E). siScrambled, n = 106 nuclei; siATRX, n = 111 nuclei. (G) Quantification of BRCA1 foci from the experiment described in (E). siScrambled, n = 106 nuclei; siATRX, n = 111 nuclei. (H) Percentage of total BRCA1 foci positive for RAD51 from the experiment described in (E). All images are at 630X magnification; scale bars are 20 μm (A) or 10 μm (E). For graphs, values represent percent total ± 95% CI except for (G) which is mean number of BRCA1 foci ± SEM; **, $p< 0.01$; ***, $p< 0.001$ by z-scores (B-D, H) or student t-test (G).

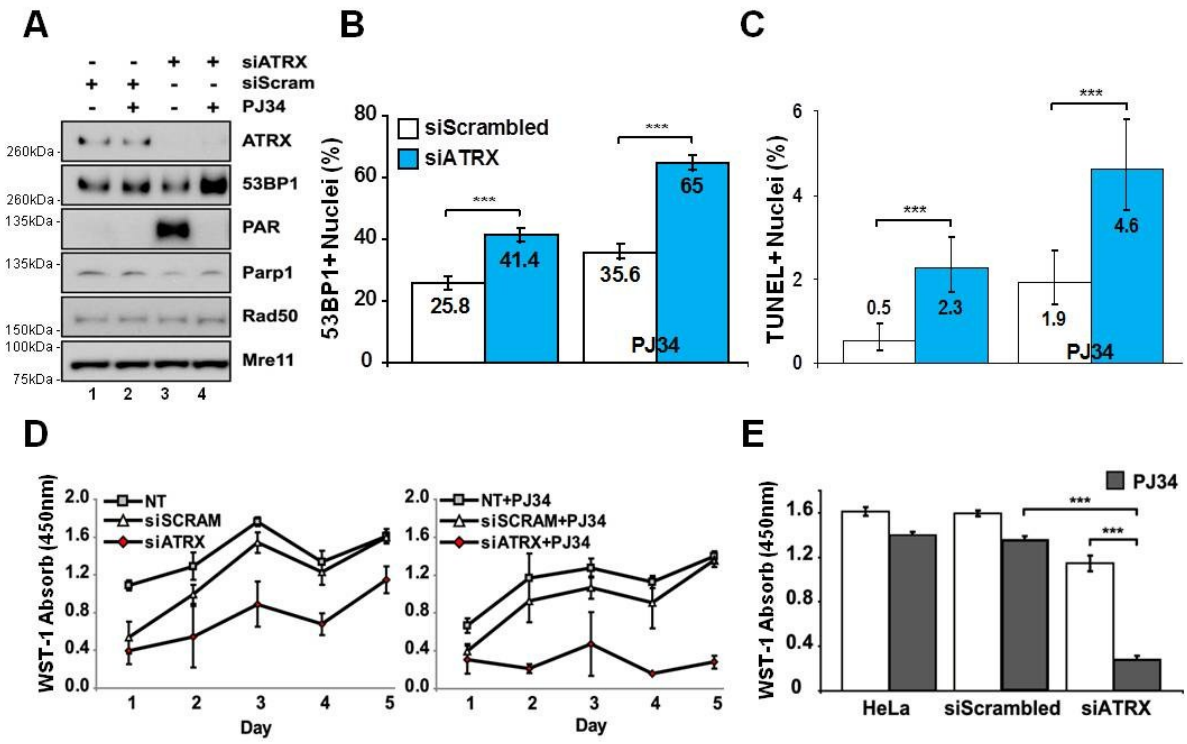

Figure 4. PARP inhibition induces DNA breaks and causes growth suppression in ATRX KD cells. (A) Immunoblot analysis of PARP inhibition by PJ34 in ATRX knockdown HeLa cells. As indicated, HeLa cells were transfected with siScrambled and siATRX. 48 hours after transfection, cells were treated with 5μM of PARP inhibitor PJ34 (+) or untreated (-) for another 24 hours. Whole cell extracts were harvested 72 hours post transfection. (B) Percentage of total nuclei containing ≥5 bright 53BP1 foci in siScrambled versus siATRX transfected HeLa cells at 96 hours post transfection. 72 hours after transfection, cells were treated with 5μM of PARP inhibitor PJ34 (right) or untreated for another 24 hours (left). Cells were fixed 96 hours post transfection and stained for 53BP1. Values represent percent total ± 95% CI. siScrambled (n = 1420); siATRX (n = 1607); siScrambled + PJ34 (n = 1473); siATRX + PJ34 (n = 1492). (***) $p < 0.001$ by z-scores. (C) Percentage of total nuclei containing TUNEL positive apoptotic nuclei in siScrambled versus siATRX transfected HeLa cells at 72 hours post transfection. 48 hours after transfection, cells were treated with 5μM of PARP inhibitor PJ34 (right) or untreated for another 24 hours (left). Cells were fixed 72 hours post transfection and TUNEL stained. Values represent percent total ± 95% CI. siScrambled (n = 2251); siATRX (n = 2031); siScrambled + PJ34 (n = 1802); siATRX + PJ34 (n = 1455). (***) $p < 0.001$ by z-scores. (D) WST-1 cell viability time course of untreated (NT), siScrambled, siATRX transfected HeLa cells. Cells were seeded equally 24 hours following transfection (left panel) or treated with 5μM PJ34 24 hours later (right panel). Viability measurements were assessed at Day 1 (72 hours post transfection) until Day 5. Values represent mean ± SEM. For all conditions, n=4. (E) WST-1 cell viability measurement at Day 5 of time courses described in (D).

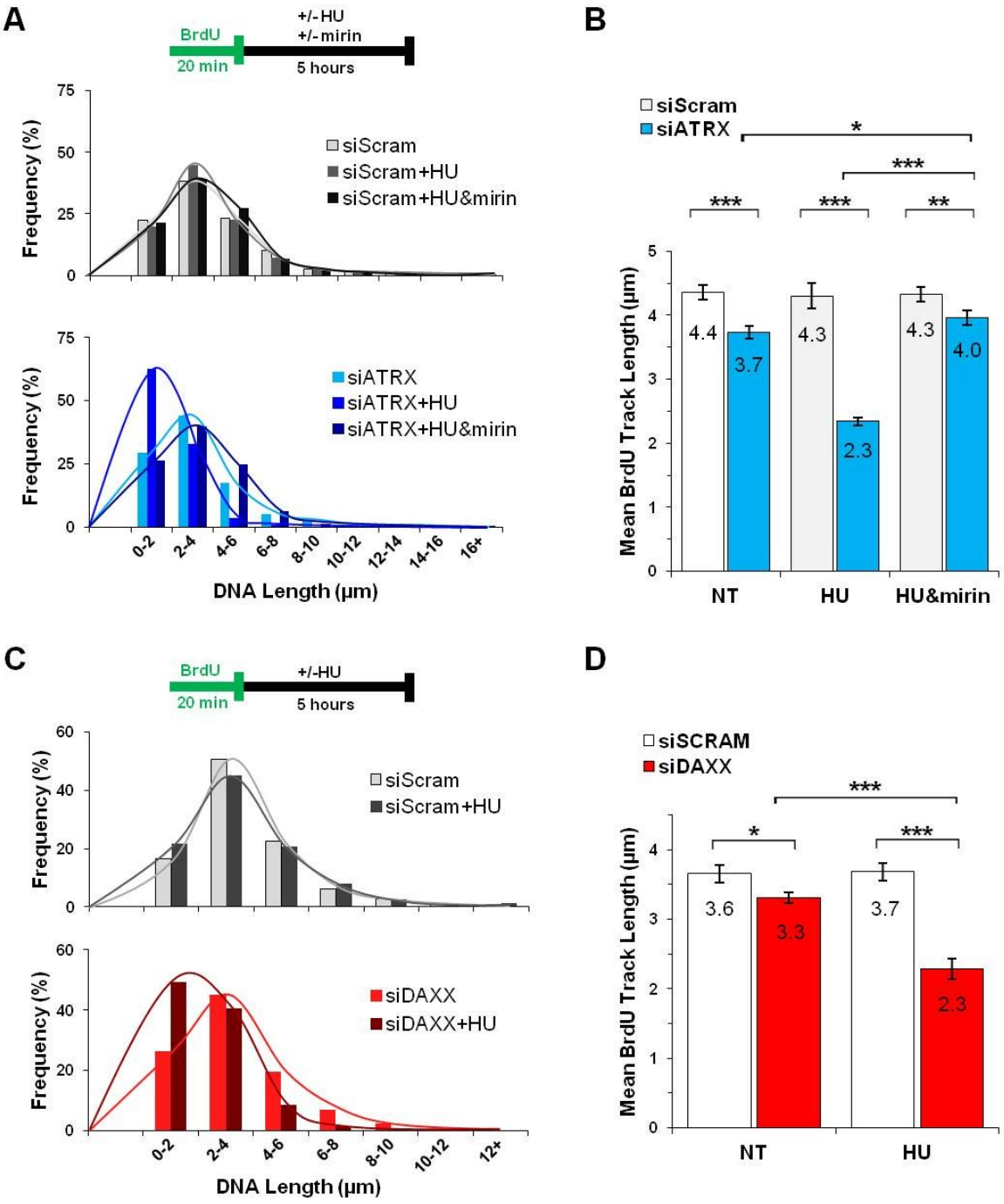
A
BrdU
20 min
+/-HU
+/-mirin
5 hours
Frequency (%)
siScram
siScram+HU
siScram+HU&mirin
siATRX
siATRX+HU
siATRX+HU&mirin
0-2
2-4
4-6
6-8
8-10
10-12
12-14
14-16
16+
DNA Length (µm)
B
siScram
siATRX
*
***
***
***
**
Mean BrdU Track Length (µm)
4.4
3.7
4.3
2.3
4.3
4.0
NT
HU
HU&mirin
C
BrdU
20 min
+/-HU
5 hours
Frequency (%)
siScram
siScram+HU
siDAXX
siDAXX+HU
0-2
2-4
4-6
6-8
8-10
10-12
12+
DNA Length (µm)
D
siSCRAM
siDAXX
***
*
***
Mean BrdU Track Length (µm)
3.6
3.3
3.7
2.3
NT
HU

Figure 5. The ATRX-DAXX pathway protects stalled DNA replication forks from degradation by MRE11 exonuclease activity. (A) DNA fiber tract length distribution histogram of siScrambled (top) and siATRX (bottom) transfected HeLa cells at 72 hr post transfection. siRNA treated cells were pulsed with BrdU and subsequently exposed to hydroxyurea (HU) and mirin as indicated in schematic. Total fibers counted for siScram experiment: no treatment, NT (n = 1782); HU (n = 1819); HU & mirin (n = 1759). Total fibers counted for siATRX treated cells: NT (n = 1527); HU (n = 1523); HU & mirin (n = 1536). (B) Mean DNA fiber tract length of experiments described in (A). (C) DNA fiber tract length distribution histogram of siScrambled (top) and siDAXX (bottom) transfected HeLa cells at 72 hr post transfection. Fibers counted for siScrambled treated cells were: NT (n = 888); HU (n = 998). Total fibers counted for siDAXX treated cells were: NT (n = 888), HU (n = 1171). (D) Mean DNA fiber tract length of experiments described in (C). For panels (B, D), the mean length ± 95% CI was plotted. (*) $p < 0.05$, (**) $p < 0.01$, (***) $p < 0.001$ by Mann-Whitney test.

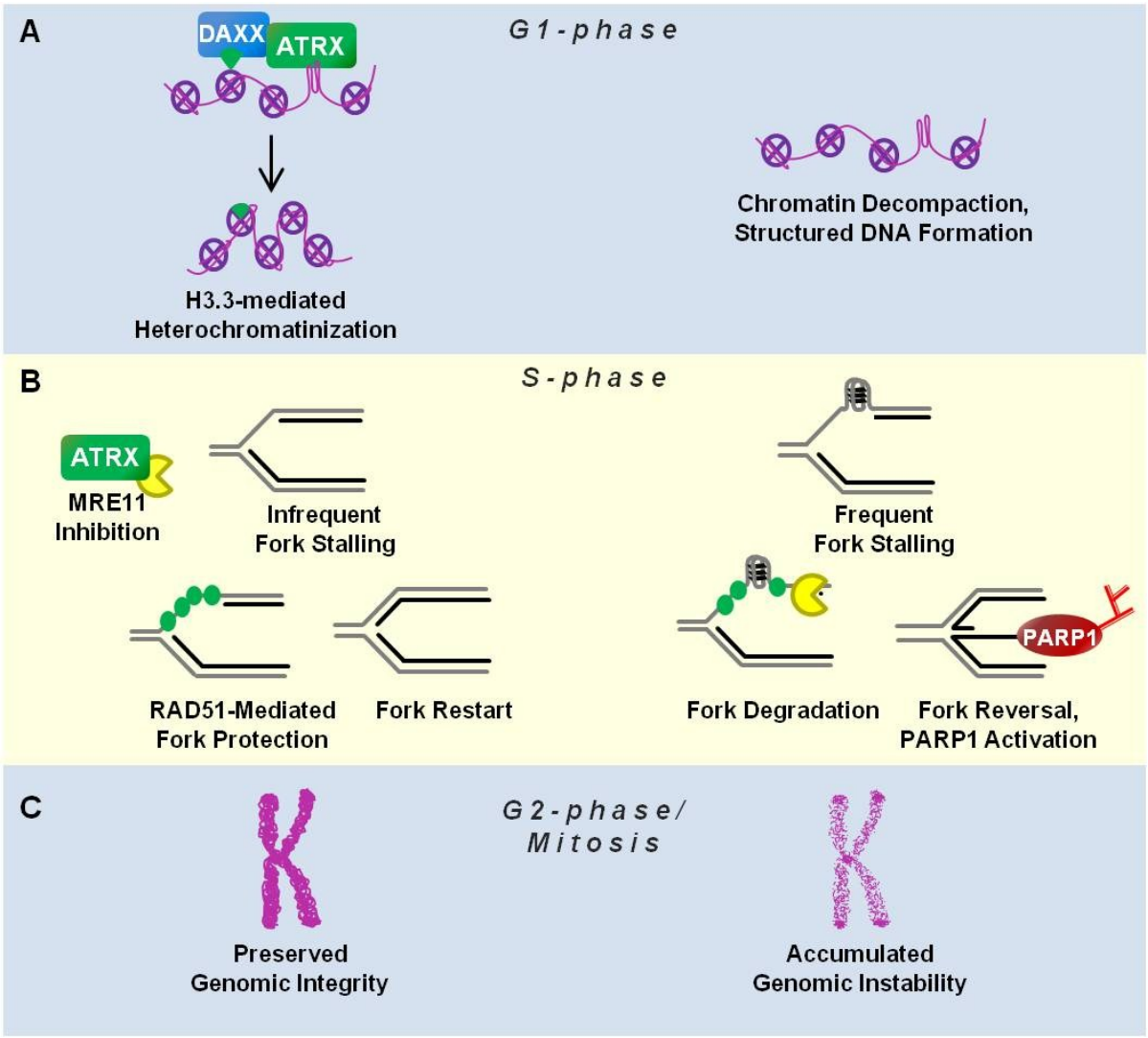

Figure 6. A model of how ATRX suppresses genomic instability during cellular proliferation. Relevant scenarios are shown during (A) G1-phase, (B) S-phase, and (C) G2/M-phase with ATRX present (left) or absent (right). (A) During G1, ATRX localizes to decompacted and structured DNA (e.g. G4-DNA) along with DAXX to chaperone H3.3-H4 dimers that serve as a beacon for further heterochromatinization. When cells progress into S-phase (B), DNA replication forks experience more frequent stalling events when ATRX is absent due to an increased incidence of structured DNA. ATRX physically interacts with MRE11 and inhibits excessive MRE11-mediated resectioning of stalled replication forks, which subsequently require RAD51-mediated protection of nascent DNA. In the absence of ATRX, PARP1 activation is upregulated in an attempt to reverse stalled replication forks and protect against further MRE11 resectioning. Cells with frequent fork stalling that progress into G2-phase and mitosis (C) are more prone to double strand DNA breaks and mutagenic non-allelic homologous recombination events (NAHR) resulting in genomic instability.

8. Curriculum Vitae

Objective

To pursue an education and a career regarding the investigation of novel concepts in biochemistry and molecular genetics, with special focus given towards understanding the mechanisms required for the development of complex organs such as the brain.

Technical Skills

- Laboratory experience in biochemistry and molecular biology:
  - Cell culture(primary mammalian, bacterial)
  - Mouse neuro-anatomy
  - Flow cytometry
  - Fluorescent confocal microscopy and live cell imagining
  - Transfection, nucleofection, and infection (adenoviral, lentiviral) of cultured cells
  - Real-time quantitative PCR
  - Chromatin/protein immunoprecipitation
  - Sub-cellular fractionation and western protein analysis
  - Computer skills: laboratory analysis software (e.g. BLAST, PubMed), MS Office (Word, Excel, PowerPoint)
- Certified by the Canadian Council on Animal Care's National Institutional Animal User Training program with experience handling and breeding transgenic mice
- Certified for WHMIS, Radiation Safety & Emergency Preparedness and Standard First Aid with CPR Level A.

Publications

- Stalled replication forks within heterochromatin require ATRX for protection. (2016) Huh MS#, **Ivanochko D#,**Hashem E,Curtin M, Delorme M, Goodall E, Yan K, & Picketts DJ. *Cell Death and Disease. (In press);* # denotes equal contribution
- PHF6 Degrees of Separation: The multifaceted roles of a chromatin adaptor protein. (2015) Todd MAM, **Ivanochko D**, Picketts DJ. *Genes* 6(2), 325-352
- Snf2h-mediated chromatin organization and histone H1 dynamics govern cerebellar morphogenesis and neural maturation. (2014) Alvarez-Saavedra M, De Repentigny Y, Lagali PS, Raghu Ram EV, Yan K, Hashem E, **Ivanochko D**, Huh MS, Yang D, Mears A, Todd MA, Corcoran CP, Bassett EA, Tokarew NJ, Majumder R, Ioshikhes I, Wallace VA, Kothary R, Meshorer E, Stopka T, Skoultchi A, Picketts DJ. *Nature Communications* 5, 4181

Employment & Volunteer History

- University of Ottawa, Department of Biochemistry (***January to April 2015, 2016***)
  – Teaching Assistant: Lab demonstrator BCH3346
- University of Ottawa, Peer Help Centre (***September 2012 to Present***)
  – Tutor
- "Let's Talk Science" (***2013 to Present***)
  – Volunteer at Stem Cell Talks symposiums and classroom demonstrations
- Ottawa Hospital Research Institute:
  Laboratory of Dr. David Picketts (***May to August 2013; May to August 2014***)
  – Summer Research Student

Education

- **University of Ottawa (*2014- Present*)**
  MSc Biochemistry with Specialization in Human Molecular Genetics
  Thesis title: "*ATRX Protects Cells From Replication Induced Genomic Instability*"
  Supervisor: Dr. David Picketts PhD

Graduate courses	
BCH8111 – Chromosome and Chromatin Biology	A+
HMG8105 – Molecular Biology of Human Disease II	A

- **University of Ottawa (*2010 – 2014*)**
  BSc Honours with Specialization in Biochemistry

4th Year		3rd Year	
BCH4040 – Biochemistry Honours Project (equiv. to 3 courses)	A+	BCH3170 – Molecular Biology	B+
BCH4300B – Statistics for Biochemistry	A+	BCH3356 – Molecular Biology LAB	A-
BCH4932D – Biochemistry Seminar	A+	CHM3120 – Organic Chemistry	A
BPS4129 – Chemical Biology	A+	CHM3122 – Applications of Spectroscopy	A
BCH4300A – Stem Cells	B+	BPS3101 – Genomics	A-
CHM4155 – Polymer & Applied Chemistry	A+	BCH3120 – Metabolism	B+
CHM4328 – Carbohydrate Chemistry	A+	BCH3125 – Protein Structure and Function	A-
BIM4316 – Bio-Analytical Chemistry	A-	BCH3346 – Biochemistry II LAB	A-
		BIO3153 – Cell Biology	

Undergraduate Honour's Research Project:
Identification and Characterization of Mus musculus ISWI Target Genes During Granule Neuron Progenitor Differentiation
Supervisor: Dr. David Picketts PhD

- **York University (*2008 – 2009*)**
  BA Linguists and Communications Double Major *
  (*I discontinued my studies after completing my first year to pursue science)

Awards

- NSERC - Postgraduate Scholarship - Doctoral Program (***Commences September 2016***)
  Value: $63000 / 36 months

- CIHR - Frederick Banting and Charles Best Canada Graduate Scholarship (***May 2015***)
  Value: $17500

- Queen Elizabeth II Graduate Scholarship in Science and Technology (***Declined***)
  Value: $15000

- University of Ottawa Excellence Scholarship (***May 2015***)
  Value: $8000

- University of Ottawa Admission Scholarship (***September 2014***)
  Value: $7500

- The BMI Undergraduate Research Excellence Award (Received: ***April 2014***)

- Dean's Honour List (***2013-2014***)